

Fall 2005

# Development of palladium nanowires

Chuanding Cheng  
*Louisiana Tech University,*

Follow this and additional works at: <https://digitalcommons.latech.edu/dissertations>

 Part of the [Chemical Engineering Commons](#), and the [Materials Science and Engineering Commons](#)

---

## Recommended Citation

Cheng, Chuanding, "" (2005). *Dissertation*. 583.  
<https://digitalcommons.latech.edu/dissertations/583>

This Dissertation is brought to you for free and open access by the Graduate School at Louisiana Tech Digital Commons. It has been accepted for inclusion in Doctoral Dissertations by an authorized administrator of Louisiana Tech Digital Commons. For more information, please contact [digitalcommons@latech.edu](mailto:digitalcommons@latech.edu).

# NOTE TO USERS

This reproduction is the best copy available.

**UMI**<sup>®</sup>



# DEVELOPMENT OF PALLADIUM NANOWIRES

by

Chuanding Cheng, B.E.

A Dissertation Presented in Partial Fulfillment of  
the Requirement for the Degree of  
Doctor of Philosophy in Engineering

COLLEGE OF ENGINEERING AND SCIENCE  
LOUISIANA TECH UNIVERSITY

November 2005

UMI Number: 3192317

### INFORMATION TO USERS

The quality of this reproduction is dependent upon the quality of the copy submitted. Broken or indistinct print, colored or poor quality illustrations and photographs, print bleed-through, substandard margins, and improper alignment can adversely affect reproduction.

In the unlikely event that the author did not send a complete manuscript and there are missing pages, these will be noted. Also, if unauthorized copyright material had to be removed, a note will indicate the deletion.

**UMI**<sup>®</sup>

---

UMI Microform 3192317

Copyright 2006 by ProQuest Information and Learning Company.

All rights reserved. This microform edition is protected against unauthorized copying under Title 17, United States Code.

ProQuest Information and Learning Company  
300 North Zeeb Road  
P.O. Box 1346  
Ann Arbor, MI 48106-1346



## APPROVAL FOR SCHOLARLY DISSEMINATION

The author grants to the Prescott Memorial Library of Louisiana Tech University the right to reproduce, by appropriate methods, upon request, any or all portions of this Dissertation. It is understood that "proper request" consists of the agreement, on the part of the requesting party, that said reproduction is for his personal use and that subsequent reproduction will not occur without written approval of the author of this Dissertation. Further, any portions of the Dissertation used in books, papers, and other works must be appropriately referenced to this Dissertation.

Finally, the author of this Dissertation reserves the right to publish freely, in the literature, at any time, any or all portions of this Dissertation.

Author Chuanzhong  
Date 11/09/2005

## ABSTRACT

Inherent limitations of traditional lithography have prompted the search for means of achieving self-assembly of nano-scale structures and networks for the next generation of electronic and photonic devices. The nanowire, the basic building block of a nanocircuit, has recently become the focus of intense research. Reports on nanowire synthesis and assembly have appeared in the scientific literature, which include Vapor-Liquid-Solid mechanism, template-based electrochemical fabrication, solvothermal or wet chemistry, and assembly by fluid alignment or microchannel networks. An ideal approach for practical application of nanowires would circumvent technical and economic constraints of templating. Here we report on the self-assembly of highly-ordered metallic nanowires directly from a palladium acetate solution under an applied alternating current (AC) electric field of relatively high intensity and frequency.

DNA-templated nanowires are first presented here. DNA molecules were stretched and positioned by electric field, followed by metallization by palladium acetate solution. Palladium nanowire arrays have been found to grow directly between microelectrodes without any template, under an alternating electric field of relatively high intensity and frequency. The wires grew spontaneously along the direction of the electric field and have high uniformity and conductivity.

Single 75 nm-diameter palladium nanowires have also been self-assembled from aqueous solution at predefined locations between 15  $\mu\text{m}$ -gap electrodes built on a  $\text{SiO}_2$  substrate. Nanowire assembly was initiated by application an electric field, and it occurred only along the direction of field lines where the field is strongest. Related metals did not support single nanowire assembly under comparable conditions. Current-limiting circuits for controlled nanowire synthesis, electric field simulation, and growth mechanism were studied. The simple and straightforward approach to nanowire assembly outlined here will provide a means of nano-/micro-scale device interconnection at precise positions at room temperature and good potential for device development, integration, and packaging.

## TABLE OF CONTENTS

ABSTRACT.....	iii
LIST OF TABLES.....	vii
LIST OF FIGURES.....	viii
ACKNOWLEDGMENTS.....	xii
CHAPTER 1 INTRODUCTION.....	1
1.1 Background.....	1
1.2 Nanowire Synthesis.....	2
1.2.1 Catalyzed Growth by VLS Mechanism.....	2
1.2.2 Template-Based Electrochemical Synthesis.....	3
1.2.3 Synthesis in Solvothermal or Wet Chemistry.....	6
1.3 Nanowire Assembly.....	6
1.3.1 Fluid Alignment.....	6
1.3.2 Microchannel Networks.....	6
1.4 Electric-Field Assisted Synthesis and Assembly.....	7
1.4.1 Synthesis by Electric Field.....	7
1.4.2 Assembly by Electric Field.....	8
1.5 Objective and Methodology.....	9
CHAPTER 2 CONDUCTIVE NANOWIRES TEMPLATED BY DNA.....	10
2.1 Fundamentals of DNA Molecule.....	10
2.2 DNA Stretching and Positioning.....	14
2.2.1 Molecular Combing.....	15
2.2.2 Electrophoretic Stretching.....	18
2.2.3 Hydrodynamic Stretching.....	21
2.2.4 DNA Positioning.....	22
2.3 DNA Metallization.....	24
2.4 Electrode Fabrication.....	32
2.4.1 LOR Photoresist Lift-Off.....	32
2.4.2 Process of LOR Photoresist Lift-Off.....	33
2.5 Materials and Methodology.....	35
2.6 Experimental Results and Discussion.....	37

CHAPTER 3 DIRECT GROWTH OF ARRAYS OF PALLADIUM NANOWIRES...	44
3.1 Introduction.....	44
3.2 Electrode Structure.....	45
3.3 Materials and Methodology.....	45
3.4 Characterizations.....	46
3.5 Discussion.....	47
CHAPTER 4 SINGLE PALLADIUM NANOWIRES AT PRESCRIBED LOCI.....	55
4.1 Electrode Structure.....	55
4.2 Materials and Methodology.....	56
4.3 Characterizations.....	56
4.4 Other Materials.....	59
CHAPTER 5 CIRCUIT DESIGN FOR CONTROL OF NANOWIRE GROWTH.....	67
5.1 Melting Problem.....	67
5.2 Current-Limiting Circuit Design.....	69
5.3 Circuit Simulation Results.....	70
CHAPTER 6 MECHANISM DISCUSSION.....	74
6.1 Palladium and Its Complex.....	74
6.2 Electric Field Simulation.....	76
6.3 Discussion.....	80
CHAPTER 7 CONCLUSION AND FUTURE WORK.....	85
7.1 Conclusion.....	85
7.2 Future Work.....	86
REFERENCES.....	89

## LIST OF TABLES

Table 2-1	Stretching and positioning of DNA for nanowire fabrication.....	14
Table 2-2	Recommended LOR spin coating parameters.....	34
Table 2-3	Preparation of DNA. Storage temperature: -20 °C.....	35
Table 4-1	EDX data.....	58
Table 4-2	Effect of voltage and concentration on wire growth.....	64
Table 5-1	Truth value of ADG 431.....	70
Table 6-1	Ionic mobilities in water at 298 K.....	82
Table 6-2	Period time at different frequency.....	82

## LIST OF FIGURES

Figure 1-1	Schematic illustration of vapor-liquid-solid nanowire growth mechanism which includes three steps: 1) alloying, 2) nucleation, 3) axial rowth.....	3
Figure 1-2	Nanoporous membrane.....	4
Figure 2-1	Schematic diagram of the structure of double-stranded DNA. Each subunit consists of a phosphate group, a sugar and one of the four bases: adenine (A), thymine (T), guanine (G) or cytosine (C). Molecular recognition by Watson-Crick base pairing means that A pairs with T only, and G pairs with C only. Two classes of binding site for DNA-templated metallic nanowire fabrication are shown: negatively charged phosphate groups in the polymer backbone, and N7 atoms of bases G and A and N3 atoms of bases C and T.....	11
Figure 2-2	Molecular combing. A) Schematic diagram of the mechanism. Redrawn from ref. 59. The distance between the coverslip and substrate is typically on the order of microns, depending on droplet volume, coverslip mass, surface properties, and so on. The meniscus generates a surface tension during evaporation which stretches DNA. B) Fluorescence micrograph of bacteriophage $\lambda$ DNA stained with the fluorescent dye YOYO-1 (Molecular Probes, Inc., USA) and combed on silanized glass. The average length of stretched molecules is $\sim 21 \mu\text{m}$ . The scale bar represents $10 \mu\text{m}$ .....	16
Figure 2-3	Stretching of DNA with floating potential electrodes. A) Schematic diagram of the electrodes. Redrawn from ref. 69. B) $\lambda$ DNA molecules stretched and positioned between floating potential electrodes. DNA was stained with a fluorescent dye, Yo-Pro-1 (Molecular Probes Inc., USA). The image was taken with a fluorescence microscope. Copyright 2000 IEEE.....	20
Figure 2-4	Stretching DNA by hydrodynamic flow. A) Schematic diagram of apparatus. Reprinted with permission from ref. 73. Copyright 1994 American Association for the Advancement of Science. B) Time-averaged fluorescence micrograph of a DNA molecule ( $67.2 \mu\text{m}$ ) stretched in a $0.95 \text{ cP}$ fluid flow with a velocity of 2, 4, 6, 8 or $10 \mu\text{m/s}$ . The ratio of extended length to the contour length was 19, 33, 44, 50 and 55% (left to right). Copyright 1995 American Association for the Advancement of Science.....	22

Figure 2-5	Visualization by fluorescence microscopy of stretched DNA molecules between Au electrodes. A) Middle of parallel electrodes. B) End of parallel electrodes. The gap size is $\sim 16 \mu\text{m}$ . DNA is stained with YOYO-1. Arrows stretched DNA molecules. (By Dr. Qun Gu, 2005).....	23
Figure 2-6	Characterization of metallized DNA. A) Atomic force microscope image of a 100 nm wide Ag nanowire using DNA-templated assembly. B) I-V characteristics of the nanowire. Copyright 1998 Macmillan Publishers Ltd.....	24
Figure 2-7	Characterization of Pd nanowires. A) Scanning electron micrograph of a $\sim 60$ nm-wide Pd nanowire. The measured resistance was $34.3 \text{ k}\Omega$ . B) Temperature dependent resistance of three Pd wires. Copyright 2002 Springer-Verlag.....	26
Figure 2-8	Co nanowire fabrication and characterization. A) UV-vis spectrum of Pd(II)-activated DNA in Co plating bath as a function of time. Spectra were taken at 0 min, 10 min, 20 min, and 40 min. The inset shows a magnified view of the spectra in the 400-600 nm range. B) AFM image of a Co nanowire. The height scale is $\sim 14$ nm. Copyright 2005 Institute of Physics Publishing.....	27
Figure 2-9	Molecular lithography. A) AFM image of RecA filament bound to $\lambda$ DNA. B) AFM image of the sample after reduction. C) AFM image of the sample after Au plating. D) SEM image of Au nanowires. The gaps in B-D show that the regions of DNA protected by RecA were not metallized. Scale bars: $0.5 \mu\text{m}$ ; $0.25 \mu\text{m}$ in inset of C. Copyright 2002 American Association for the Advancement of Science.....	29
Figure 2-10	Molecular biology meets nanotechnology. A) Ligation of aldehyde-derivatized DNA fragments (2054 bp) and underivatized fragments (1106 bp). B) Gel electrophoresis of ligated fragments. Left lane is a $\lambda$ -Hind III digest. C) SEM micrograph of Ag(0) deposited on ligated fragments. Upper panel: Two 700 nm Ag clusters are separated by a 350 nm gap. Low panel: Three 700 nm Ag clusters are separated by two 350 nm gaps. Scale bar: 330 nm. Copyright 2004 American Chemical Society.....	30
Figure 2-11	LOR photoresist process. (From <a href="http://www.microchem.com">www.microchem.com</a> ).....	33
Figure 2-12	Undercut pattern by LOR photoresist.....	35
Figure 2-13	Collection effect on DNA by dielectrophoresis.....	38
Figure 2-14	Stretching and positioning of DNA molecules.....	40
Figure 2-15	Metallization of DNA and control experiments without DNA.....	42
Figure 2-16	Metallized DNA strands.....	43
Figure 3-1	Schematic diagram of the microelectrode structure used in this research. Four pairs of parallel electrodes, with gap size ranging from 10 to $25 \mu\text{m}$ , were patterned on a silicon dioxide substrate. Dimensions are not to scale.....	45
Figure 3-2	SEM images of Pd nanowires assembled between electrodes under an applied AC signal of $10 V_{\text{rms}}$ and 300 kHz. The nanowires have an	

	approximate diameter of 100 nm. Experiments involved palladium acetate dissolved in 10 mM HEPES buffer, pH 6.5, diluted 8× from saturation. Gap spacing between electrodes: (a) 10 μm, (b) 15 μm, (c) 20 μm, (d) 25 μm. In (a), the second Pd nanowire from the left has ruptured, presumably due to high current density.....	47
Figure 3-3	Effect of concentration of palladium acetate solution on time required for assembly of nanowires after application of an alternating electric field. The field was 10 V <sub>rms</sub> and 300 kHz. A saturated solution of palladium was diluted with DI water 2, 4, 8, 16, or 32 times. No Pd nanowires were observed after 32× dilution. The whole drop of solution on electrodes was evaporated away after 15 minutes under room temperature.....	49
Figure 3-4	Effect of frequency on the growth of nanowires from Pd acetate solution. The alternating electric field applied was 8 V <sub>rms</sub> and (a) 0.3 KHz, (b) 3 KHz, and (c) 30 KHz. Palladium acetate was 8-fold diluted from saturation.....	50
Figure 3-5	A single Pd nanowire of diameter c. 200 nm. (a) Characterization by SEM. The wire self-assembled between gold electrodes under an AC electric field of 10 V <sub>rms</sub> and 300 KHz at the end of a 20-μm gap electrode. (b) <i>I-V</i> curve. The resistance was 1.69 kΩ. After cutting the wire, the sample behaved as an insulator (inset). (c) Melting test. Under high voltage, 6 Pd nanowires were destroyed one by one when an applied DC voltage shifted from the 0 to 10 V.....	52
Figure 4-1	Schematic electrode designs.....	55
Figure 4-2	Characterization of a single Pd nanowire between Au electrodes on a SiO <sub>2</sub> wafer. (a) Visualization by SEM. The wire self-assembled from Pd acetate solution between a 15 μm-gap and had a diameter of c. 75 nm. Pd acetate solution was diluted 8-fold from saturation, the source was 10 V <sub>rms</sub> at 300 KHz, and DC offset 0.8 V. Scale bar, 2 μm. (b) 4 μm x 4 μm AFM image of a portion of (a). Vertical scale, 90 nm. Irregularity in wire diameter will increase electrical resistance. (c) EDX analysis. The resistance was 149 kΩ.....	57
Figure 4-3	Single Pd nanowires assembled between different types of pointed electrode. (a) “Dull” points. (b) “Sharp” points.....	59
Figure 4-4	Test of various metal salts or complexes under an applied signal of 300 kHz 10 V <sub>rms</sub> and 0.8 V DC. (a) Pt(NH <sub>3</sub> ) <sub>2</sub> Cl <sub>2</sub> , 5 μm scale bar; (b) K <sub>2</sub> PtCl <sub>4</sub> , 5 μm; (c) K <sub>2</sub> IrCl <sub>6</sub> , 10 μm; (d) PdCl <sub>2</sub> , 5 μm; (e) Co(Ac) <sub>2</sub> ·4H <sub>2</sub> O, 10 μm; (f) Ni(Ac) <sub>2</sub> ·4H <sub>2</sub> O, 10 μm. Each solution was saturated, buffered with 10 mM HEPES at pH 6.5, and prepared at room temperature except (b), for which the concentration was 0.02 mol/L.....	60
Figure 4-5	Microwires formed with different precursors. (a) 59 mM PdAc <sub>2</sub> , applied voltage 10V, (b) 59 mM PdAc <sub>2</sub> , applied voltage 5V, (c) 75 mM PdCl <sub>2</sub> , applied voltage 10V, (d) 75 mM PdCl <sub>2</sub> , applied voltage 5V.....	63

Figure 4-6	Pd wires formed under different conditions and with PdAc <sub>2</sub> as precursor. (a) 5.9 mM Pd(NH <sub>3</sub> ) <sub>4</sub> and 5V, (b) 0.59 mM Pd(NH <sub>3</sub> ) <sub>4</sub> And 10 V.....	64
Figure 4-7	Other materials under same electric field. (a) 5.9 mM K <sub>2</sub> PtCl <sub>4</sub> , (b) 0.59 mM AgNO <sub>3</sub> .....	65
Figure 5-1	Melting problem of nanowires.....	68
Figure 5-2	Schematic diagrams of electrodes and circuits. (a) Floating electrodes. (b) Current limiting circuits. (c) Components of current limiting circuits.....	69
Figure 5-3	Simulation result of circuit before growth of nanowires.....	71
Figure 5-4	Simulation result of circuit after growth of nanowires.....	72
Figure 6-1	Structure of palladium acetate.....	76
Figure 6-2	Simulation of equal potential lines and electric field around the specific electrode structure.....	77
Figure 6-3	Electric field before nanowire growth.....	78
Figure 6-4	Electric field during nanowire growth.....	79
Figure 6-5	Palladium acetate particles.....	80
Figure 6-6	Ions drift at different frequencies.....	84
Figure 7-1	Presumed mechanism of nanowire growth.....	86

## ACKNOWLEDGMENTS

I would first like to express my sincere gratitude and thanks to my advisor, Dr. Donald T. Haynie, for enlightened discussion, endless support, and precious advice. I would also like to thank my advisory committee, Dr. Tabbetha Dobbins, Dr. Yi Su, Mr. Ji Fang, and Dr. Upali Siriwardane. Their invaluable advice, continuous guidance, and encouragement are important for completion of this dissertation. Special appreciation is extended to Dr. Louis Roemer. Without his broad love and eternal trust, my academic and research journey at Louisiana Tech could not have proceeded so smoothly and so fruitfully. Special acknowledgements also extend to faculty and staff members at Institute for Micromanufacturing, Dr. Kody Varahramyan, Dr. Alfred Gunasekaran, Mr. Philip Coane, Dr. Karen Xu, Ms. Debbie Wood, Mr. John McDonald, Mr. Dee Tatum, and Mr. Scott Williams for their great help and support in the course of the work.

Much gratitude is extended to my colleagues, Qun Gu, Ravikanth Gonela, Shivashankar Suryanarayanan, Sathish Anabathula, Kun Dai, Zhengchun Liu, Fengliang Xue, Weisong Wang, for their valuable discussion, support and contributions.

# CHAPTER 1

## INTRODUCTION

### 1.1 Background

One-dimensional nanostructures are currently a topic of intensive study. Development of such structures in photonics and electronics has been driven by limitations of traditional lithography and advantages of bottom-up self-assembly. Ordinary fabrication processes, however, such as random deposition [1] manipulation by atomic force microscopy (AFM), or micromanipulation [2], are generally inefficient or time-consuming. Direct device interconnection and assembly of nanowires at precise positions, important for commercial prospects of nanowires, therefore continue to pose considerable technical challenges.

Recently, significant progress has been made in nanowire synthesis [3-15] and self-assembly of functional devices [1, 2, 16]. Approaches to synthesis have included catalyzed growth by the vapor-liquid-solid mechanism at high temperature [3-5], template-based synthesis by electrochemical fabrication [6-13], and use of solvothermal conditions or wet chemistry [14, 15]. Nanowires grown by these ex-situ methods are free-standing, so assembly of a functional device requires the harvesting of pre-formed nanowires, transfer to specific positions, and assembly into hierarchical structures. Fluid alignment [16] and microchannel networks [17] have recently been exploited for

nanowire patterning. Although these methods can produce useful patterns, soft lithography is required to construct a micromold at a desired location before the nanowires are formed.

Electrochemical deposition has proved a convenient and versatile means of fabricating nanowires of various metals, semiconductors, and conductive polymers. Such nanowires can be dense, continuous, and highly crystalline [18]. A range of templates are known in nanowire fabrication: nanopores [6], surface step-edges [7], DNA [8, 9], polymers [10, 11], and carbon nanotubes or other nanowires [12, 13]. Direct metallic intercontact between electrodes has been obtained by dielectrophoresis in a gold particle solution [19], field emission in organometallic compound gas [20], and bipolar electrochemistry in a metal ion solution [21]. To date, however, wires prepared in these ways are microns thick [19, 21] or poorly conductive [19, 20].

## 1.2 Nanowire Synthesis

### 1.2.1 Catalyzed Growth by VLS Mechanism

Semiconductor nanowires and nanotubes are exceptionally important to the study of dimension-dependent chemical and physical phenomena, and potential for applications of self-assembly of nanoscale electronic devices. Many methods of nanowire synthesis in the field have been reported. One key feature of these approaches is the promotion of crystal growth with large variation in the aspect ratio (length to diameter ratio) by using metal nanoparticles as catalysts.

Usually three well defined steps have been clearly identified during the synthesis process: metal alloying, crystal nucleation, and axial growth (Figure 1-1). One of the

most representative examples is growth of silicon nanowires with gold nanoclusters as catalysts.

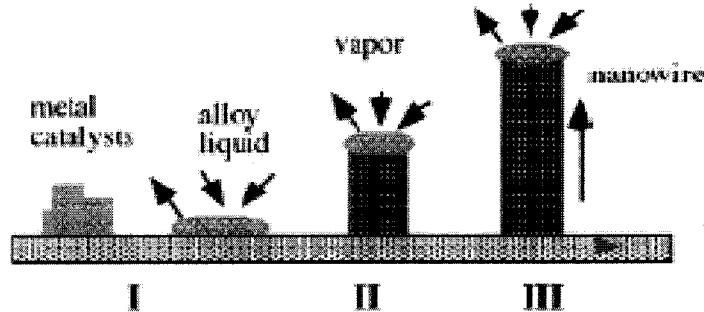


Figure 1-1 Schematic illustration of vapor-liquid-solid nanowire growth mechanism which includes three steps: 1) alloying, 2) nucleation, 3) axial growth [4].

Initially, Au clusters remain in solid state, but at high temperature, Si vapor condenses to form a biphase (solid Au and Au/Si liquid alloy). When Si vapor continues to condense into alloy and composition of Si increased up to a value, the alloy enters another biphase (Au/Si alloy and Si crystal). Once the Si nanocrystal nucleates at the liquid/solid interface, further condensation of Si vapor will promote the growth of nanowires from the alloy. When the system cools down, the alloy nanocrystals solidify as the tips of nanowires.

### 1.2.2 Template-Based Electrochemical Synthesis

Most nanowire synthesis by electrochemical fabrication is based on all kinds of template. Nanoscale channel defined by E-Beam lithography is one way to form template. Nanowire fabrication based on this method has exact position, while at the same time the approach is low efficient. To pursue high efficiency, people seek mass production of nanoporous template [6], step-edge template [7], natural biomimetic template such as DNA and polymer [8-11], and synthesized nanowire template [12, 13].

### *Nanoporous template*

Track-etch membrane and anodic porous alumina are two most popular methods to prepare nanoporous template. For the track and etch method (Figure 1-2a), a heavy-charged particle from a nuclear radiation resource is used to strike a thin film and go through it. The minimum width of the track is only 2.5 nm. The formed track can be selectively etched while other materials are left unchanged. The final channel can be controlled below 10 nm. If plasma etching is used a conical-shape channel can be formed. For the anodic porous alumina, the nanopores in the template are formed by anodizing aluminum films in an acidic electrolyte. The fabricated nanopores are ordered into a honeycomb structure as shown in Figure 1-2b.

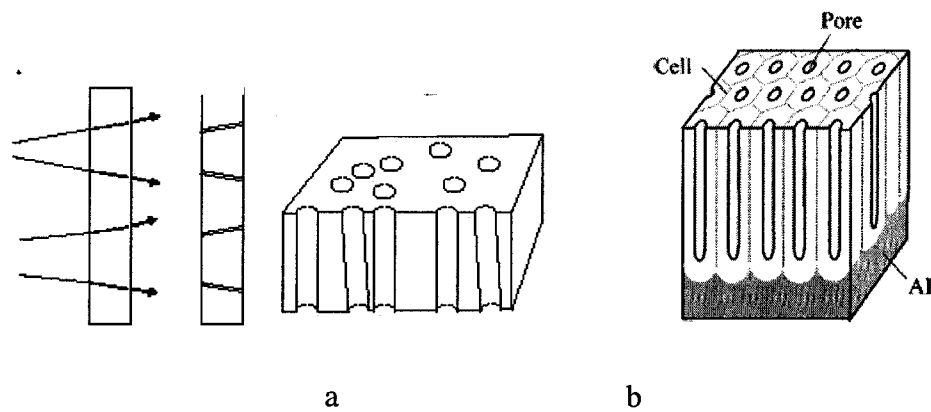


Figure 1-2 Nanoporous membrane [18].

Once nanoporous membrane is prepared, required materials can be filled into nanopores by electrochemical deposition, electroless deposition, chemical vapor deposition, etc.

### *Step-edge template*

Nanoscale surface step edges can be used as templates for nanowire synthesis. This method takes the advantages of the fact that electrochemical deposition usually happens preferably at the step edges rather than smooth surface. Many materials such as metal, metal oxide, and polymer could be selectively deposited onto the step edge to form nanowires. The nanowires could be lifted off from the surface step edge by embedding into polymer film.

### *DNA and polymer template*

DNA and polypeptide molecules are natural template to synthesize nanowires. As DNA and polypeptides molecules can self-recognize complementary parts in other copartner, they are promising for self-assembly of molecular structures and nanoelectronics. Electroless deposition is usually used to synthesize DNA or polymer templated metal nanowires. Metals ions first bind onto the active sites of molecules. When reducing, metals only, or mostly, selectively deposit onto template. As DNA molecules have negative charges on the phosphate groups of their backbones, positively charged nanoparticles could be attracted and attached onto template by electrostatic interaction.

### *Synthesized nanowire template*

A carbon nanotube can be used as template to build metal or semiconductor nanowires. The formed nanowires have diameters of similar or larger than the carbon nanotube. Metal nanostructures with hollow interiors could be also synthesized by first coating nanowire template and then followed by dissolving template.

### 1.2.3 Synthesis in Solvothermal or Wet Chemistry

Synthesis of nanowires in solution is more promising to become a general method in the future as the whole processes are conducted at a relatively low temperature, and diameters of synthesized nanowires could be controlled within several nanometers compared with nanowires grown by vapor-liquid-solid methods. Some synthesis mechanisms in solution are still unclear, but growth of crystalline 1D nanostructures didn't involve exotic nanocrystal of metals as catalyst. The seeds were generated in situ in the solution through a solution-solid phase transition.

## 1.3 Nanowire Assembly

### 1.3.1 Fluid Alignment

Most nanowires were grown in ex-situ conditions, so to build functional devices, it is required to harvest pre-formed nanowire, transfer to specific positions and assembly into hierarchical structures. The methods of random deposition, manipulation by atomic force microscopy (AFM), or micromanipulation are obviously low efficient. Recently nanowire pattern by fluid alignment [16] was reported and used to assemble functional MOS devices and MOS-based sensors. PDMS mold was first defined on the surface where the nanowires were required to be. The suspension of nanowires went through the channels and parallel nanowires patterned by fluid alignment effect. Flow speed determined the angular distribution with respect to the flow, while flow duration controlled the average space between nanowires.

### 1.3.2 Microchannel Networks

For this method microchannel networks were first patterned same as fluid alignment method. However, this strategy was based on the solvent evaporation induced

self-assembly [17]. Nanowires bundles were found to align at the corners of microsize channels. When solution evaporated, the meniscus of media receded into two corners. The solution became concentrated, and nanowires were self-organized into bundles at the places.

## 1.4 Electric-Field Assisted Synthesis and Assembly

### 1.4.1 Synthesis by Electric Field

Electric field was recently used as an efficient method to synthesize and assemble nano or microwires. Both DC and AC field were applied. Most experiments relied upon the aqueous media to carry materials, except nanowire synthesis by field emission, which were produced in gas phase. To our knowledge three kinds of growth mechanisms were reported about direct synthesis of nano or microwires by electric field: dielectrophoresis [19], field emission [20], and bipolar chemistry [21].

Nanosize gold particles could be self-assembled into microwires by dielectrophoresis effect. Dipole moment was induced on the gold particles. Dielectrophoresis force can move particles to the places where electric field strength is the strongest. Once the wires were initiated at one electrodes, gold particles were persistently brought to the tip of wires to sustain the growth until the wires reached the other electrodes. The microwire assembled by this way did not have good mechanical properties and could only exist in liquid condition. The resistivity of wires was three orders of magnitude above the bulk gold.

Field emission was presumed to cause metal nanowire synthesis from organometallic gas. Nanowire growth was started at a sharp tip where field emission was caused to occur by sufficiently high electric field. The emitted electrons dissociated

precursor molecules and charged metal ions were attracted towards tips, which led to continuous growth of a conductive nanowire. Experiments were also done to grow single nanowires at the tips of carbon nanotubes. A DC power source was controlled by feedback to provide a constant current, important to achieve sustained nanowire growth.

Micro or submicro nanowires were grown between two conductive particles separated from external electrodes. The growth process was supposed to be caused by bipolar electrochemistry. When conductive particles stay in a DC electric field, bipolar will be induced. When the overpotential at the surface is high enough, electrochemical reaction will happen on both anode and cathode. On the anode, metal will lose electrons and dissolve into solution. Metal ions move to the cathode by the action of electric field and get electrons there to transform back to metal. The aggregation of metals on the cathode surface will result in the growth of wire structures. The wires formed in this way were not uniform. Size of wires could not be well controlled and diameters of wires were usually in micro scale.

#### 1.4.2 Assembly by Electric Field

Electric field-assisted assembly technique was recently used to assemble preformed nanowires between metal electrodes patterned by lithography on the nonconductive substrate [22]. The electric field has alignment effect on the metal nanowires in solution. The force that caused alignment was the result of polarization in the applied electric field. The nanowires could be assembled along the direction of electric field. They were separated each other between parallel electrodes. Precise position could be achieved by using sharp electrodes which cause a nonuniform electric field.

Single-walled carbon nanotubes could also be aligned along electric field direction during growth initialized by catalyst. By contrast nanotube growth under on electric field exhibited no preferred orientation and they were randomly distributed between parallel electrodes. Both DC and AC electric fields were successfully applied to align carbon nanotubes.

### 1.5 Objective and Methodology

We report the self-assembly of nanowire array and single nanowires of palladium from aqueous solution at pre-defined locations, by application of an electric field [23]. The wires form bridges between electrodes where the electric field is strongest and exhibit good conductance near 300 K. By contrast, the Pd nanowires discussed here are self-assembled at pre-defined locations, but in the absence of a mold.

Here, a saturated aqueous solution of Pd acetate, buffered with 10 mM HEPES, pH 6.5, was diluted 8-fold with ultrapure water and deposited on 5 nm Cr/100 nm Au electrodes patterned by lift-off on a SiO<sub>2</sub> wafer. Nanowire assembly between electrodes was initiated by applying a 10 V<sub>rms</sub>, 300 kHz signal and a 0.8 V DC bias.

## **CHAPTER 2**

### **CONDUCTIVE NANOWIRES**

#### **TEMPLATED BY DNA**

##### 2.1 Fundamentals of DNA Molecule

One-dimensional nanowires are widely recognized as important elements in the development of certain futuristic nanoscale devices. Nanowire-based sensors can be used to detect trace quantities of biomolecules and chemicals in nano-electro-mechanic systems [24-26]. Co, Ni and Fe, and binary nanowires of these elements with giant magneto-resistance, have shown promise for high density storage memory [27-29].

Great effort has been made to develop new strategies for the realization of such tiny one-dimensional structures. Conventional photolithographic fabrication, by contrast, faces increasing difficulties in continuous miniaturization of circuit features due to the wave nature of light. Non-lithographic “bottom-up” nanofabrication has become widely accepted as the successor of lithography because small building blocks can be assembled from even smaller components—nanoparticles, molecules, and atoms. Various nanofabrication methods have been investigated to prepare nanowires, including vapor-liquid-solid growth, laser-assisted catalytic growth, and template-based methods. We have reported a novel non-template-based approach to the assembly of conductive Pd

nanowires from aqueous solution with an applied alternating current field [23]. Figure 2-1 shows the structure of double-stranded DNA.

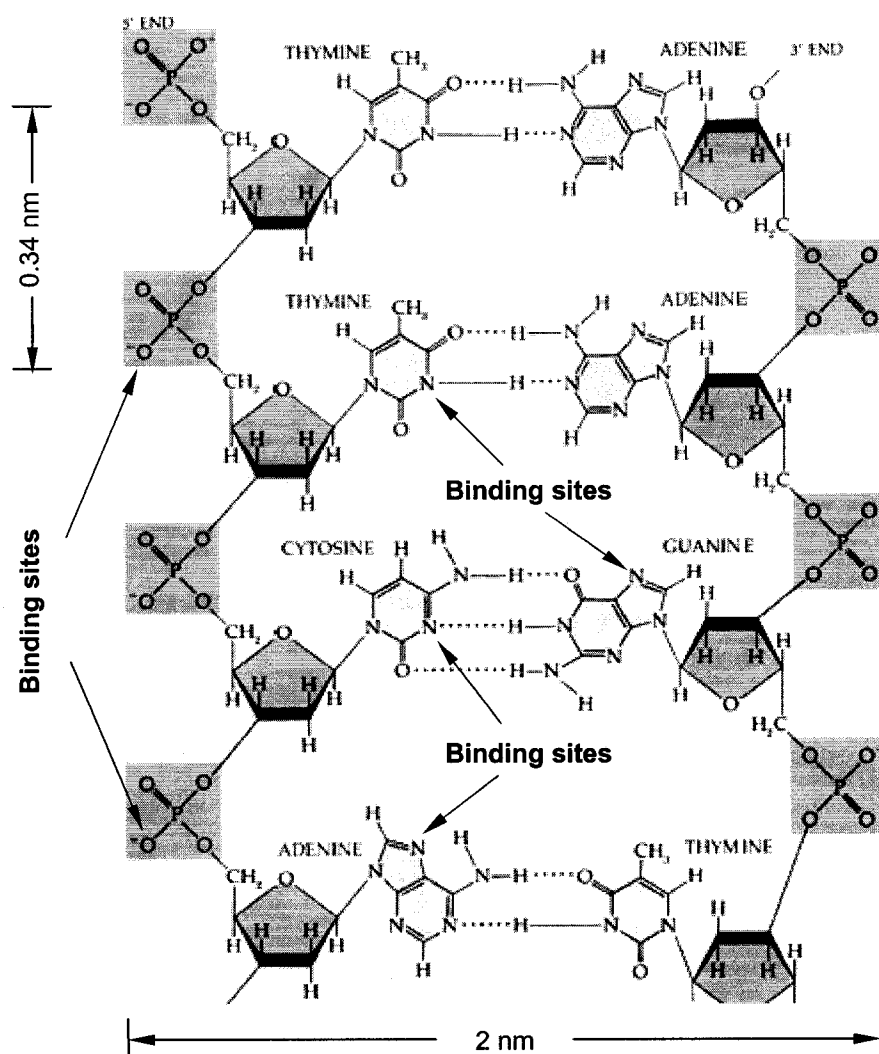


Figure 2-1 Schematic diagram of the structure of double-stranded DNA. Each subunit consists of a phosphate group, a sugar and one of the four bases: adenine (A), thymine (T), guanine (G) or cytosine (C). Molecular recognition by Watson-Crick base pairing means that A pairs with T only, and G pairs with C only. Two classes of binding site for DNA-templated metallic nanowire fabrication are shown: negatively charged phosphate groups in the polymer backbone, and N7 atoms of bases G and A and N3 atoms of bases C and T. Original figure Copyright 1992 Worth Publishers, Inc.

DNA template-based approaches are attractive for the development of 1-D nanostructures. In the mid-1990s, Braun et al. [8] fabricated the first conductive nanowires from Ag nanoparticles and single DNA molecules. Since then, the development of DNA-templated nanowires has progressed rapidly. Metallic nanowires of Pd [9, 30-31], Pt [32-35], Au [36-41], and Cu [42, 43] have been prepared by this approach. Gu et al. have fabricated magnetic Co nanowires, using Pd nanonuclei for selective catalysis of Co deposition on DNA [44]. In addition, DNA templates have been used to assemble materials other than metals, including semiconductors [45-47], conductive polymers and semiconducting polymers [48-50].

The DNA molecule is a natural template for nanofabrication. The linear polynucleotide chain has a width of 2 nm and a length of 0.34 nm per nucleoside subunit (Figure 2-1). A wide range of molecular lengths, from nanometers to microns, can be realized with established technology in molecular biology, for example DNA ligation, enzymatic digestion, and polymerase chain reaction. DNA-templated nanowires could be prepared with an almost unlimited range of aspect ratio. A DNA molecule has two classes of binding site, negatively charged phosphate groups and aromatic bases (Figure 2-1). The polyanionic backbone of the molecule, composed of alternating sugar and phosphate groups, binds metallic cations or cationic nanoparticles by electrostatic interaction. Various transition metal ions bind to the nitrogen atoms of the DNA bases and form metal-DNA complexes by coordination coupling involving unfilled *d* orbitals. For example, the N7 atoms of the bases guanine and adenine form strong complexes with Pt(II) and Pd(II) ions [52-54], and the N3 atoms of the bases thymine and cytosine strongly interact with Pd(II) ions [55]. Both classes of binding site have been utilized in

nanowire fabrication [9, 30-35, 38-39, 42-44]. DNA is uniquely suited to molecular recognition: A pairs specifically with T, and G pairs specifically with C (Figure 2-1). Loweth et al. [56] have used Watson-Crick base pairing to assemble two or three individual Au nanocrystals on specific sites of single-stranded DNA (ssDNA) molecules. DNA-templated metallic nanowires tend to look different from semiconductor nanowires fabricated by a different approach because metal nanoparticle arrays on DNA prepared by wet chemistry lack crystallinity and uniformity [9, 30-44]. As discussed below, the specific molecular recognition capability could be developed to assemble highly uniform nanowires on a ssDNA template. A distinguishing feature of nanoassembly with ssDNA is that the precision of the spatial arrangement of assembled nanostructures can be on the order of a few nanometers.

Control of DNA-templated nanostructures requires the ability to manipulate DNA molecules on a surface prior to further processing. Individual DNA molecules must be separated and stretched to serve as templates for nanowire fabrication. The length of a DNA nanowire will be determined by the stretching process. Table 2-1 summarizes three common methods of DNA stretching. Appropriate “interfacing” of DNA and conductive elements by chemical modification or adjustment of conditions is indispensable to the interconnection of DNA-templated nanowires to devices in a nanoscale electronic circuit. Interconnection can be realized by a number of different approaches to the specific coupling of DNA to a conductive surface. Advanced manipulation of DNA can be important for the precise positioning of templates.

Table 2-1 Stretching and positioning of DNA for nanowire fabrication

Method	Surface	Chemical Modification	Variables	References
Molecular combing	hydrophobic, hydrophilic	not required	hydrophobicity, meniscus	(4, 30-31, 36-37, 40, 42-44), 57-63
Electrophoretic stretching	Au, Al, beads	thiol, biotinylation	field strength, frequency	64-72
Hydrodynamic Stretching	Au, beads, mica	thiol, biotinylation	velocity, viscosity	(3, 32, 41), 73-77

## 2.2 DNA Stretching and Positioning

At equilibrium, a DNA molecule in aqueous solution will usually be randomly structured as a result of thermal fluctuations. Entropy will shorten the end-to-end distance, often to a much smaller size than the contour lengths. A DNA molecule therefore must be stretched to serve as a nanowire template. Many approaches have been used to stretch and align DNA molecules, including molecular combing [57-63], electrophoretic stretching [64-72], hydrodynamic stretching [73-77], and van der Waals interaction [78]. A common strategy is to tether one end to a surface and then to stretch the molecule by an external force, for example, surface tension. Details of the mechanics of stretching are complex and beyond the scope of this review. The focus here is on principles and practical aspects of DNA stretching and metallization.

Molecular combing is the simplest method of stretching DNA templates in nanowire fabrication and thus the most widely used one (Table 2-1). No chemical

modification of DNA molecules is required. Combing can be performed on various hydrophobic or hydrophilic surfaces. Combed DNA molecules can be well dispersed and strongly bound to the substrate, a situation favorable for subsequent metallization and characterization of nanowires. Both direct current (DC) and alternating current (AC) electric fields can be used to stretch DNA. An advantage of the electrophoretic approach is that nanowire templates can be stretched and positioned directly between electrodes. After metallization, electrical properties of nanowires between two electrodes can readily be characterized. DNA must be modified by thiolation or biotinylation to be stretched by a DC field. Otherwise, optical tweezers must be used to tether one end of a DNA molecule before stretching. DNA to be stretched by dielectrophoresis does not require chemical modification. Spin stretching is a simplified hydrodynamic stretching without the requirement of chemical modification of DNA. Molecules stretched by this method have been used in nanowire fabrication (Table 2-1). Similar to stretching by a DC field, conventional hydrodynamic stretching requires chemical modification.

### 2.2.1 Molecular Combing

Molecular combing was first described by Bensimon et al. [57]. Individual DNA molecules or bundles of molecules are stretched by a receding meniscus between the substrate and coverslip (Figure 2-2). DNA solution is deposited on silanized glass and covered. A terminus reacts with surface vinyl groups, anchoring the molecules on the substrate. Surface tension, which acts parallel to the meniscus, extends DNA during movement, because this force is greater than the entropic force but smaller than the force needed to break covalent bonds. Figure 2-2 shows bacteriophage  $\lambda$  DNA molecules

(48.5 kb,  $\sim 16 \mu\text{m}$ ) stretched by molecular combing. The average end-to-end distance is  $\sim 21 \mu\text{m}$ , 131 % of the crystallographic length.

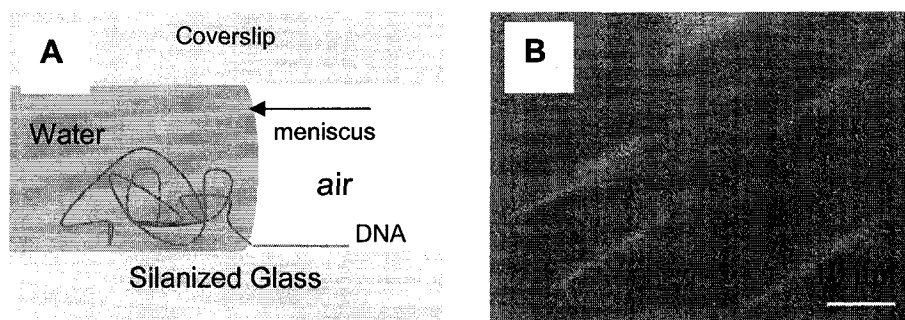


Figure 2-2 Molecular combing. A) Schematic diagram of the mechanism. Redrawn from ref. 59. The distance between the coverslip and substrate is typically on the order of microns, depending on droplet volume, coverslip mass, surface properties, and so on. The meniscus generates a surface tension during evaporation which stretches DNA. B) Fluorescence micrograph of bacteriophage  $\lambda$  DNA stained with the fluorescent dye YOYO-1 (Molecular Probes, Inc., USA) and combed on silanized glass. The average length of stretched molecules is  $\sim 21 \mu\text{m}$ . The scale bar represents  $10 \mu\text{m}$ .

In later work, Bensimon et al. [58] found that the end-to-end distance of combed bacteriophage  $\lambda$  DNA molecules depended on the character of the substrate surface. On a silanized hydrophobic surface, the length was  $21\text{-}24 \mu\text{m}$ , but on an anti-dioxigenin hydrophilic surface it was  $16\text{-}18 \mu\text{m}$ . The estimated extension force was  $\sim 160 \text{ pN}$  on silanized glass and  $\sim 54 \text{ pN}$  on anti-dioxigenin-coated glass, in both cases greater than the entropic force. Various surfaces, for example polystyrene, polymethylmethacrylate, and polylysine, have been shown suitable for molecular combing [59]. The effectiveness of combing on a hydrophobic surface is highest near pH 5.5.

Yokota et al. [60] improved the basic idea of molecular combing through mechanical control of meniscus movement after deposition of DNA solution on a silanized substrate. A coverslip is attached to a motor-driven droplet-spreading apparatus that drags the coverslip across the substrate at a certain rate, for example  $3 \text{ cm/min}$ .

Surface tension coupled to controlled movement of the meniscus stretches DNA molecules with high uniformity. Deposition of non-target blocking DNA on the substrate prior to combing compensates for variation in affinity between target DNA molecules and the surface. Addition of a small amount of  $\text{MgCl}_2$  to the solution increases the number of stretched molecules on the substrate;  $\text{Mg}^{2+}$  binds to the sugar-phosphate backbone of DNA. Otake et al. [61] have stretched DNA by moving the substrate instead of the coverslip, with the substrate mounted on a computer-controlled microscope stage. DNA droplets are dispensed on silanized glass through the capillary tip of a microinjector. Relative displacement between capillary tip and substrate controls movement of the meniscus. The shear force generated at a displacement rate of 15 cm/min was found to stretch bacteriophage  $\lambda$  DNA to  $\sim 21 \mu\text{m}$ . An advantage of this method is that DNA molecules can be precisely localized on the substrate and visualized after combing.

Molecular combing can also be achieved by dipping a silanized coverslip into DNA solution [62]. Termini of DNA molecules bind spontaneously to the substrate. After 5 minutes of incubation, the coverslip is removed from solution at a constant speed of  $300 \mu\text{m/s}$ . The meniscus exerts a constant force on DNA molecules and aligns them. The long molecules become oriented in a single direction over the entire coverslip. For preparation of templates for nanowire fabrication, the length distribution can be narrowed by moving the meniscus at a steady speed to generate a constant extension force on the molecules.

A large surface tension in molecular combing, often  $>65 \text{ pN}$  on a hydrophobic surface, can extend DNA molecules 30-50 % above the contour length. This is called

“overstretching”. Gueroui et al. [63] reduced the surface tension by coating a layer of 1-dodecanol on PMMA or 7-octenyltrichlorosilane substrates. Without 1-dodecanol treatment, the mean end-to-end distance of combed T7 DNA (38 kb) on the hydrophobic surfaces was 19.5  $\mu\text{m}$ , ~50 % longer than its crystallographic length. The average length was only 13  $\mu\text{m}$  on the dodecanol-coated surface, close to the contour length.

### 2.2.2 Electrophoretic Stretching

#### *DC Electrophoretic Stretching*

Gel electrophoresis is widely used in molecular biology to separate DNA fragments by length. Application of a uniform electric field causes polyanionic chains to migrate toward the anode. The same principle is used to stretch DNA in a DC field [64-66]. DNA molecules tethered at one end in solution are stretched by an applied electrophoretic force. Tethering is accomplished in a variety of ways. For example, a terminus of a DNA molecule can be bound to a bead trapped by optical tweezers or immobilized to a solid support by chemical coupling.

Schurr et al. [64] and Smith et al. [65] have studied the relationship of DNA extension to external electric field strength by assuming that DNA molecules are uniform polyionic chains. Plasmid DNA (66 kb) and bacteriophage  $\lambda$  DNA (48.5 kb) were immobilized in agarose gel. Both molecules behaved like entropic springs and became fully extended in a low electric field. In the absence of an electric field,  $\lambda$  DNA molecules are random coils and the average end-to-end distance is only ~1.47  $\mu\text{m}$ . Stretching DNA in agarose gel may not be useful in preparation of nanowire templates. Zimmermann et al. have developed a method to stretch DNA by “free electrophoresis” (without a gel) [66]. A gold surface was coated by a layer of biotin thiol.  $\lambda$  DNA

biotinylated at one end was bound to the substrate by way of streptavidin-labeled beads. DNA thus tethered was stretched in a 5 V/cm DC field. The non-covalent bonds of the Au-biotin-streptavidin-biotin-DNA construct held fast and allowed concatemers of  $\lambda$  DNA molecules (~200 kb) to be stretched to full length.

#### *Dielectrophoretic Stretching*

Dielectrophoresis (DEP) is a non-uniform field effect. It aligns dipolar objects parallel to the direction of electric field. A DNA molecule is polarizable because its polyanionic backbone is surrounded by a cloud of counterions at equilibrium. When the frequency and field strength are high, the applied electric field stretches polarized DNA molecules to their full length by dielectrophoresis. The molecules become oriented parallel to the field in the process and migrate, by dielectrophoresis not fluid flow. If the electrode is made of electrochemically active metal such as aluminum, the DNA end in contact with the electrode can become permanently anchored.

Washizu et al. [67-69] have studied effects of DEP on DNA. In a 1 MHz and  $>1 \times 10^6$  V/m field, bacteriophage  $\lambda$  DNA was stretched and positioned between two electrodes. Termini of the DNA molecules became tightly bound to the electrodes. In some cases, however, one end only of DNA becomes bound to an electrode, and an applied field generates thermal hydrodynamic flow and fluctuation of liquid near the electrodes, decreasing reproducibility. Floating-potential electrodes (FPEs) have been designed to reduce thermal fluctuations (Figure 2-3A). The potential is not applied to the floating electrodes, reducing thermal flow near them. The two outer electrodes (Figure 2-3A) generate a dielectrophoretic force that influences DNA structures. This approach was

found to increase the number of stretched and positioned DNA molecules. Figure 2-3B shows bacteriophage  $\lambda$  DNA molecules stretched between and positioned on electrodes.

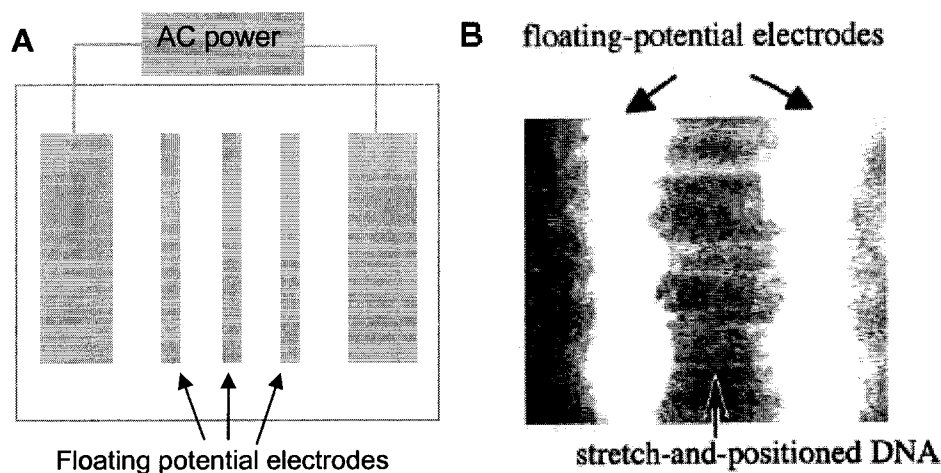


Figure 2-3 Stretching of DNA with floating potential electrodes with a gap of 15  $\mu\text{m}$ . A) Schematic diagram of the electrodes. Redrawn from ref. 69. B)  $\lambda$  DNA molecules stretched and positioned between floating potential electrodes. DNA was stained with a fluorescent dye, Yo-Pro-1 (Molecular Probes Inc., USA). The image was taken with a fluorescence microscope. Copyright 2000 IEEE.

DEP has been used by Namasivayam et al. [70] to stretch DNA in a polymer-enhanced medium, 3.75 wt % polyacrylamide in Tris-HCl buffer.  $\lambda$  DNA (48.5 kb) was elongated to 21  $\mu\text{m}$  in this medium, in a 1 MHz and  $3 \times 10^5$  V/cm field. Germishuizen et al. [71] have studied effects of DEP on the stretching of DNA immobilized on a gold surface. A 300-500 kHz AC field was found to achieve extension of  $\lambda$  DNA up to 15  $\mu\text{m}$ , but the molecules did not become fully elongated. Stretching of bacteriophage T4 DNA (165.6 kb) in agarose gel has been studied by Kaji et al. [72] in a low frequency and low field strength AC field. They found that optimal conditions for stretching were 10 Hz and 200 V/m in 1% agarose.

### 2.2.3 Hydrodynamic Stretching

Another widely used method is to stretch DNA by hydrodynamic flow. DNA tethered at one end is stretched by the shear force generated by the momentum gradient between applied flow and DNA chain. Aligned molecules are oriented in the direction of flow. The end-to-end distance of extended DNA depends mainly on the velocity of flow and viscosity.

Perkins et al. [73, 74] have investigated extension and relaxation of DNA in applied steady flow. Figure 2-4A shows a schematic diagram of the apparatus. One end of a DNA molecule is attached to a 1  $\mu\text{m}$  bead trapped by optical tweezers. A drag force is provided by constant hydrodynamic flow. DNA molecules are stretched by a flow of 2  $\mu\text{m/s}$  or greater (Figure 2-4B). The fractional extension is related to the viscosity, velocity, and contour length by a power law, consistent with the worm-like chain model for DNA extension under an applied force. The same authors have also studied relaxation of fully extended DNA. Immediately after cessation of flow, free ends of DNA recoil rapidly and visual length decreases by 30% within a few seconds. Relaxation is slower thereafter. For example, a 39.1  $\mu\text{m}$ -long DNA molecule recoiled to  $\sim 6 \mu\text{m}$  during the initial 50 seconds of relaxation. At the end of relaxation, some molecules appeared as  $\sim 1 \mu\text{m}$  diameter compact balls. Smith et al. [75] have studied the mechanics of single DNA molecules. Force-measuring laser tweezers were used to stretch  $\lambda$  DNA to its contour length by a  $\sim 10$  pN force. A  $\sim 65$  pN force extended DNA to  $\sim 170\%$  of its contour length. The structure of B-DNA is altered by overstretching.

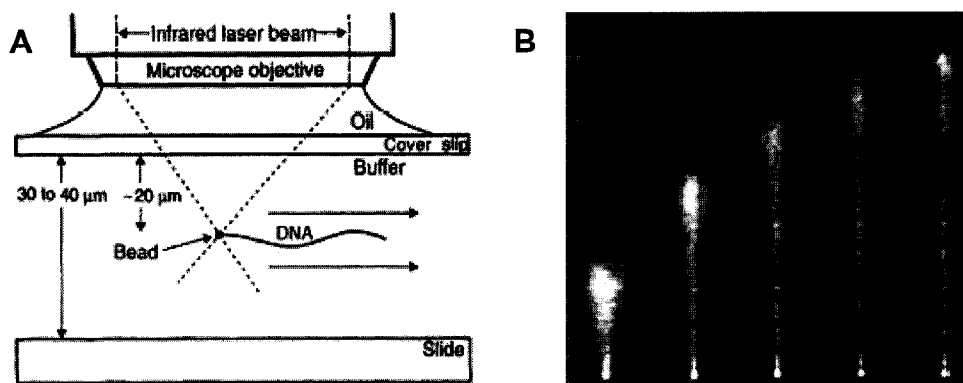


Figure 2-4 Stretching DNA by hydrodynamic flow. A) Schematic diagram of apparatus. Reprinted with permission from ref. 73. Copyright 1994 American Association for the Advancement of Science. B) Time-averaged fluorescence micrograph of a DNA molecule ( $67.2 \mu\text{m}$ ) stretched in a  $0.95 \text{ cP}$  fluid flow with a velocity of 2, 4, 6, 8 or  $10 \mu\text{m/s}$ . The ratio of extended length to the contour length was 19, 33, 44, 50 and 55% (left to right). Copyright 1995 American Association for the Advancement of Science.

Spin stretching is a simple and effective method of aligning DNA [76, 77].

Viscous force generated by rotational flow extends the polymer. DNA molecules on silanized glass spun at 3000-5000 rpm become aligned and stretched. At the periphery of the DNA solution, molecules are more extended than those near the center. The higher linear speed at the periphery leads to a higher viscous force on the DNA molecules and a greater end-to-end distance after stretching.

#### 2.2.4 DNA Positioning

Reliable preparation of the interface between a nanowire and a specific surface is crucial for the development of nanoscale electronic devices. Nanowires could be interconnected to circuit elements by the sort of DNA-surface coupling used in DNA stretching. Two conventional coupling mechanisms, Au-thiol and biotin-streptavidin, play an important role in positioning single DNA molecules on a specific surface.

Figure 2-5 shows two  $\lambda$  DNA molecules stretched and positioned between two Au electrodes. The electrode gap is 16  $\mu\text{m}$ , and the molecules are immobilized by Au-thiol coupling. The sticky ends of  $\lambda$  DNA are ligated to two thiol-capped oligonucleotides, each of which is bound to an Au electrode. After one end of DNA was immobilized to one electrode, a flow of 50-100  $\mu\text{m/s}$  was applied. The other end of stretched DNA molecules became bound to the other electrode by Au-thiol coupling. (By Dr. Qun Gu, 2005)

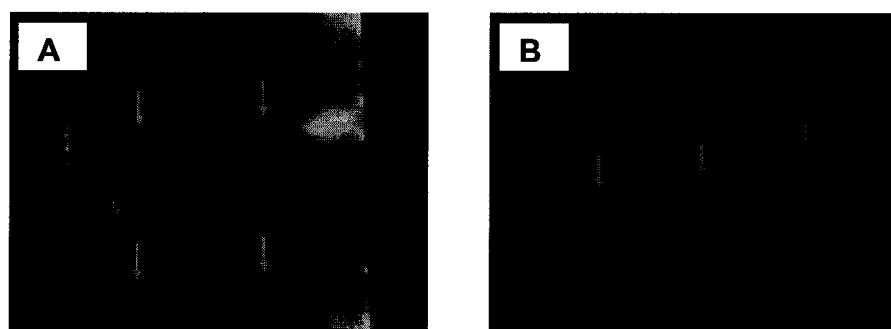


Figure 2-5 Visualization by fluorescence microscopy of stretched DNA molecules between Au electrodes. A) Middle of parallel electrodes. B) End of parallel electrodes. The gap size is  $\sim 16 \mu\text{m}$ . DNA is stained with YOYO-1. Arrows stretched DNA molecules. (By Dr. Qun Gu, 2005)

A major difficulty in the development of nanowires in electronics is precise and reproducible positioning of structures on a 2-D substrate. A key advantage of DNA-based assembly over other assembly methods is the unique molecular recognition properties of DNA. Mbindyo et al. [79] have positioned oligonucleotide-modified Au nanowires on a 2-D substrate coated with complementary oligonucleotides. After hybridization, only nanowires capped with oligonucleotides were positioned on the surface. “Self-wiring” could possibly be achieved in electronics by DNA-based molecular recognition.

### 2.3 DNA Metallization

Unmodified DNA has a low conductivity, limiting its usefulness for electronics [80, 81]. DNA, however, can be metallized by virtue of its electrostatic properties. Braun et al. [8] have used silver nanoparticles for this purpose. Conductivity was enhanced. Ag ions bind to DNA by Ag-Na ion exchange. Hydroquinone can reduce DNA-bound Ag ions to Ag(0) metallic clusters, which then autocatalyze further reduction of Ag ions from solution. DNA stretching and positioning were achieved by hydrodynamic flow and Au-thiol coupling. Figure 2-6 shows a prepared Ag nanowire between two Au electrodes. The diameter is  $\sim 100$  nm. The resistivity,  $3.4 \times 10^{-3} \Omega\text{-m}$ , is higher than that of bulk silver. Nevertheless, the method has become the prototype for metallization of single DNA molecules.

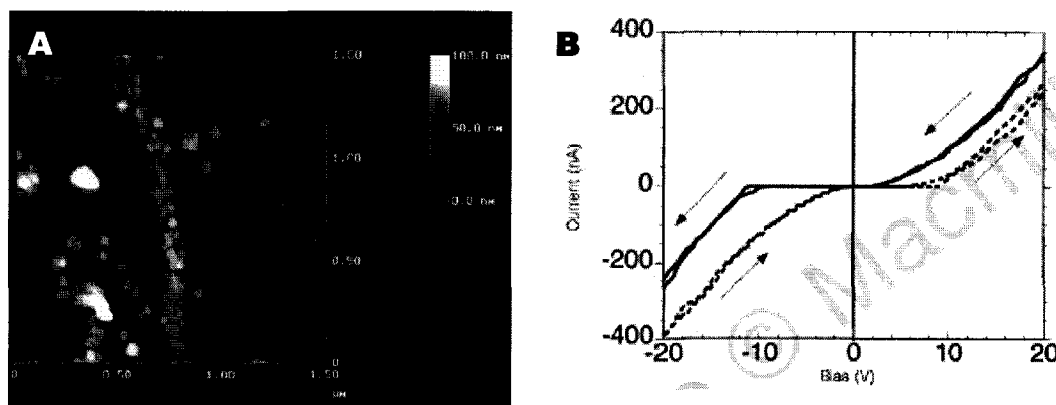


Figure 2-6 Characterization of metallized DNA. A) Atomic force microscope image of a 100 nm wide Ag nanowire using DNA-templated assembly. B) I-V characteristics of the nanowire. Copyright 1998 Macmillan Publishers Ltd.

DNA-templated assembly has led to great progress in nanowire fabrication in the past few years. A variety of metallic nanowires made in this way have been reported: Pd, Pt, Au, Cu, and Co. Fabrication is based on principles of electroless plating, a mature technology widely used in industry to make metallic films. During the step known as

DNA “activation”, metallic cations bind to bases or phosphate groups of the DNA molecule. Pd(II) and Pt(II), for example, bind to nitrogenous bases of B-DNA, mainly on the N7 sites of purines [9, 30-35]; Cu(II) binds to polyanionic backbones of DNA by the electrostatic interaction [42-43]. Activated metal-DNA complexes are then reduced by a chemical agent, resulting in one-dimensional metallic clusters on DNA, normally 1-7 nm in diameter. The clusters act as nucleation centers to catalyze metallic growth of continuous nanowires.

Richter et al. [9, 30] have used bacteriophage  $\lambda$  DNA as a template to fabricate conductive nanowires of Pd. The wires had an average diameter of 50 nm and an estimated conductivity of  $2 \times 10^4 \text{ S cm}^{-1}$ , only 10-fold smaller than bulk Pd. During activation, Pd(II) ions became bound to bases of DNA. Dimethylamine borane, a common reducing agent, reduced DNA-bound Pd(II) to clusters with a diameter of 2–4 nm. A second treatment with Pd plating bath led to continuous nanowires, catalyzed by pre-formed Pd nuclei. In recent work [31], the same authors measured the temperature-dependent resistance of ~60 nm diameter Pd nanowires that were pinned between two electrodes with a space of 5  $\mu\text{m}$  (Figure 2-7A). Interesting electrical properties were found. At temperatures above 30 K, the Pd nanowires displayed ohmic behavior and resistance decreased linearly with decreasing temperature. Below 30 K, resistance increased with decreasing temperature (Figure 2-7B). Such behavior differs from that of most bulk metals. The authors ascribed the phenomenon to quantum effects. Increased resistance at low temperature may result from weak localization and electron-electron interaction in the nanoscale materials [82-84]. Annealing of Pd nanowires was found to

improve conductivity by reducing structural disorder. A 9-10 fold decrease in resistance was found after heating at 200 °C.

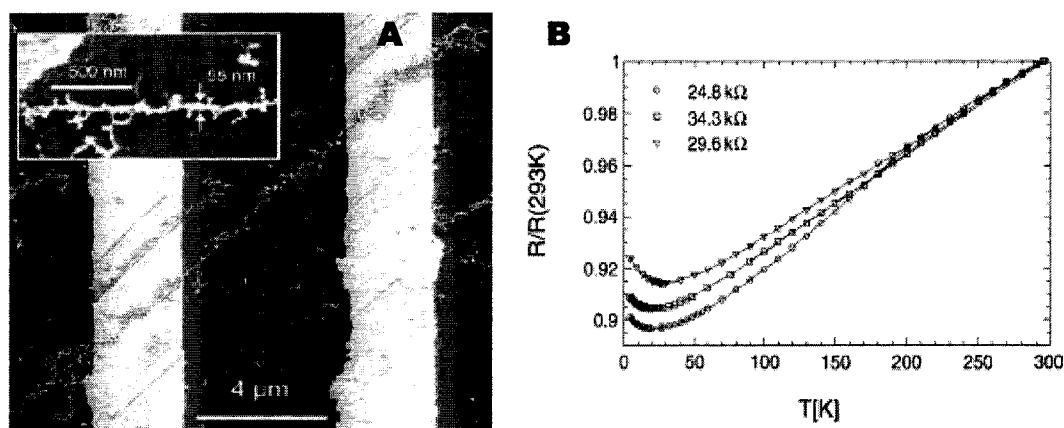


Figure 2-7 Characterization of Pd nanowires. A) Scanning electron micrograph of a ~60 nm-wide Pd nanowire. The measured resistance was 34.3 k $\Omega$ . B) Temperature dependent resistance of three Pd wires. Copyright 2002 Springer-Verlag.

Catalytic metal nanoclusters can not only initiate deposition of the same type of metal, but also catalyze growth of a second type of metal. This is so-called heterogeneous nucleation and growth. Ford et al. [32] have used this approach to metallize DNA with Au. Pt(II)-activated DNA was reduced by sodium borohydride, and ~1 nm Pt nanoclusters were found on the template. Electroless plating with Au resulted in 4-6 nm Au nanoparticles being deposited on the DNA template. Recently, we have reported the assembly of Co nanowires on DNA by heterogeneous nucleation and growth [44]. Pd nanoclusters were used to catalyze growth of Co nanowires of average diameter 10-20 nm. Reaction of Pd(II):DNA with Co reducing bath was monitored by spectrophotometry (Figure 2-8A). A shoulder is evident at 260 nm in the spectra of activated DNA taken at early time points, indicating that reduced Pd and Co nanoclusters had not yet fully coated DNA. The shoulder is barely visible at later time points. Adsorption of Pd(0) and Co(0) onto DNA alters spectral properties of the macromolecule. The inset shows the

spectrophotometric signal at 515 nm as a function of reaction time. 10 min post-mixing, the Co(II) signature peak is noticeably decreased, implying that cations are being deposited from solution onto DNA. 40 min later, the Co(II) ions were almost completely reduced to Co(0) from catalysis by Pd(0), as the peak at 515 nm has nearly disappeared. Figure 2-8B shows an AFM image of a single Co nanowire of height  $\sim 14$  nm.

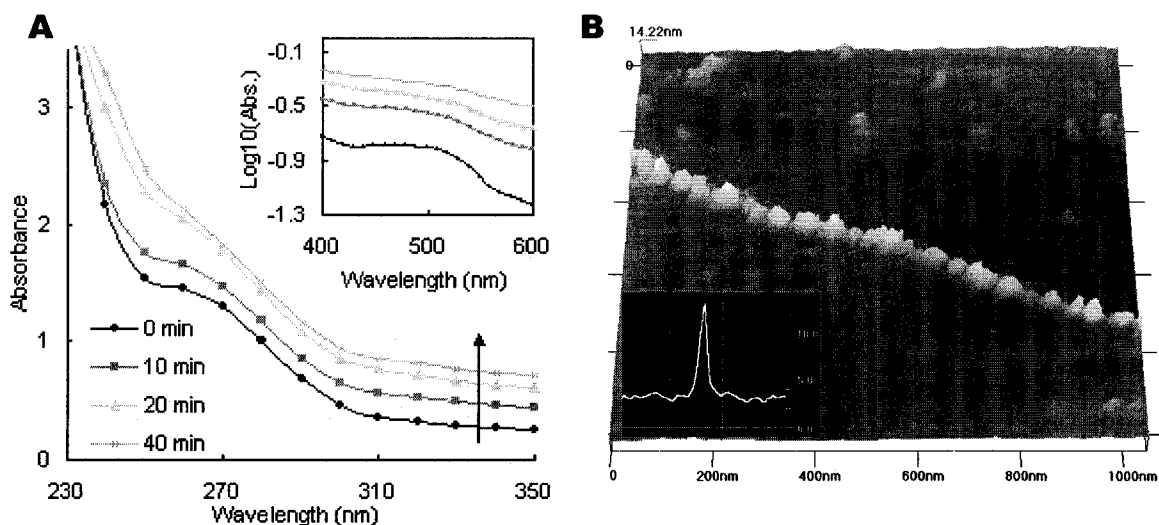


Figure 2-8 Co nanowire fabrication and characterization. A) UV-vis spectrum of Pd(II)-activated DNA in Co plating bath as a function of time. Spectra were taken at 0 min, 10 min, 20 min, and 40 min. The inset shows a magnified view of the spectra in the 400-600 nm range. B) AFM image of a Co nanowire. The height scale is  $\sim 14$  nm. Copyright 2005 Institute of Physics Publishing.

Activation of DNA is a critical step in DNA nanowire assembly. How metal ions bind to DNA will determine the coverage of metal deposits on templates and heterogeneity of the resulting nanowires. Seidel et al. [33] have investigated effects of the activation process on the heterogeneity of prepared nanowires. They found that DNA was not metallized by Pt(0) without prior activation by Pt(II). By contrast, DNA activated with Pt(II) at 37 °C for 16 h was uniformly metallized by 3-5 nm Pt(0). Mertig et al. [34] have used first-principles molecular dynamics to simulate effects of activation on

clustering of Pt(0) on a DNA substrate. Pt(II)-DNA adducts prepared in the activation process could control the structure and heterogeneity of Pt(0) clusters on DNA after chemical reduction. A long activation time was required to deposit Pt(0) nanoparticles that are able to initiate growth of nanowires with high coverage and heterogeneity. This was confirmed by Seidel et al. [35] in an extensive study on the synthesis of Pt nanocluster chains on DNA templates. The authors have suggested that Pt metallization of DNA obeys the so-called “DNA-controlled” mechanism. Electronic affinity of Pt(II)-DNA complexes are greater than Pt(II) ions in solution due to the heterocyclic bases of DNA, favoring nucleation on DNA templates. Pt(II)-DNA is reduced to Pt(I)-DNA or Pt(0)-DNA in an early stage of the reaction. Then Pt(II) ions in solution diffuse to Pt(I)-DNA and form Pt(I)-Pt(II) dimers, limiting reduction of Pt(II) ions in solution. This explains the favorable growth of metallic nanoclusters on the templates.

Complete confinement of growth of metallic particles on templates, however, is difficult when fabricating nanowires in aqueous solution. Inevitably, metallic ions are reduced in solution and become randomly deposited on the substrate. This leads to low nanowire heterogeneity, despite favorable growth on the templates by the “DNA-controlled” mechanism. Typically low heterogeneity nanowires show irregular branching and necklace structures. Keren et al. [36] have developed a new scheme of metallization to help overcome this difficulty. Aldehyde bound to DNA by a Michael-type addition functions as a reducing agent for Ag(I). Reduced Ag(0) clusters deposit predominantly on the template where the reducing agent is localized before metallization. Figure 2-9B shows Ag nuclei on DNA prepared by this approach. Au nanowires with low background were grown by catalysis during a subsequent electroless plating step (Figure 2-9D).

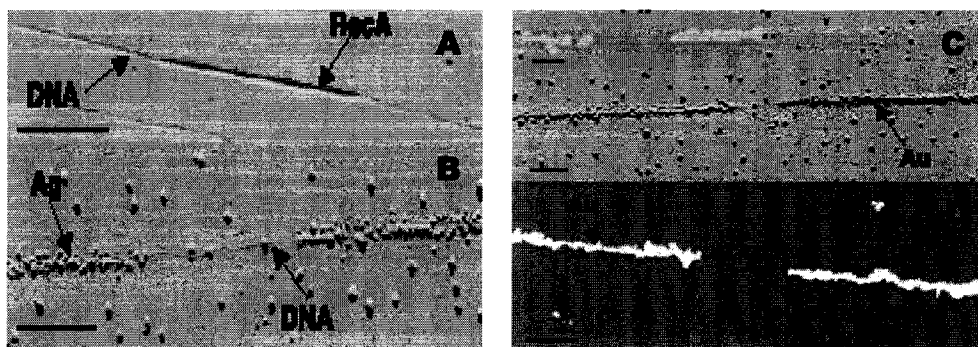


Figure 2-9 Molecular lithography. A) AFM image of RecA filament bound to  $\lambda$  DNA. B) AFM image of the sample after reduction. C) AFM image of the sample after Au plating. D) SEM image of Au nanowires. The gaps in B-D show that the regions of DNA protected by RecA were not metallized. Scale bars: 0.5  $\mu\text{m}$ ; 0.25  $\mu\text{m}$  in inset of C. Copyright 2002 American Association for the Advancement of Science.

Highly compact nanocircuits will require the precise patterning and interconnection of wires at the molecular level. A single nanowire can be patterned by molecular recognition of DNA by protein—a type of “molecular lithography”. In a recombination reaction, RecA nucleoprotein filament binds to segments of aldehyde-derivatized DNA at specific nucleotide sequences (Figure 2-9A). RecA (2027 bases,  $\sim 678$  nm) then prevents the Ag(0) deposition that occurs elsewhere on aldehyde-derivatized DNA. As a result, a 678 nm-long insulating gap is formed on a single nanowire after Au metallization (Figure 2-9C, D).

Molecular lithography has been improved by standard tools of molecular biology: restriction digestion and DNA ligation [37]. Restriction enzymes and ligase act on aldehyde-derivatized DNA as effectively as unmodified DNA. A 2054 bp ( $\sim 700$  nm) fragment of DNA treated with aldehyde, and a 1106 bp ( $\sim 350$  nm) fragment not treated with aldehyde were digested by *Hga I* and then ligated. This yielded DNA fragments with alternating aldehyde-derivatized and non-aldehyde-derivatized parts (Figure 2-10A,

B). The fragments were then metallized with Ag. Prepared Ag structures were isolated by 350 nm gaps because the non-aldehyde-derivatized parts did not become metallized (Figure 2-10C).

Localization of a reducing agent on templates may enhance heterogeneity of metallized DNA. Bereril et al. [43] have reported a method to reduce background called “ionic surface masking”.  $K^+$  or  $Cs^+$  ions bind to  $SiO_2$ . The resulting cationic surface provides a physical and electrostatic barrier to adsorption of  $Ag(I)$  and  $Cu(II)$  during activation. Ag and Cu nanowires can then be assembled on the surface. A 51% decrease in non-specifically deposited Ag nanoparticles was found by this approach, and a 74% decrease in non-specifically deposited Cu nanoparticles.

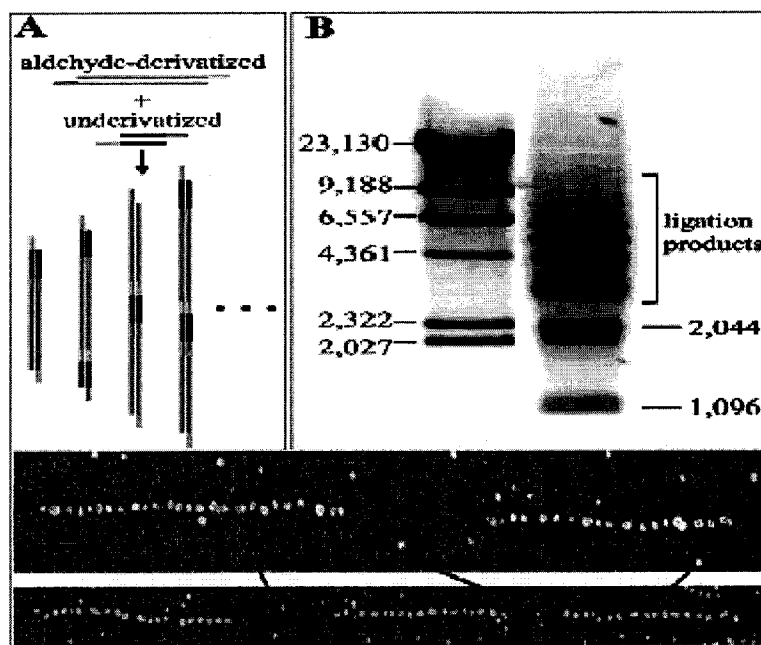


Figure 2-10 Molecular biology meets nanotechnology. A) Ligation of aldehyde-derivatized DNA fragments (2054 bp) and underivatized fragments (1106 bp). B) Gel electrophoresis of ligated fragments. Left lane is a  $\lambda$ -Hind III digest. C) SEM micrograph of  $Ag(0)$  deposited on ligated fragments. Upper panel: Two 700 nm Ag clusters are separated by a 350 nm gap. Low panel: Three 700 nm Ag clusters are separated by two 350 nm gaps. Scale bar: 330 nm. Copyright 2004 American Chemical Society.

Another method to enhance heterogeneity and decrease background is to localize nuclei on DNA templates [44]. This way, random deposition is limited because the reducing agent does not react with Co ions without catalysis of previously-reduced Pd(0) nuclei bound to DNA. In most reports, metal ions in solution or bound to DNA are reduced during metallization. Ideally, the reducing agent would react with catalytic metal ions only, when localized on a DNA template only, and target metal ions would be reduced on the surface of catalytic nuclei only.

Nucleation and growth of metal clusters on DNA is the main approach to DNA nanowire assembly. DNA-directed assembly of nanoparticles, however, has also received a good deal of attention. Kumar et al. [38] and Sastry et al. [39], for example, have reported that linear arrays of lysine-capped colloidal Au (~4 nm) can be assembled on DNA by electrostatic interaction between the polyanionic DNA backbone and positively charged Au nanoparticles. Patolsky et al. [40] have developed an approach to nanowire assembly in which nanoparticles bind directly to DNA bases. 1.4 nm Au particles labeled with amino psoralen are intercalated into a poly-A and poly-T DNA duplex by a photochemical reaction. UV irradiation catalyzes covalent binding of amino psoralen to bases of DNA. ~4 nm high Au nanowires can be assembled by this approach. Harnack et al. [41] have shown that a nanowire can be fabricated from DNA by separate nucleation and growth. 1-2 nm trisphosphine-labeled Au particles bind densely to DNA as catalytic seeds. Then Au electroless plating is used to grow the nanowire. The resulting nanowires are 30-40 nm wide and show ohmic behavior with a conductivity ~1/1000 of bulk Au.

Quake et al. [85] have shown that DNA can be metallized in a dry environment. Evaporated Au is directly deposited on a DNA molecule bridged between electrodes. The average width of the resulting Au-clad DNA is ~10 nm. A similar non-chemical approach to metallization of DNA was recently proposed by Hopkins et al. [86].  $\text{Mo}_{21}\text{Ge}_{79}$  nanowires ~10 nm in diameter were fabricated by sputtering materials onto two single DNA molecules, suspended across a ~100 nm wide trench. The resulting superconducting wires could be useful in the development of quantum interference devices.

## 2.4 Electrode Fabrication

### 2.4.1 LOR Photoresist Lift-Off

Metal electrodes designed for this study were patterned by lift-off: 5 nm Cr and 40 nm Au on a silicon dioxide wafer. Lift-off lithography is the critical process to get the correct electrode pattern. For the best lift-off an obvious undercut is required below photoresist. In the initial experiments we use chlorobenzene to soak photoresist-coated wafer before development and after exposure. Development speed of exposed areas and underpart of unexposed areas is much fast than that of surface of unexposed areas, so undercut pattern will form. However, chlorobenzene is toxic and chlorobenzene process can be easily spoiled by even little contamination. This lift-off process is not closed. LOR process (Figure 2-11) was applied in the experiments.

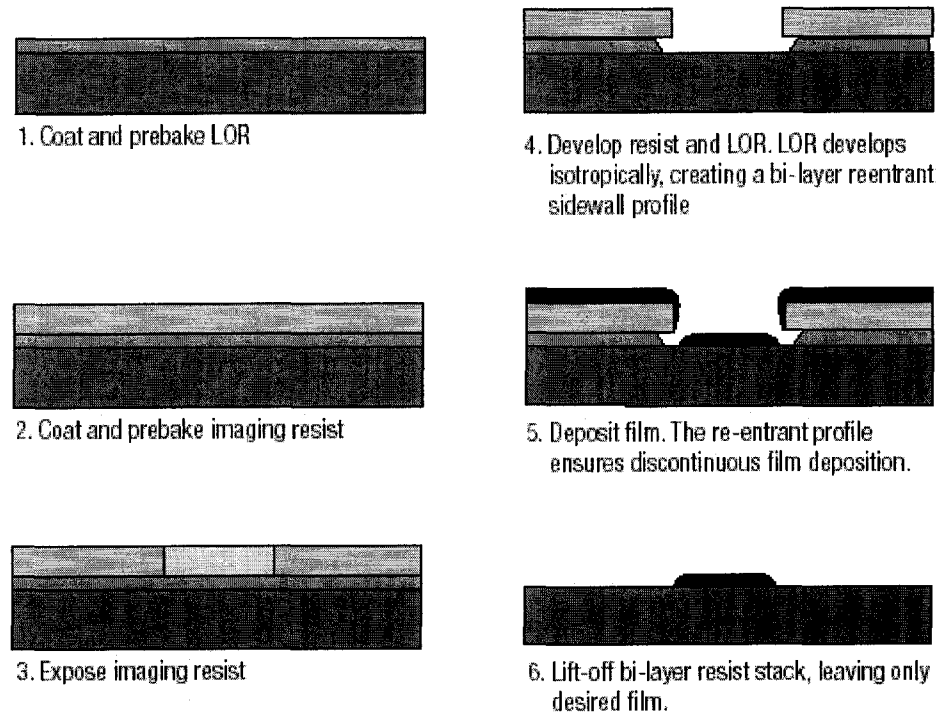


Figure 2-11 LOR photoresist process. (From [www.microchem.com](http://www.microchem.com))

LOR photoresist lift-off is a simple bi-layer processing without extra flood exposure, develop, or toxic chemical soak steps, and can reach submicron linewidth control.

#### 2.4.2 Process of LOR Photoresist Lift-Off

Following process is optimized for fabrication of  $2\ \mu\text{m}$  linewidth pattern.

- (1) Clean wafer with acetone and water.
- (2) Prebake the wafer 30 min at the temperature of  $250\ ^\circ\text{C}$ .
- (3) LOR spin coating with parameters as in Table 2-2.

Table 2-2 Recommended LOR spin coating parameters

Process Step	Process Parameters
Dispense time	4 seconds
Dispense spin speed	400 rpm
Acceleration	10.000 rpm/second
Terminal spin speed	3,000 rpm
Spin time	45 seconds

- (4) LOR bake 5 min at the temperature of 190 °C.
- (5) PR 1813 spin coating.
- (6) Soft bake 60 s at the temperature of 115 °C.
- (7) Expose with UV light 8 s, soft contact mode.
- (8) Develop with MF-319 20 s.
- (9) Rinse with DI water immediately.
- (10) E-beam or sputter Cr and 40 nm Au.
- (11) Lift off with acetone in ultrasonic bath for 10 min.

Undercut pattern is controlled by development time, LOR baking time, and exposing time, among which the development time is most important. The development time should be determined by often observation under optical microscopy. For this experiment development time is around 20 s. With the optimized processes mentioned above, we can get undercut of 1  $\mu\text{m}$  length and 0.5  $\mu\text{m}$  height (Figure 2-12). With the good undercut pattern, the lift off process can be easily completed by immersing wafer into acetone in ultrasonic bath.

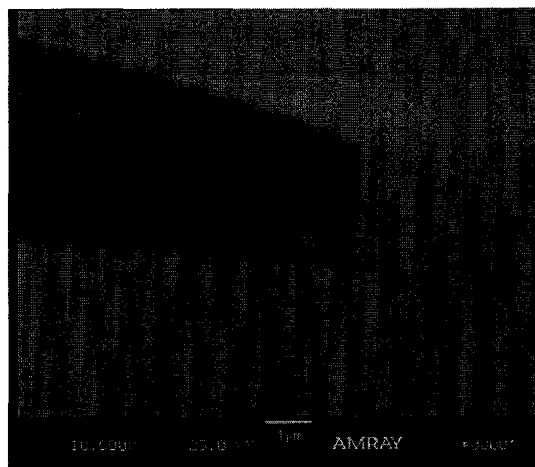


Figure 2-12 Undercut pattern by LOR photoresist.

## 2.5 Materials and Methodology

Preparation of  $\lambda$ DNA with different concentration as shown in Table 2-3 (48,000 bp, 500  $\mu\text{g}/\text{ml}$  or 15.87 nM, from New England Biolabs).

Table 2-3 Preparation of DNA. Storage temperature:  $-20\text{ }^{\circ}\text{C}$

Objective DNA concentration	DNA solution		TE buffer
	concentration	volume	
1 nM	15.87 nM	10 $\mu\text{l}$	148.7 $\mu\text{l}$
100 pM	1 nM	20 $\mu\text{l}$	180 $\mu\text{l}$
10 pM	100 pM	20 $\mu\text{l}$	180 $\mu\text{l}$
1 pM	10 pM	20 $\mu\text{l}$	180 $\mu\text{l}$
0.1 pM	1 pM	20 $\mu\text{l}$	180 $\mu\text{l}$

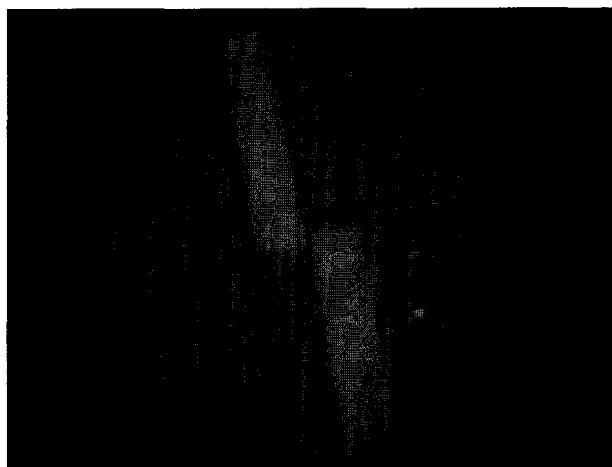
- Preparation of TE buffer 250 ml (10 mM, Tris-HCl, pH 8.0, and 1mM EDTA).
  - (1) Tris 0.30285 g and EDTA 0.10405 g.
  - (2) Dissolve both into 230 DI water.
  - (3) Add HCl to adjust until pH = 8.
  - (4) Fill in DI water until 250 ml.
- Dye  $\lambda$ DNA with YOYO with ratio of 5 bp/dye or 1  $\lambda$ DNA/10<sup>4</sup> YOYO.
  - (1) Warm up YOYO and DNA solution in room temperature.
  - (2) Dilute YOYO 10,000 times (100nM). Put 1 $\mu$ l YOYO into 10 ml TE buffer (10 mM, Tris-HCl, pH 8.0, and 1mM EDTA).
  - (3) Mix 10 pM DNA solution 100 $\mu$ l with diluted YOYO solution 100 $\mu$ l.
  - (4) Samples for fluorescence microscopy.
- Stretching and positioning of DNA molecules by dielectrophoresis.
  - (1) Clean prepared electrodes with acetone and DI water.
  - (2) Prepare YOYO-dyed DNA as mentioned above.
  - (3) Solder conductive wires to both electrodes.
  - (4) Drop 20  $\mu$ l DNA solution and cover with thin slide.
  - (5) Apply AC source (sin wave, 300 kHz, and 5.2 V) and observe in-situ under fluorescence microscopy.
- Metallization of DNA by palladium.
  - (1) Prepare Pd solution. Put 5 mg Pd(CH<sub>3</sub>COO)<sub>2</sub> into 1 ml HEPES buffer (pH 6.5, 10 mM) in ultrasonic bath 2 min then centrifuge 5 min to get saturated solution. Then dilute 8 times with buffer solution.
  - (2) Mix DNA solution and Pd solution with volume ratio of 3:1 for 2 h.

- (3) Drop 20  $\mu\text{l}$  mixed solution, then stretch DNA molecules between electrodes as mentioned above.
- (4) At the same time add in 10  $\mu\text{l}$  reduction solution (2.5 g/l sodium citrate, 2.5 g/l 85% lactic acid, 0.25 g/l dimethylamine borane, pH 7.4).
- (5) Wait 10 min and stop the power.

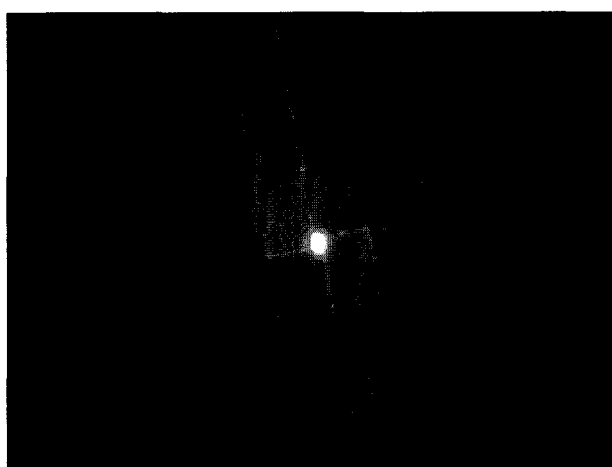
## 2.6 Experimental Results and Discussion

DNA molecules can be collected in the areas where electric field is the strongest by application of AC electric field. As shown in Figure 2-13, the electric field at the meeting areas between two electrodes are strongest, so DNA were collected there and showed green color because of dyes of YOYO.

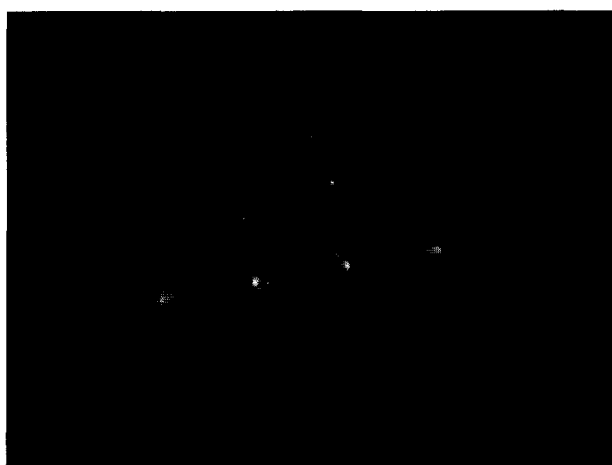
YOYO-dyed DNA molecules show green color under fluorescence microscopy. Without application of electric field, DNA molecules distribute evenly in the liquid media, and moving around with flow. When electric field is turned on, DNA molecules will move to the area where paired electrodes meet each other and stay there. The collection process usually takes several seconds. After the electric field is turned off, most DNA molecules will diffuse around rapidly. Figure 2-13a shows YOYO-dyed DNA molecules before applying an electric field. As the limitation of amplifying times of optical microscopy and camera, we can only see the green background. Single DNA molecules could be detected by photo counting intensified camera. From Figure 2-13b we can observe liquid media moving after applying an electric field. Moving direction is vertical to the DNA stretching. Figure 2-13c shows an electrode array used to collect DNA molecules.



(a)



(b)



(c)

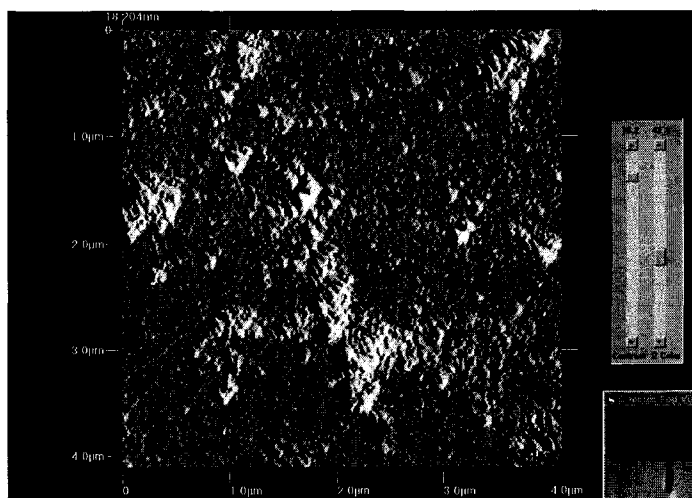
Figure 2-13 Collection effect on DNA by dielectrophoresis.

The counterion cloud around DNA molecules is assumed to be responsible for dielectrophoresis. The interaction of induced dipole moments with the surrounding electric field leads to an electrokinetic movement and orientation parallel to the electric field direction or called positive dielectrophoresis. When the properties of electric field and surrounding liquid media are such that the movement of DNA molecules is vertical to the electric field direction, it is called negative dielectrophoresis. In our experiments we find DNA molecules along electric field direction at 300 KHz and  $10V_{\text{rms}}$ . No negative dielectrophoresis phenomenon was observed.

From Figure 2-14 we can see single DNA molecules bridged between electrodes. After the buffer solution was removed, DNA still stayed there. The DNA molecules could stand the soft rinse of DI water. We consider the adhesion is the physical absorption. Chemical adhesion is the ideal as chemical bonding can provide strong enough strength against exterior forces between DNA molecules and substrate, and if functionalization of substrate is site-selective, positioning of DNA molecules could be individually addressable. The most widely used chemical bonding between DNA and gold is thiol bond. To obtain this bond, the ends of DNA should be modified by  $-S-H$  chemical group. The reaction happens at room temperature. In AFM picture, several single DNA molecules were stretched and aligned on the surface. Some particles are also observed on the surface. The contamination could come from DNA solution, YOYO solution, or soldering process. The materials and processes need to be improved to reduce background contamination.



(a)



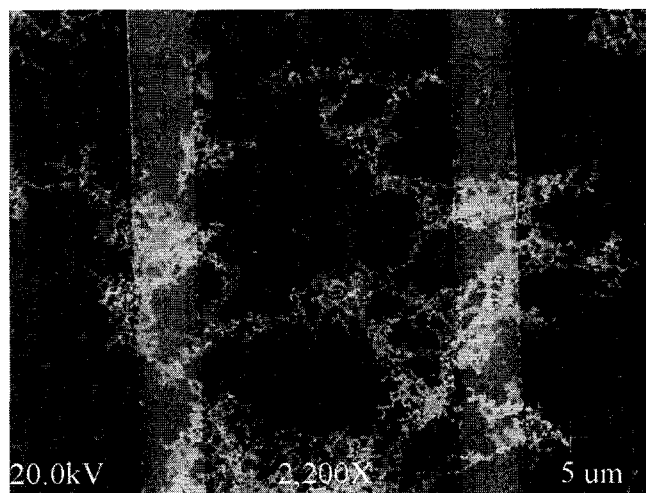
(b)

Figure 2-14 Stretching and positioning of DNA molecules.

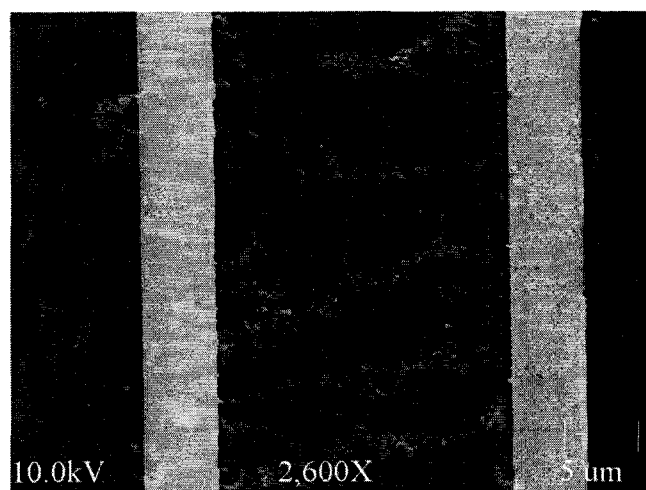
As we know, to build conductive DNA nanowires between electrodes, two main processes are usually applied, stretching and positioning, and metallization. When the electric field is on, DNA molecules are stretched between electrodes. At this time, both ends of DNA contact electrodes, but not bond there. Also by the influence of liquid flow, the ends of DNA will not be static, they are vibrating. So it is hard to get both ends of

DNA anchored to respective electrodes, even using sulfur modified DNA. In this experiment we integrate two assembly processes into one. In other words, stretching, position, and metallization are conducted in the same one process. When metallization happens at the time of stretching, metal is grown around DNA molecules fast and big enough that many DNA will bridge permanently between electrodes.

Figure 2-15 shows a metallized DNA network between electrodes. Some electrodes are spanning two electrodes. The control experiment was done under the same condition but only without DNA molecules. The interesting thing is that similar wire structures still formed between electrodes, due to reduction of Pd ions in the solution to Pd particles. The Pd particles are assembled by dielectrophoresis into wire structures. After metallization DNA strands were left on the substrate. The distance between two parallel gold electrodes is 20  $\mu\text{m}$ . We can see DNA molecules were nonuniformly distributed on the substrate. Some DNA covered on the electrodes. Aggregation of DNA molecules are presumed to form during the metallization process. Metallized DNA molecules modified their stretched form. Another explanation is that, when reducing reaction happened actively in the solution, irregular movement of ions led to dynamic flow around DNA molecules, which changed the stretched form into coils. DNA molecules after metallization have diameters around 100 nm. Branched are found in metallized DNA molecules which is presumably caused by the processes of reduction and deposition.



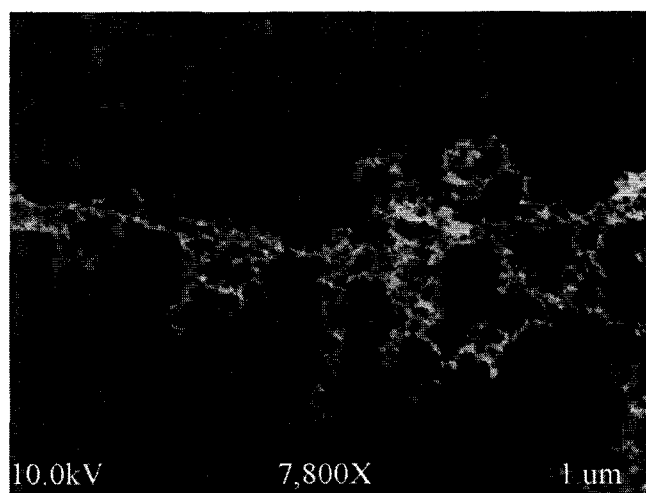
(a)



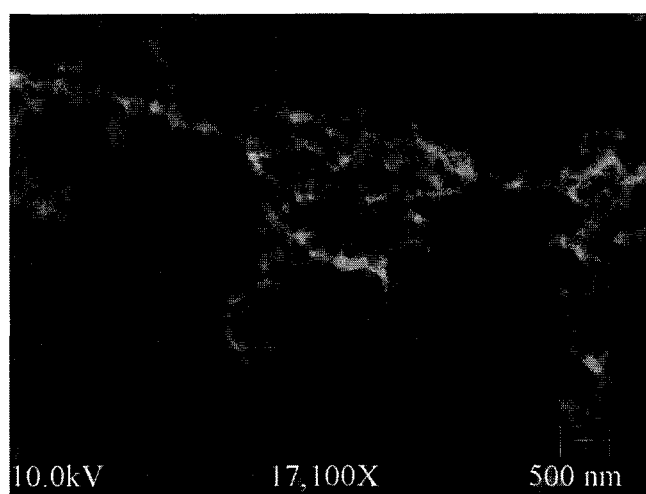
(b)

Figure 2-15 Metallization of DNA and control experiments without DNA.

Figure 2-16 shows two magnified DNA strands with magnification of 7800 and 17100 times, respectively. Further experiments were proceeded without reduction bath, and uniform nanowire arrays were observed growth between electrodes and had specific pattern which will be presented in the following chapter.



(a)



(b)

Figure 2-16 Metallized DNA strands.

## **CHAPTER 3**

### **DIRECT GROWTH OF ARRAYS OF PALLADIUM NANOWIRES**

#### **3.1 Introduction**

The nanowire, the basic building block of a nanocircuit, has recently become the focus of intense research. Many methods of nanowire synthesis and assembly are ex-situ or are based on templating—DNA molecules, nanopores, surface step-edges, or channels patterned by lithography are required for the nanowire fabrication process. An ideal approach for practical application of nanowires would circumvent technical and economic constraints of templating. Here we report the self-assembly of highly ordered metallic nanowires directly from palladium acetate solution under an applied alternating current (AC) electric field of relatively high intensity and frequency.

There are examples in the scientific literature of an applied electric field being used to fabricate nanowires between electrodes. Most such studies, however, involved pre-formed nanoparticles or nanowires. Our approach has no such requirement. Moreover, in the latter chapter, this approach has been used to self-assemble single nanowires at specified locations between electrodes or devices. In any case, the results of the present study challenge current nanowire methodologies and could lead to direct assembly of nanoscale electronic structures and systems.

### 3.2 Electrode Structure

Metal electrodes designed for this study were patterned by lift-off: 5 nm Cr and 40 nm Au on a silicon dioxide wafer. Four pairs of parallel electrodes differed in gap width (Figure 3-1), enabling simultaneous study of different electric field strengths. Results shown below indicate that the behavior of palladium acetate solution in this context depended significantly on field intensity.

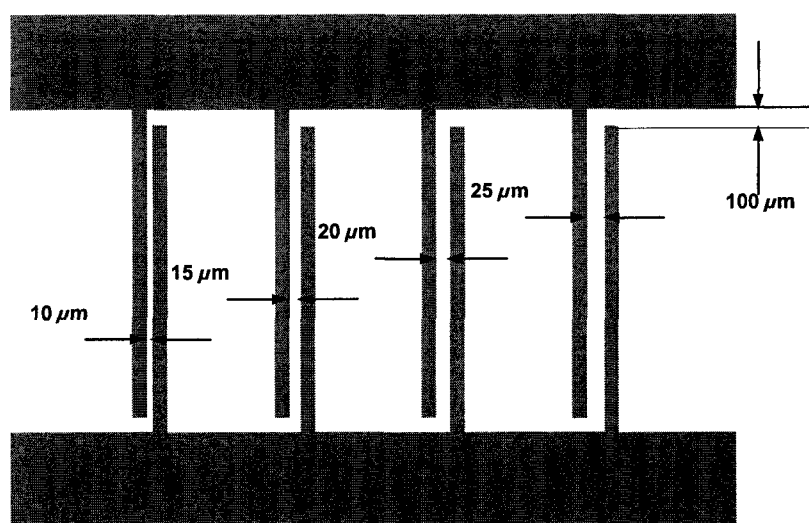


Figure 3-1 Schematic diagram of the microelectrode structure used in this research. Four pairs of parallel electrodes, with gap size ranging from 10 to 25  $\mu\text{m}$ , were patterned on a silicon dioxide substrate. Dimensions are not to scale.

### 3.3 Materials and Methodology

In a typical experiment, palladium acetate solution was prepared by dissolution of crystalline  $\text{Pd}(\text{acetate})_2$  in 10 mM HEPES buffer, pH 6.5. Saturated solution was diluted by a given amount using DI water; buffer species were diluted with palladium ions. A sinusoidal signal of defined potential and frequency was applied to the electrodes on which the palladium solution was deposited. Nanowire formation was found to vary with concentration of palladium, applied voltage, and frequency.

### 3.4 Characterizations

Palladium nanowires resulting from the fabrication process were visualized by scanning electron microscopy. Figure 3-2 shows typical examples of 100-nm-diameter Pd nanowires formed under an AC signal of 10 V<sub>rms</sub> and 300 kHz. Wires are arrayed perpendicular to the electrodes and parallel to the direction of the electric field. The density of nanowires varied with electrode gap size and hence peak electric field strength. Nanowires self-assembled along the entire length of the 10 μm- and 15 μm-wide electrodes (Figures 3-2a and 3-2b). By contrast, when the gap size was 20 μm or 25 μm, in some cases a few nanowires formed (Figures 3-2c and 3-2d), but in most cases only a single nanowire formed, mainly at an electrode “end” (Figure 3-5a, below).

Nanowire self-assembly was detected *in situ* and real time by optical microscopy. In all cases nanowire formation became evident 0.5-4 min after applying the electric field, the time depending on concentration of palladium, field strength, and frequency, and formation of a complete array of nanowires was complete within seconds. Most nanowires grew approximately simultaneously for a given set of conditions. Some, however, developed before others and then melted, due apparently to high current density (Figure 3-2a). The very high field strength at a narrow broken gap in a nanowire will lead to hydrolysis, producing bubbles and inhibiting “self-healing” by “secondary assembly.” After a number of nanowires had bridged a pair of electrodes, there was a sharp reduction of voltage and therefore electric field. Short-circuiting of electrodes prevents growth of new nanowires and protects existing ones from destruction.

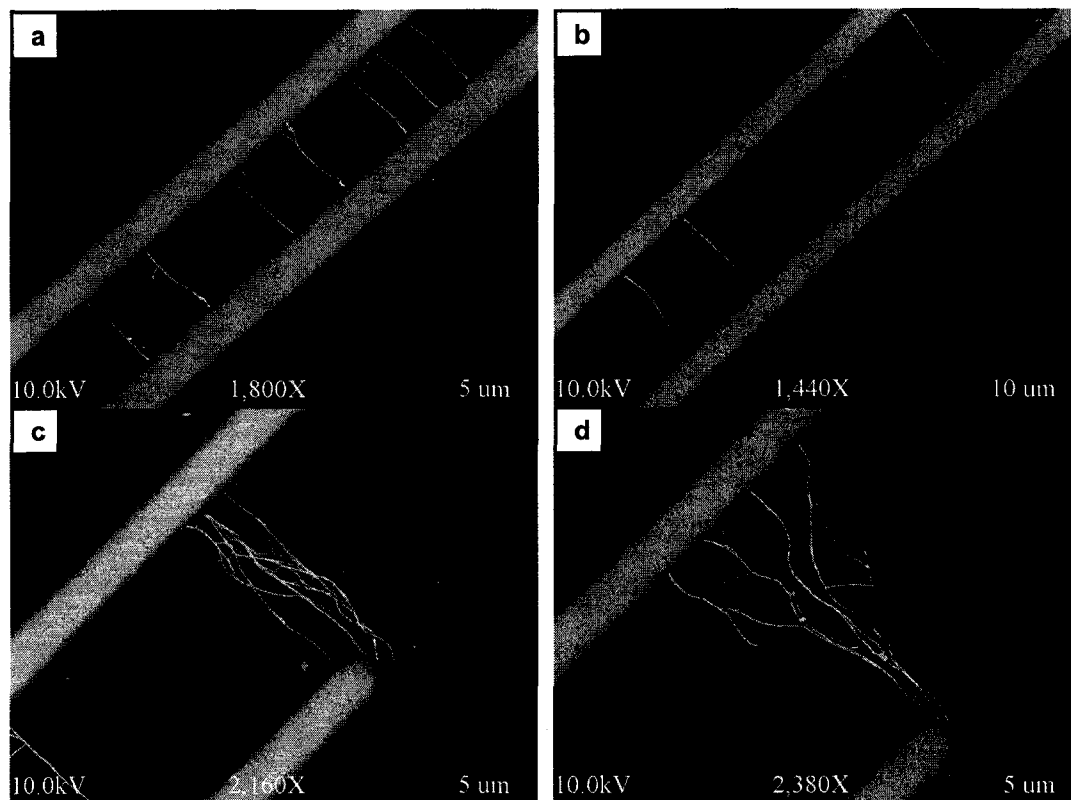


Figure 3-2 SEM images of Pd nanowires assembled between electrodes under an applied AC signal of  $10 V_{\text{rms}}$  and 300 kHz. The nanowires have an approximate diameter of 100 nm. Experiments involved palladium acetate dissolved in 10 mM HEPES buffer, pH 6.5, diluted  $8\times$  from saturation. Gap spacing between electrodes: (a)  $10 \mu\text{m}$ , (b)  $15 \mu\text{m}$ , (c)  $20 \mu\text{m}$ , (d)  $25 \mu\text{m}$ . In (a), the second Pd nanowire from the left has ruptured, presumably due to high current density.

### 3.5 Discussion

Formation of regular arrays of nanowires can be explained by reduction of electric field strength following initiation of nanowire growth. Formation of a conductive metallic nanowire between electrodes will decrease the local electric field, inhibiting the growth nearby of new nanowires.

Magnitude of applied voltage and therefore electrode field intensity had marked influence on nanowire growth. The applied potential for which nanowire formation was observed to occur using the electrode structure illustrated in Figure 3-1 was  $8\text{--}10 V_{\text{rms}}$ .

This corresponds to a maximum field intensity of 0.4–1.0 MV/m, depending on electrode spacing. When the applied voltage was too “low,” the energy provided by the electric field was insufficient to initiate nanowire growth.

The effect of the concentration of Pd solution on the growth of nanowires was investigated when the electric field was constant at  $10 V_{\text{rms}}$  and the frequency was 300 kHz. We found no obvious dependence of diameter of nanowires on concentration of Pd solution. Here, as initial concentration of palladium acetate was low, so after dilution the concentration got even lower. In other words, the result of no effect of palladium concentration on nanowire thickness is based on the low concentration of palladium. In the later experiment we used palladium ammonium complex because it can easily dissolve into water and different concentration could be prepared. The dependence of concentration was observed for palladium ammonium complex and thickness varied from 100 nm to 2  $\mu\text{m}$ . The length of time between application of the field and onset of assembly of nanowires, however, was largely dependent on ion concentration (Figure 3-3). At higher concentrations, more Pd complex was reduced to form Pd nuclei at one time, and less time was needed to reach the threshold condition required to initialize assembly. When 32 $\times$ -diluted Pd solution was used, the concentration was so low that no nanowires were observed to grow between electrodes.

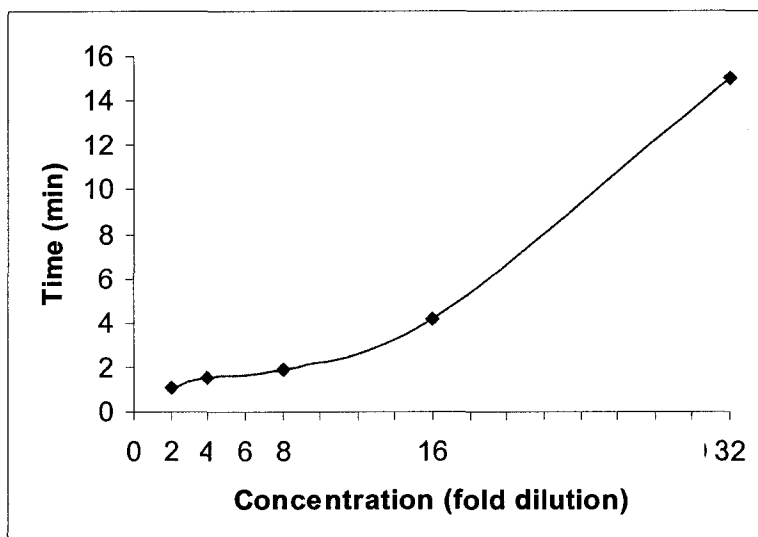
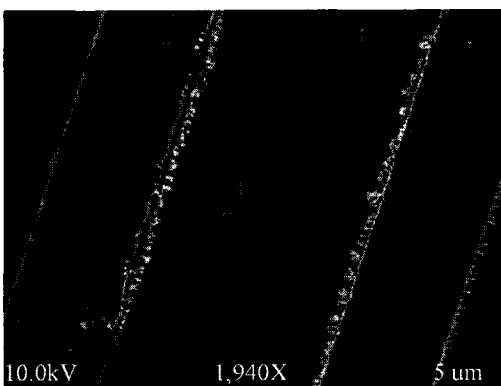
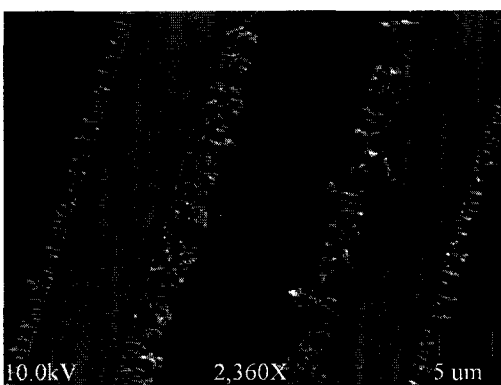


Figure 3-3 Effect of concentration of palladium acetate solution on time required for assembly of nanowires after application of an alternating electric field. The field was 10  $V_{\text{rms}}$  and 300 kHz. A saturated solution of palladium was diluted with DI water 2, 4, 8, 16, or 32 times. No Pd nanowires were observed after 32 $\times$  dilution. The whole drop of solution on electrodes was evaporated away after 15 minutes under room temperature.

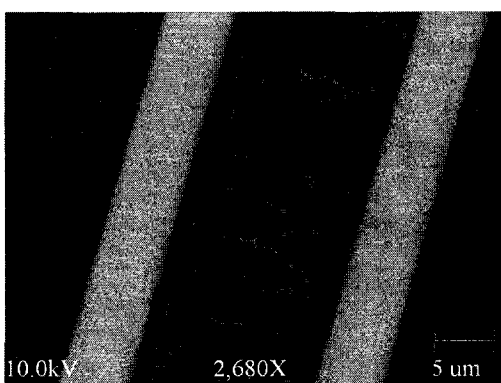
Our experiments have revealed that the assembly of nanowires in the present context depended substantially on the frequency of the applied electromotive force. At low frequencies, including DC, no nanowires were formed; material deposition, apparently of palladium, occurred along the entire length of electrodes and was disorganized. As frequency increased, however, material began to self-assemble between electrodes into structures of increasing likeness to wires (Figure 3-4). Uniform nanowire self-assembly occurred only at relatively high frequency ( $\sim$ 300 kHz; Figure 3-2).



(a)



(b)



(c)

Figure 3-4 Effect of frequency on the growth of nanowires from Pd acetate solution. The alternating electric field applied was 8 V<sub>rms</sub> and (a) 0.3 KHz, (b) 3 KHz, and (c) 30 KHz. Palladium acetate was 8-fold diluted from saturation.

The mechanism of this behavior is not entirely unclear. The applied AC field may induce a frequency-dependent orientation of soluble matter, notably palladium ions, or the character of the electric field between electrodes may be frequency dependent, owing to dispersive properties of the solution. It would appear, in any case, that when the frequency is sufficiently high material aligns parallel to the field, enabling the growth of nanowires in the same direction. At low frequency, dissipation due to thermal fluctuations and joule heating outcompete alignment due to the field, and material is deposited only irregularly at the edge of electrodes (Figure 3-4a and 3-4b) or forms dendritic structures between them (Figure 3-4c).

The resistance of an array of nanowires on an electrode, formed as described above, was found to be 50–200  $\Omega$ . Electrical properties of a single nanowire of diameter *c.* 200 nm at the end of a 20- $\mu\text{m}$  electrode (Figure 3-5a) were determined after electrical isolation. Figure 4b shows clear evidence that the  $I$ - $V$  curve of this nanowire was ohmic at room temperature. The measured resistance was 1.69 k $\Omega$ , corresponding to a resistivity of *c.* 212  $\mu\Omega\cdot\text{cm}$ . This value is only about 20-fold greater than that of bulk palladium, suggesting that the nanowires are composed mostly of palladium. The relatively high resistivity can be attributed to deposition of other materials during the assembly of the nanowire, for example acetate ions, non-ideality of wire shape, grain boundaries, or high contact resistance between nanowire and electrodes. When the nanowire shown in Figure 4a was severed using the probe tip of a Keithley probe station, the sample behaved like an insulator (Figure 3-5b, inset). Clearly the nanowires are metallic.

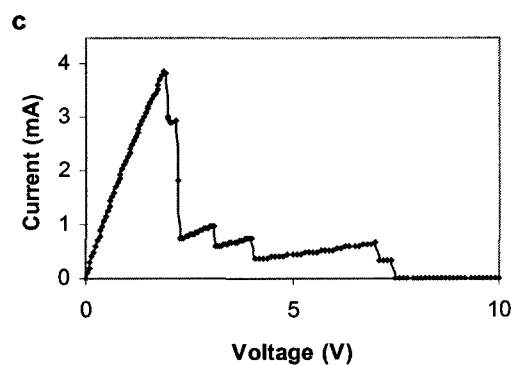
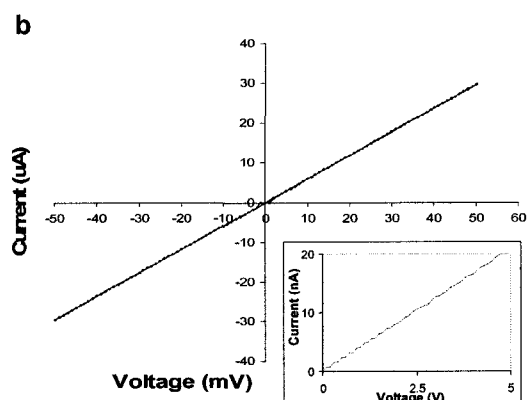
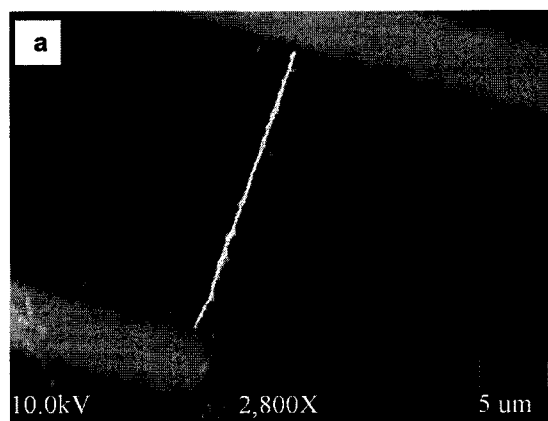


Figure 3-5 A single Pd nanowire of diameter c. 200 nm. (a) Characterization by SEM. The wire self-assembled between gold electrodes under an AC electric field of 10 V<sub>rms</sub> and 300 KHz at the end of a 20-μm gap electrode. (b) *I-V* curve. The resistance was 1.69 kΩ. After cutting the wire, the sample behaved as an insulator (inset). (c) Melting test. Under high voltage, 6 Pd nanowires were destroyed one by one when an applied DC voltage shifted from the 0 to 10 V.

We have also studied breakage characteristics of the nanowires under high voltage. In one case, a 20- $\mu\text{m}$  electrode featuring 6 nanowires was selected. A DC potential was applied to the electrode and made to increase gradually from 0 to 10 V. The nanowires melted in succession. Analysis of the  $I$ - $V$  curve collected during this process (Figure 3-5c) has revealed that the respective resistances were in the range 1.0–23.2  $\text{k}\Omega$ , increasing with applied potential. The result is consistent with the discussion of broken nanowires above (Figure 3-2a).

Nanowire arrays were characterized in other ways. Soaking an array for 10 min in a reducing aqueous environment (25  $\text{gL}^{-1}$  sodium citrate, 25  $\text{gL}^{-1}$  85 % lactic acid solution, and 2.5  $\text{gL}^{-1}$  dimethylamine borane, pH 7.4) or annealing it for 2 h in vacuum at 400  $^{\circ}\text{C}$  gave no obvious change in electrical resistance. Because palladium acetate reacts rapidly with a reducing agent and decomposes at 220  $^{\circ}\text{C}$ , the data prove that the wires were made largely if not exclusively of palladium. It remains to be determined whether our approach will be suitable for other metals.

Possible mechanisms of metallic nanowire formation are the following. There was a time delay in all cases between application of the AC signal and nanowire formation, and delay length was inversely related to palladium concentration. This suggests a threshold of palladium concentration for initiation of nanowire growth. The conductive properties of the nanowires suggest that palladium ions somehow arrange themselves in the time-varying electric field between electrodes. Presumably nanowire growth begins in a region of inhomogeneity of palladium ion concentration and of the electric field, which itself will be an artifact of electrode fabrication. The nanowire self-assembly process, apparently a type of electrochemical deposition, may involve

dielectrophoresis [19] and electrothermal flow. The applied electric field continually brings palladium ions to the tip of a growing nanowire and sustains its growth until the nanowire reaches the opposite electrode and the electric field is shorted out in the local area. Electrothermal flow was apparently not the dominant cause of self-assembly, as fluid flow was often observed perpendicular to the direction of growth of nanowires.

We consider an electrochemical reaction proceeding at the tip of a nanowire during growth, and the formation of metallic bonds in a nanowire structure. Electrochemical deposition involving membrane templates tends to yield dense, continuous, and highly crystalline nanowires [18]. The nanowires reported here appear are similar in character but easier to fabricate. Moreover, our nanowires have substantially greater mechanical stability than gold-nanoparticle microwires [19], in which the strength of interparticle interaction is comparable to that of a hydrogen bond. Our nanowires are stable following drying and withstand rinsing with DI water, while the gold-nanoparticle microwires are easily fragmented or destroyed by capillary forces [19].

## CHAPTER 4

### SINGLE PALLADIUM NANOWIRES

#### AT PRESCRIBED LOCI

##### 4.1 Electrode Structure

Metal electrodes designed for this study were patterned by lift-off: 5 nm Cr/100 nm Au on a silicon dioxide wafer. Three electrode structures (Figure 4-1) were designed to investigate the effect of electric field on growth of single palladium nanowires.

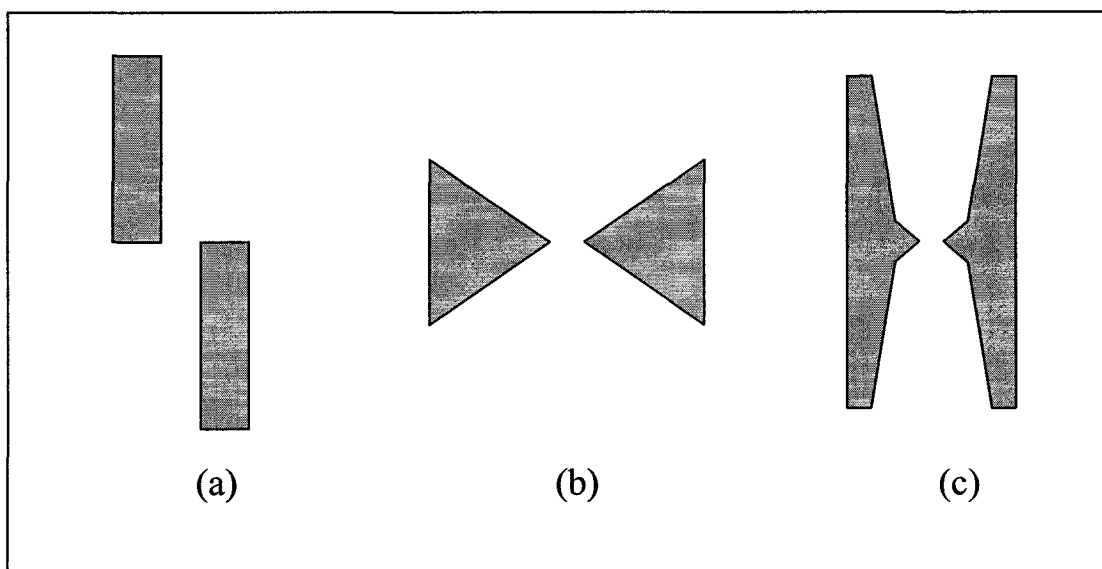


Figure 4-1 Schematic electrode designs.

## 4.2 Materials and Methodology

Here, a saturated aqueous solution of Pd acetate, buffered with 10 mM HEPES, pH 6.5, was diluted 8-fold with ultrapure water and deposited on 5 nm Cr/100 nm Au electrodes patterned by lift-off on a SiO<sub>2</sub> wafer, and palladium nanowire assembly between electrodes was realized *in situ* by application of a 10 V<sub>rms</sub>, 300 kHz signal on a 0.8 V DC bias potential. The resulting nanowires have been characterized by various methods.

## 4.3 Characterizations

Scanning electron microscopy has revealed that the indicated conditions can yield single nanowire bridges between a 15 μm-gap electrode (Figure 4-2). This is consistent with our previous work, in which several nanowires of diameter 100-200 nm were formed between parallel electrodes. The wire shown has a diameter (Figure 4-2a) and “height” (Figure 4-2b) well below 100 nm. What is more important here, however, is that conductive nanowires can be formed at prescribed locations, given an appropriate electrode structure. In the electrode design in Figure 4-2a, one nanowire only was formed, at the meeting point of the two parallel electrodes. This location is close to where the field is strongest, and the wire is oriented in the direction of the field. The small “branches” from the nanowire close to the upper electrode may be a result of irregular fluid flow. The apparently failed nanowire (left side of lower electrode) may have altered the local field and thereby inhibited wire formation. Other electrode designs (Figures 4-3a and 4-3b) also yielded single nanowire formation exclusively at defined locations, assembly proceeding parallel to the direction of the electric field, and only where the field is strongest, independent of gross electrode structure.

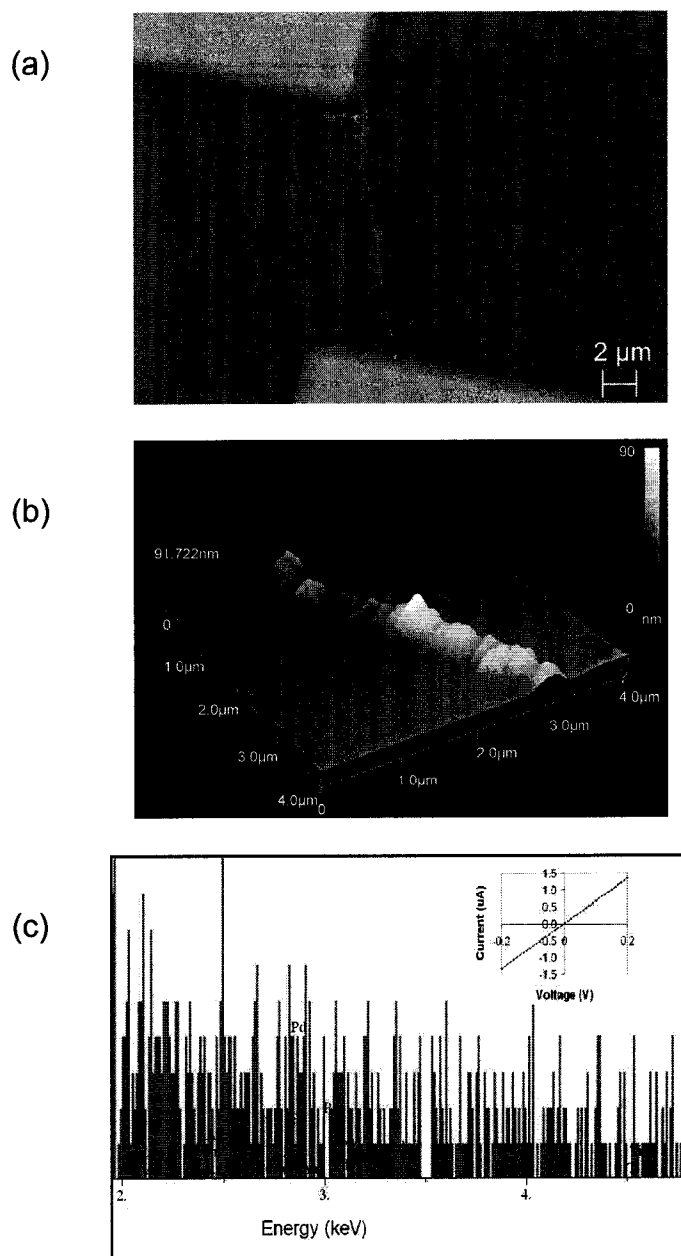


Figure 4-2 Characterization of a single Pd nanowire between Au electrodes on a  $\text{SiO}_2$  wafer. (a) Visualization by SEM. The wire self-assembled from Pd acetate solution between a  $15 \mu\text{m}$ -gap and had a diameter of *c.*  $75 \text{ nm}$ . Pd acetate solution was diluted 8-fold from saturation, the source was  $10 \text{ V}_{\text{rms}}$  at  $300 \text{ KHz}$ , and DC offset  $0.8 \text{ V}$ . Scale bar,  $2 \mu\text{m}$ . (b)  $4 \mu\text{m} \times 4 \mu\text{m}$  AFM image of a portion of (a). Vertical scale,  $90 \text{ nm}$ . Irregularity in wire diameter will increase electrical resistance. (c) EDX analysis. Pd intensity was  $0.41 \text{ c/s}$ . The resistance was  $149 \text{ k}\Omega$ .

Electron-dispersive X-ray analysis of the single nanowire in Figure 4-2a and Table 4-1 has revealed that the wire was composed almost exclusively of Pd (though some organic material might be present), consistent with our earlier study. Moreover, the wire exhibited ohmic contact behavior at ambient temperature (inset, Figure 4-2c). The measured resistance, 149 k., corresponds to a resistivity  $\sim 10^2$  greater than that of bulk Pd. The melting of nanowires shortly after growth occurred in some experiments (Figure 4-3a), apparently due to high current density. The nanowire in Figure 4-2a withstood an estimated current density of *c.*  $1.5 \times 10^6$  A/cm<sup>2</sup> – the same order of magnitude as in lithographically-defined metal interconnections [87]. An automated electronic or photonic means of opening or shorting out the circuit could be developed to protect the newly-formed nanowire.

Table 4-1 EDX data

Elt.	Line	Intensity (c/s)	Error 2-sig	Atomic Wt %	Conc	Units
O	Ka	63.74	2.914	77.146	65.565	wt.%
Si	Ka	134.21	4.229	22.772	33.974	wt.%
Pd	La	0.41	0.235	0.082	0.461	wt.%
Au	La	0	0	0	0	wt.%
			Total	100	100	wt.%

In previous study we found that, when the frequency of the applied AC signal was low, Pd ions deposit in an irregular pattern all along parallel electrodes. Here, addition of a 0.8 V DC bias to a suitable AC signal for Pd nanowire assembly increased the rate of nanowire formation. In the absence of the bias potential, minutes elapsed prior to initial

detection of Pd nanowire formation on application of the 300 kHz 10 V<sub>rms</sub> signal. Addition of the DC offset reduced the time to well below 1 min. When the bias was above 0.8 V, Pd deposition occurred but nanowires did not form. Figure 4-3 shows single nanowires formed at different electrode structures.

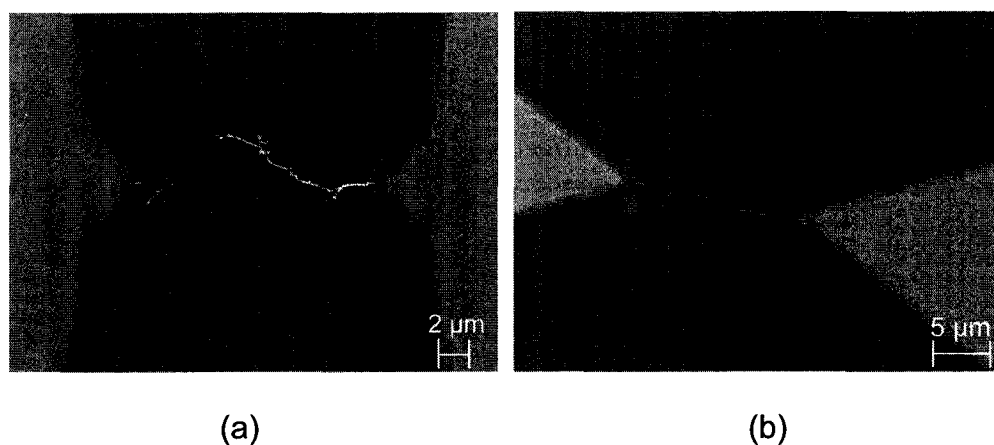


Figure 4-3 Single Pd nanowires assembled between different types of pointed electrode. (a) “Dull” points. (b) “Sharp” points.

#### 4.4 Other Materials

We have also studied whether other salts or complexes in the platinum group might be suitable for nanowire formation from aqueous solution. Analysis of such materials might lead to results of practical value, or it could help to clarify the relevant mechanisms of mechanical nanowire assembly. Platinum (II) diammine dichloride, potassium tetrachloroplatinate, potassium hexachloroiridate (IV), palladium (II) chloride, cobalt (II) acetate tetrahydrate, and nickel (II) acetate tetrahydrate have been tested using the conditions indicated above. It was assumed that the likelihood of formation of nanowires at ambient temperature was maximal if the solution was at or close to saturation. Figure 4-4 shows that  $\text{Pt}(\text{NH}_3)_2\text{Cl}_2$  alone of the indicated materials yielded

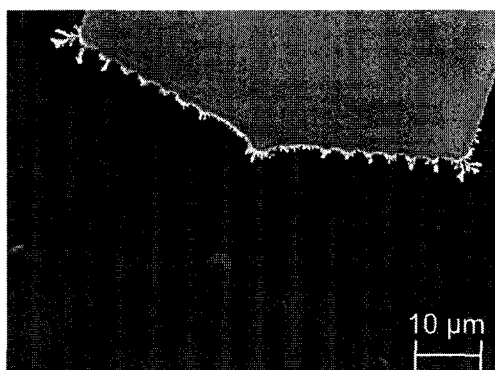
nanowires between electrodes; the other materials aggregated at one of the electrode tips (Figures 4-4b, 4-4d and 4-4e) or along the sides (Figure 4-4c), compare with Figure 4-4g and 4-4h, and Ni acetate damaged the electrodes (Figure 3f).



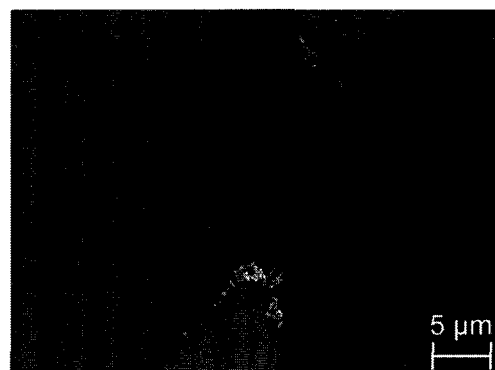
(a)



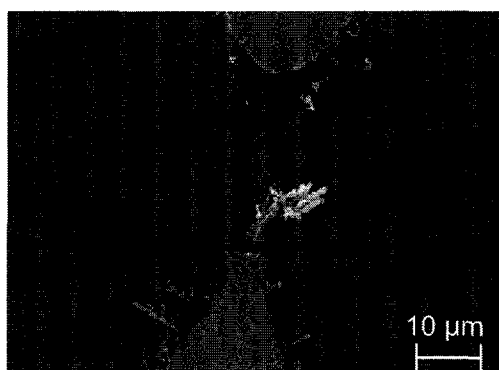
(b)



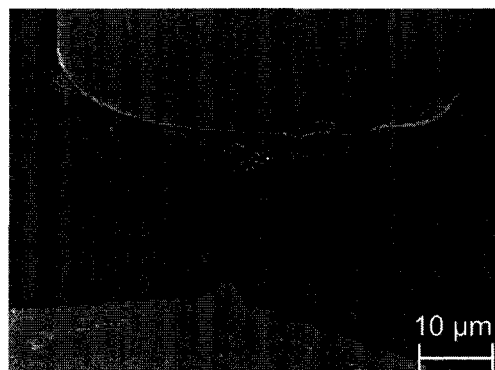
(c)



(d)



(e)



(f)

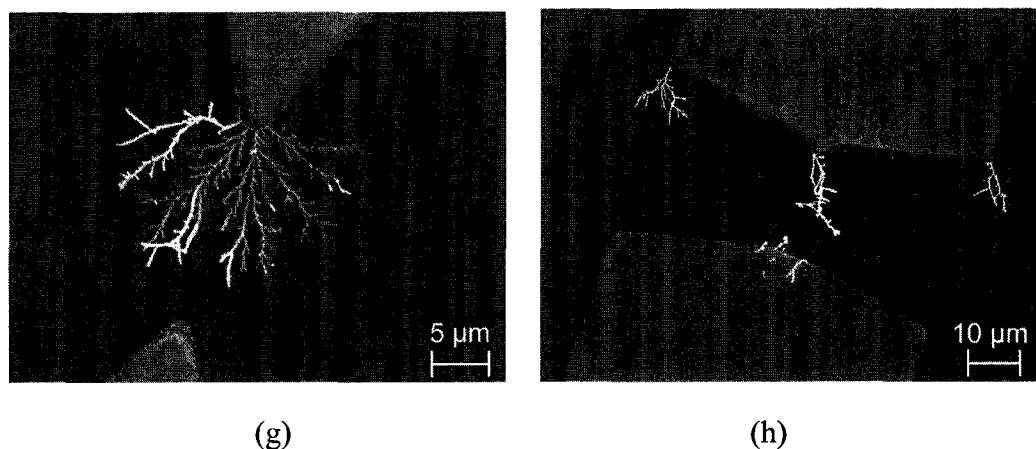


Figure 4-4 Test of various metal salts or complexes under an applied signal of 300 kHz  $10 V_{\text{rms}}$  and 0.8 V DC. (a)  $\text{Pt}(\text{NH}_3)_2\text{Cl}_2$ , 5  $\mu\text{m}$  scale bar; (b)  $\text{K}_2\text{PtCl}_4$ , 5  $\mu\text{m}$ ; (c)  $\text{K}_2\text{IrCl}_6$ , 10  $\mu\text{m}$ ; (d)  $\text{PdCl}_2$ , 5  $\mu\text{m}$ ; (e)  $\text{Co}(\text{Ac})_2 \cdot 4\text{H}_2\text{O}$ , 10  $\mu\text{m}$ ; (f)  $\text{Ni}(\text{Ac})_2 \cdot 4\text{H}_2\text{O}$ , 10  $\mu\text{m}$ . Each solution was saturated, buffered with 10 mM HEPES at pH 6.5, and prepared at room temperature except (b), for which the concentration was 0.02 mol/L.

Nanowires of Pt formed from saturated solution of  $\text{Pt}(\text{NH}_3)_2\text{Cl}_2$  have different growth characteristics from Pd nanowires. The structure of the former is dendritic (Figure 4-4a; see also Figure 4-4g and 4-4h). Dendritic structures are also formed by field emission in gases of  $\text{W}(\text{CO})_6$  [20],  $\text{Cr}(\text{CO})_6$  [88], and  $\text{Mo}(\text{CO})_6$  [89]. Pt wires formed slowly during constant application of the source in a 15  $\mu\text{m}$ -gap electrode, where there was a high radius of curvature (Figure 4-4h), and the wires were stable for 3-5 s. The mechanisms underlying this behavior remain to be determined. What is clear now, though, is that Pd nanowires differ from Pt nanowires. The former grow much faster than the latter, so that growth cannot manually be interrupted after detection by visual inspection and before wire formation is complete.

The experiments on the materials mentioned above are based on saturated solution as some materials are not easily dissolved into water or buffer solution. We do not know the exact concentrations of respective metal ions. Because both  $\text{PdAc}_2$  and

$\text{PdCl}_2$  can largely dissolve into ammonia water solution, here, I put, respectively, 8 mg Pd acetate and 8 mg  $\text{PdCl}_2$  in 500  $\mu\text{l}$  HEPES buffer (10mM, pH6.5), then added in 100 $\mu\text{l}$   $\text{NH}_3\cdot\text{H}_2\text{O}$  (28%), and followed by 15 min ultrasonic vibration. The solutions prepared are colorless and don't contain any solid residues, with the concentration of 59 mM for  $\text{PdAc}_2$  and 75 mM for  $\text{PdCl}_2$ , respectively.  $\text{Pd}(\text{NH}_3)_4$  complex are supposed to form in both solutions.

We compared experimental results under the same conditions including the same electric field.  $\text{Pd}(\text{NH}_3)_4$  complex can form micrometer wires under the conditions mentioned above and whatever  $\text{PdAc}_2$  or  $\text{PdCl}_2$  used as precursor resulted in almost no difference (Figure 4-5). The resulted single microwires have very low resistance (around 30  $\Omega$ ), and no melting problem happened because such low resistance made AC power output voltage largely reduced, which can not cause large enough current density to damage the grown wires. Higher applied voltage (10 V) could lead to more active hydrolysis and more bubbles were formed between electrodes, which resulted in non-uniform wire structures. When applied voltage is around 5 V, single wire formed almost without branches. However, when voltage reduced to below 2 V, electric field was not high enough to initiate the growth of microwires. The results of these experiments are significative in that conductive wires directly grew between microelectrodes and no melting problem was met, although the wires were micro size in thickness. Because the resistance of grown single nanowires was around 20  $\Omega$ , the low resistance resulted a sharp voltage dropping at power source, which protected grown nanowires.

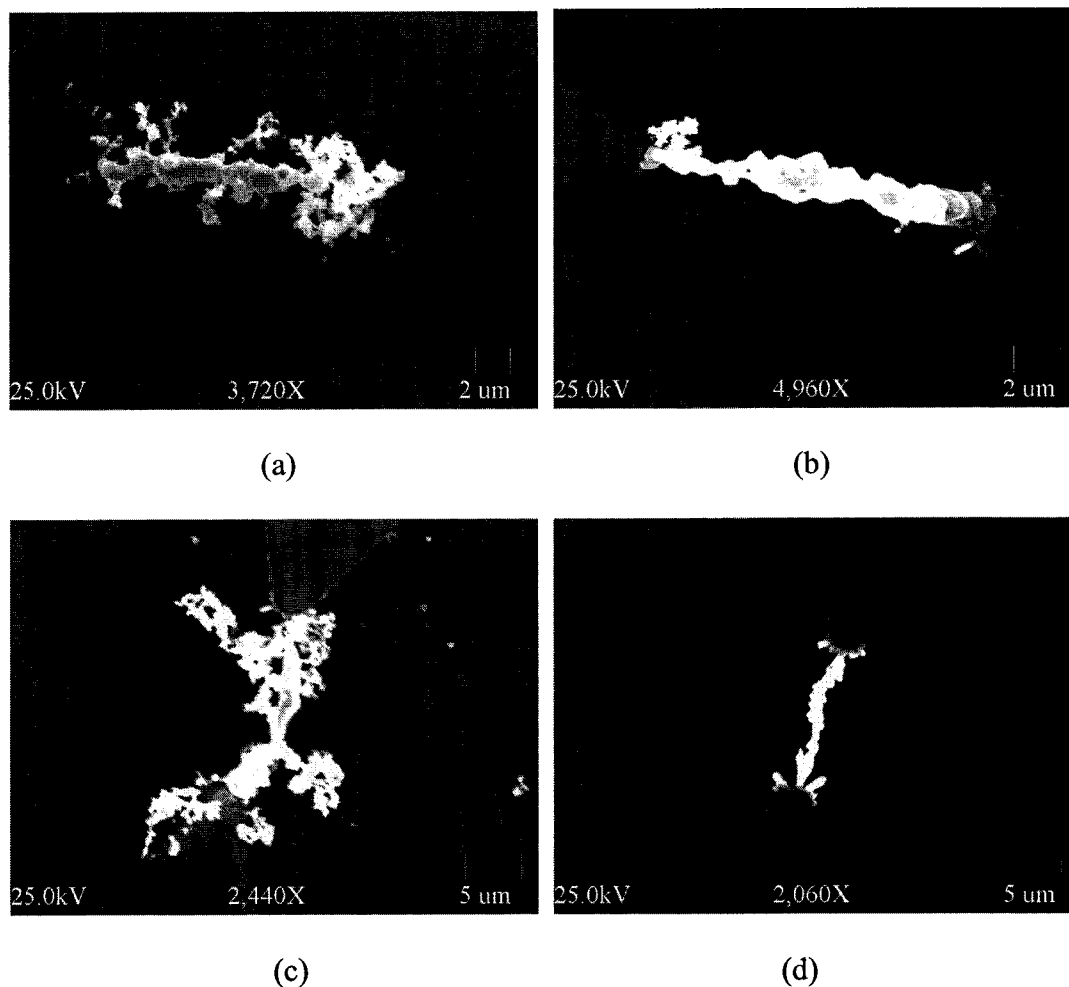


Figure 4-5 Microwires formed with different precursors. (a) 59 mM PdAc<sub>2</sub>, applied voltage 10V, (b) 59 mM PdAc<sub>2</sub>, applied voltage 5V, (c) 75 mM PdCl<sub>2</sub>, applied voltage 10V, (d) 75 mM PdCl<sub>2</sub>, applied voltage 5V.

The applied voltage between paired electrodes and concentration of used material Pd complex have a big impact on the wire growth, and even wire thickness. When the applied voltage was 5 V and the concentration of Pd(NH<sub>3</sub>)<sub>4</sub> complex was 5.9 mM, a fairly uniformly microwire was formed with resistance 30Ω, corresponding to 15.7 times resistivity of bulk palladium (Figure 4-6a). This value is in the same scale compared with the nanoscale wires synthesized from palladium acetate solution. When the applied voltage was kept at 5 V but the concentration was decreased 10 times to 0.59 mM, no

wire was found to form. At the low concentration it is hard to initialize the wire growing by low applied voltage. However, when we kept the low concentration but increased the applied voltage to 10 V, nanoscale wires were also found to grow (Figure 4-6b), although they were melted by presumably high current density. Table 4-2 compared the nanowire growth at different concentration and voltage.

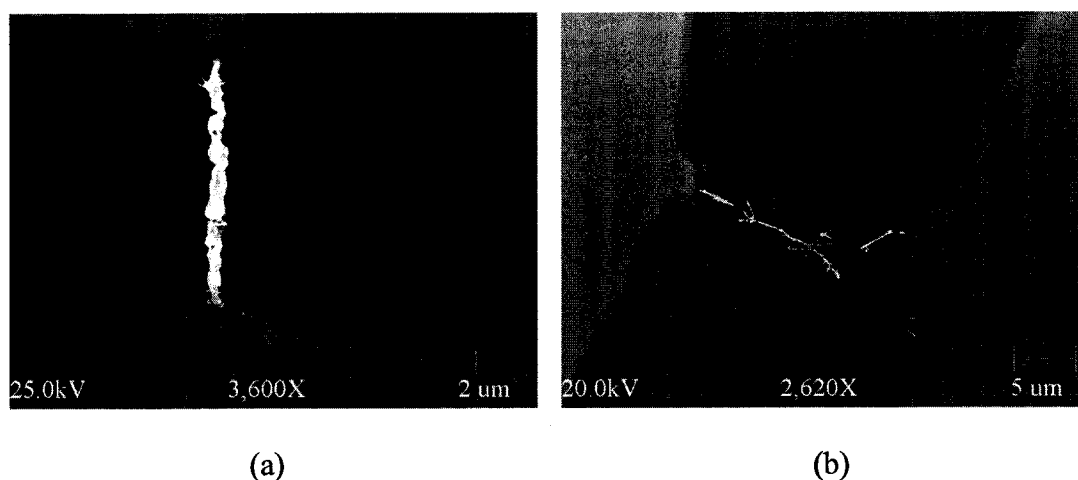


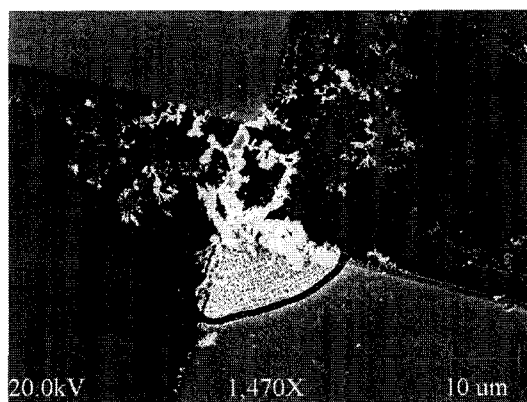
Figure 4-6 Pd wires formed under different conditions and with PdAc<sub>2</sub> as precursor. (a) 5.9 mM Pd(NH<sub>3</sub>)<sub>4</sub> and 5V, (b) 0.59 mM Pd(NH<sub>3</sub>)<sub>4</sub> and 10 V.

Table 4-2 Effect of voltage and concentration on wire growth

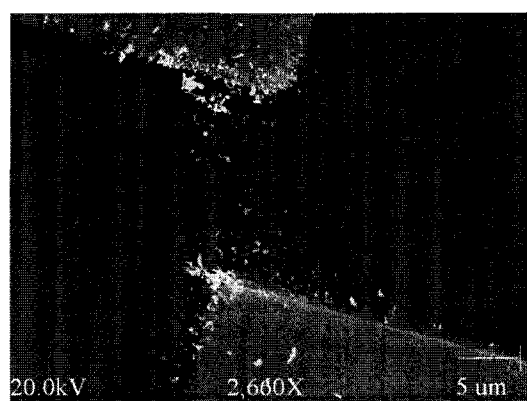
Concentration \ Voltage	59 mM	5.9 mM	0.59 mM
5 V	■	■	NO
10 V	*	NA	—

Table symbol:                   ■ stands for micro-thick wires;  
   — stands for nano-thick wires;  
   \* stands for micro-thick wires and a lot of branches;  
   NA stands for no experiments done under this condition;  
   NO stands for no wire structures formed.

Experiments were also done with 5.9 mM  $K_2PtCl_4$  and 0.59 mM  $AgNO_3$ . The applied voltage was 10 V. But no wire structures were found (Figure 4-7).



(a)



(b)

Figure 4-7 Other materials under same electric field. (a) 5.9 mM  $K_2PtCl_4$ , (b) 0.59 mM  $AgNO_3$ .

Figure 4-7 shows metal ions deposited and did mainly between electrodes where electric field is highest. This makes sense as any ions in an electric field will move against field gradient, pushed by electric field force. However no similar nanowires were found, this is probably due to different chemical characters of elements, such as chemical bond, crystal structure, or reducing potential, etc.

# CHAPTER 5

## CIRCUIT DESIGN FOR CONTROL OF NANOWIRE GROWTH

### 5.1 Melting Problem

The melting phenomenon after growth is a basic barrier which obstructs the following researches and nanowires' applications. In our experiments, Pd nanowires were self-assembled only under relatively high electric field (0.4—1.0 MV/m); while the high electric field resulted in a high current density which melted the grown nanowires (Figure 5-1).

The problem of melting in arrays of palladium nanowires showed not serious, since between parallel electrodes a lot of nanowires grow almost at the same time. When they spanned electrodes like bridges the voltage output of power source suddenly dropped (from 10 V to 1-2 V). The induced low voltage and resulted low current density would not damage the grown nanowires. At the same time the growing of new nanowires also stopped. When we built the single nanowires between electrodes, the melting phenomena were often observed when in-situ monitoring the process (Figure 5-1). The situation for single nanowires is different from nanowire array. As soon as single nanowires were grown across the gap of electrodes, a high current would go through these nanowires until the nanowires melted. At the broken position bubbles would come

out because of high electric field, which prevent the self-healing of the nanowires. If large or whole portion of a nanowire flaked away from electrodes, a new nanowire would start to grow, and the process would go around and around.

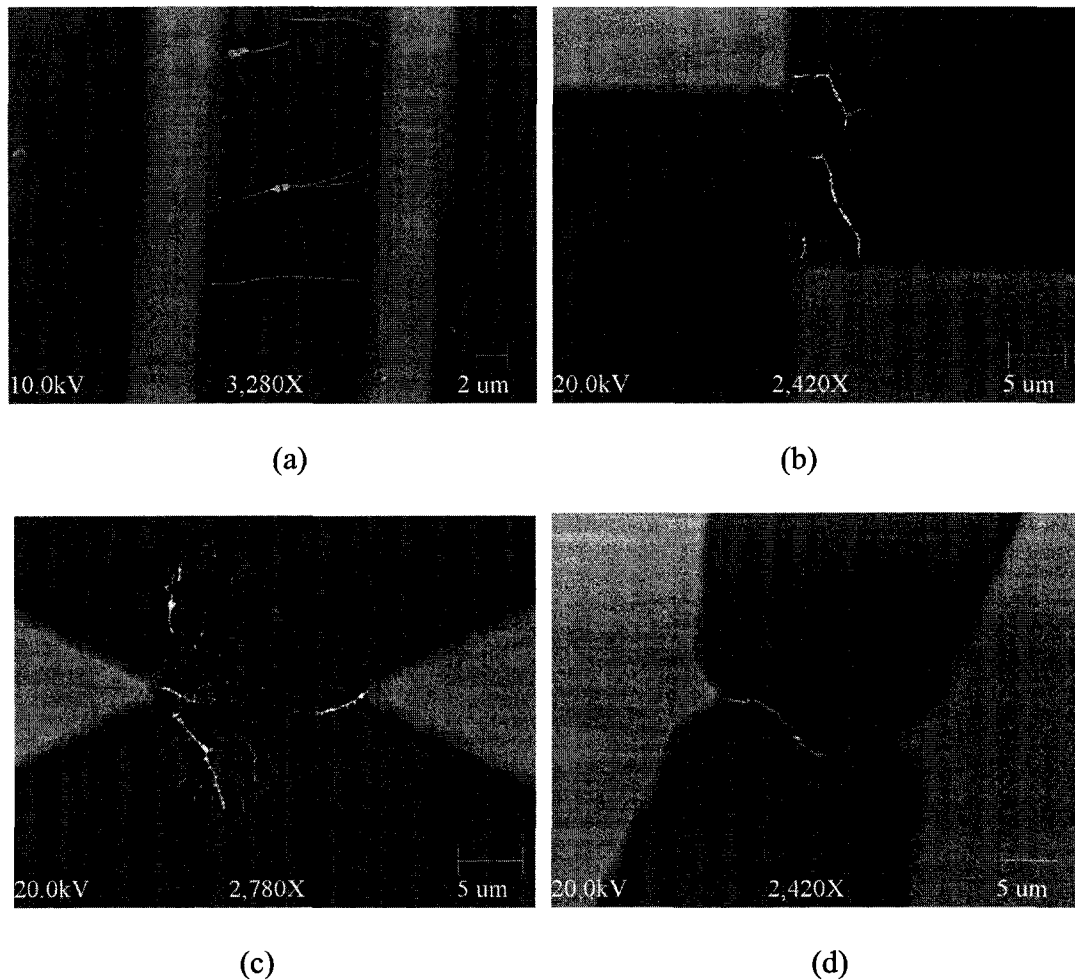


Figure 5-1 Melting problem of nanowires.

Figure 5-1 shows the melting phenomena in an array of palladium nanowires between parallel electrodes and single nanowires on the varied electrodes structures. We can see the melting points are randomly in the middle or at the end of nanowires.

## 5.2 Current-Limiting Circuit Design

Although there exist some other possibilities to solve the problem such as materials methods, self-annealing by applying a small voltage (for the case of narrow gap in nanowires, see the melted nanowire in the center of Figure 5-1a) and floating electrodes to separate the source electrodes and floating electrodes (Figure 5-2a and 5-2b), we consider a thorough way is to design a current-limiting circuits (Figure 5-2c), which can sense the current change and cut off or short circuit to protect the growth nanowires before melting.

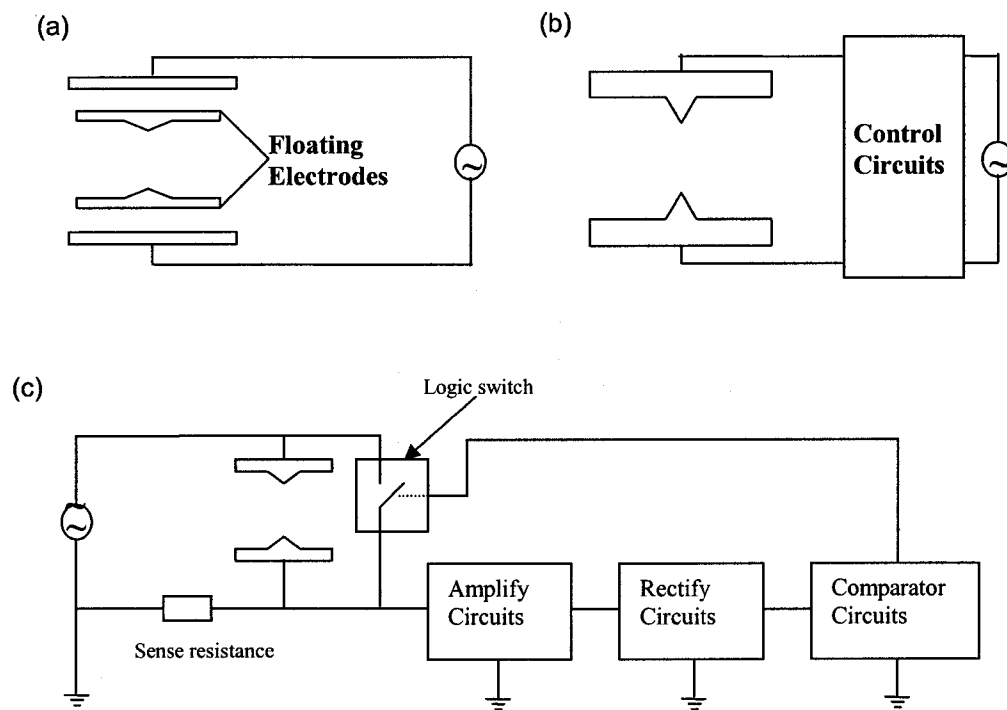


Figure 5-2 Schematic diagrams of electrodes and circuits. (a) Floating electrodes. (b) Current limiting circuits. (c) Components of current limiting circuits.

The bridge of nanowires between electrodes will cause a current jump in the circuits. The sense resistance collects this current change and converts it to voltage signal. The amplify circuits, rectify circuits, and comparator circuits process this signal

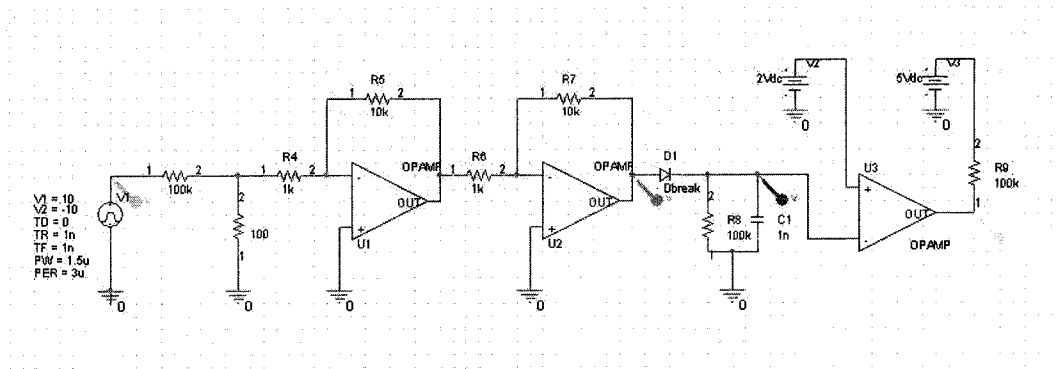
and in turn produce a trigger signal to turn on/off the logic switch. As soon as the switch is on, it shorts the electrodes and protects the grown nanowires. Analog Devices' SPST switches ADG431/ADG432 (Table 5-1), with  $\pm 15$  V analog signal range, low on resistance ( $<24 \Omega$ ), and fast switching times ( $t_{\text{on}} < 165$  ns,  $t_{\text{off}} < 130$  ns), is one good choice for logic switch.

Table 5-1 Truth value of ADG 431

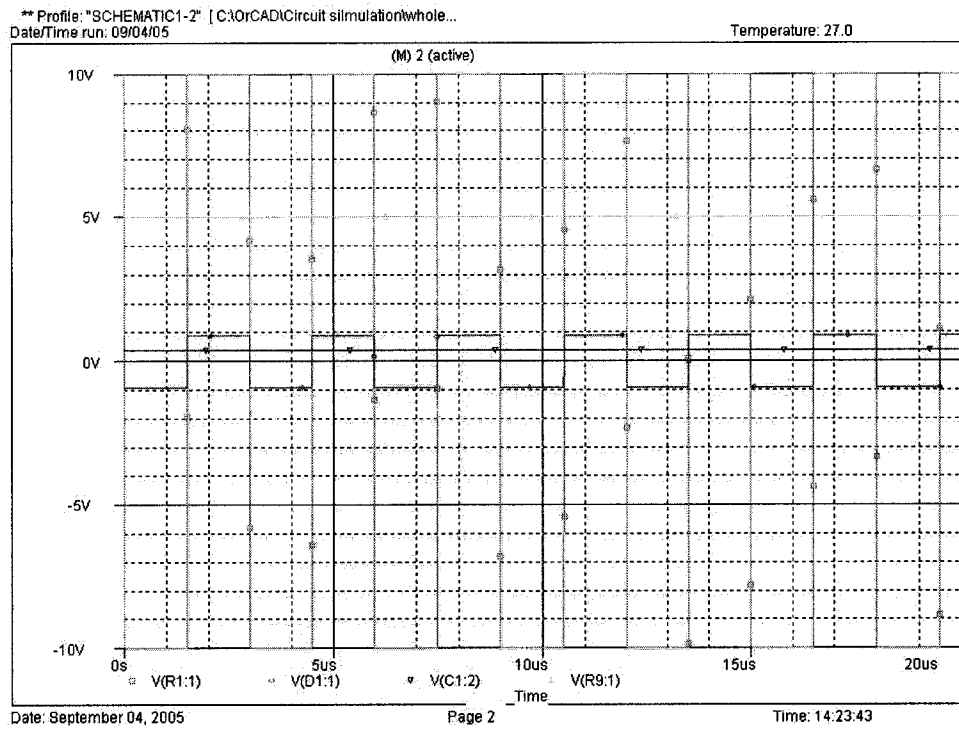
ADG431 In	Switch Condition
0	On
1	Off

### 5.3 Circuit Simulation Results

The palladium nanowires were synthesized in aqueous solution. When AC electric field was applied between electrodes, AC current went through the liquid media between electrodes, so an equivalent resistant could be supposed to exist in the working circuit in serial with power source. We estimated the value of the resistance is around  $100 \text{ k}\Omega$  based on the solution of saturated palladium acetate solution buffered by 10 mM HEPES buffer (pH 6.5) and then 8-time diluted by DI water. The resistance of grown single nanowires is supposed below  $10 \text{ k}\Omega$  in simulation. We simulated and compared the output results of circuits before and after nanowires formed. (Figure 5-3 and 5-4).



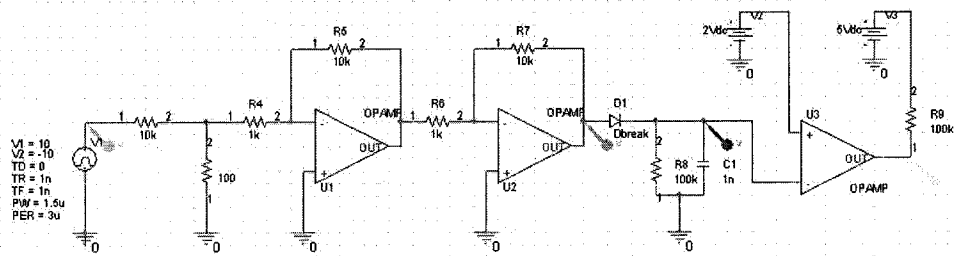
(a)



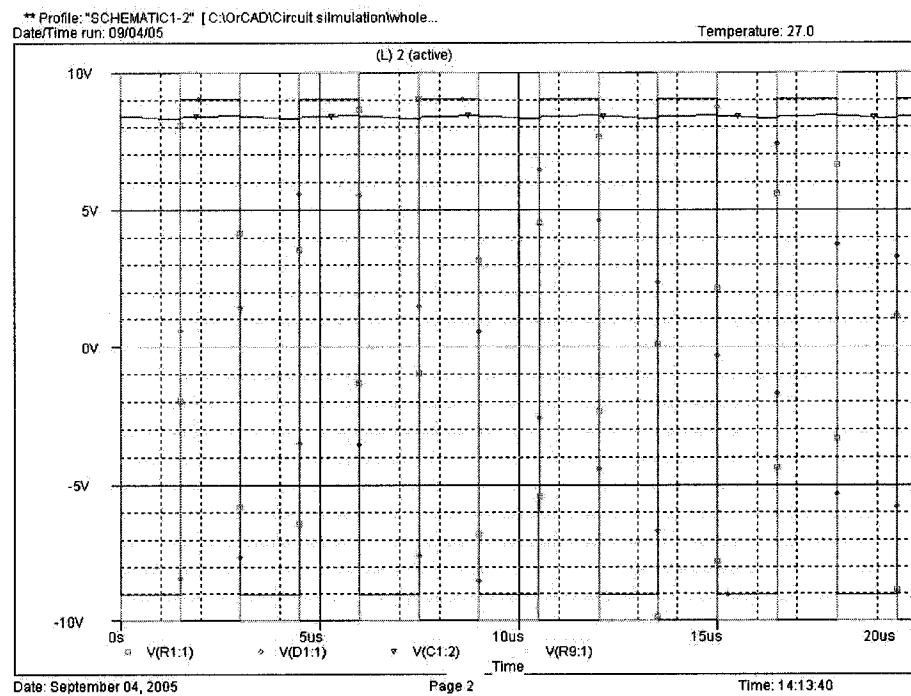
(b)

Figure 5-3 Simulation result of circuit before growth of nanowires.

- : Input voltage
- ◇: Voltage after amplifying
- ▽: Voltage after rectifying
- △: Output voltage



(a)



(b)

Figure 5-4 Simulation result of circuit after growth of nanowires.

- : Input voltage
- ◇: Voltage after amplifying
- ▽: Voltage after rectifying
- △: Output voltage

From the simulation results we can see when the equivalent resistance was changed from 100 k $\Omega$  to 10 k $\Omega$ , the signal after rectifying shifted from 0.4 V to 8.3 V. This sharply raised voltage of input of the comparator would result in an output jump from high (5 V) to low (0 V), and this low output would trigger the analog switch to short off circuits to protect the grown single nanowires.

As in real electrode system there is also an equivalent capacitor parallel to the resistance. The existence of the capacitor made design of current-limiting circuit much more complicated. It is a bad choice to use linear filter circuits to filter out a concomitant sharp wave as the resistance change itself is not a linear phenomenon. The further investigation of a more valid current-limiting circuit and a constant-current AC source are being studied.

## CHAPTER 6

### MECHANISM DISCUSSION

#### 6.4 Palladium and Its Complex

Palladium and other five chemical elements ruthenium, osmium, rhodium, iridium, and platinum are known as the platinum metals. All of them are rare elements with an abundance of less than  $10^{-6}$ %. The metals are chemically inert especially when massive.

Palladium, with atomic number 46, is fully filled electrons on its valance orbital. It has 0.179 nm atomic radius and cubic face centered crystal structure. Bulk palladium has resistivity of  $10 \mu\Omega \cdot \text{cm}$ , melting point of  $1554.9 \text{ }^\circ\text{C}$  and density of  $12020 \text{ kg/m}^3$ . Palladium is steel-white, does not tarnish in air, and is the least dense and lowest melting of the platinum group metals. When annealed, it is soft and ductile. At room temperature, palladium is capable of absorbing up to 900 times its own volume of hydrogen. In this case palladium is used to purifying of  $\text{H}_2$  since hydrogen can readily diffuse through heated palladium film. Palladium could be also used as sensor for  $\text{H}_2$  as the absorption of hydrogen can largely increase the resistivity of palladium. Moreover, palladium is widely used in autocatalysts, electronics, dentistry, jewelry, fuel cells, oil refining, photography, etc.

Complexes of palladium (II) are square or five-coordinate complexes with the formulas  $ML_4^{2+}$ ,  $ML_5^{2+}$ ,  $ML_3X^+$ , *cis*- and *trans*- $ML_2X_2$ ,  $MX_4^-$ , and  $ML_3X_2$ , where L is a neutral ligand and X a uninegative ions [90]. The palladium complexes are thermodynamically and kinetically less stable than their Pt analogs. In crystal the square complexes are often stacked one above the other. Even though the metal-metal distances may be too long for true bonding, weak interactions can occur between d orbitals on adjacent metal atoms. Some complexes have stacked cations and anions so that there are chains of metal atoms. There is an increased electrical conductivity along the directions of metal chains.

Palladium acetate is an important substance with many significant uses. Not only it catalyses many organic reactions, but it also used as a starting materials for synthesis of other palladium compounds as well as for the preparation of palladium catalysts and their precursors. In the solid state, the structure of palladium acetate is trinuclear with ideal symmetry in which each of the three palladium atoms is in a square planar environment and there are six bridging acetate groups (Figure 6-1). In solution, the structure of palladium acetate has remained somewhat controversial. Claims have been made supporting the persistence of the trinuclear molecules in solution, while other evidence is said to support the formation of various aggregates of  $[Pd(Ac)_2]_n$ , ( $n = 1, 2, 3$ , etc).

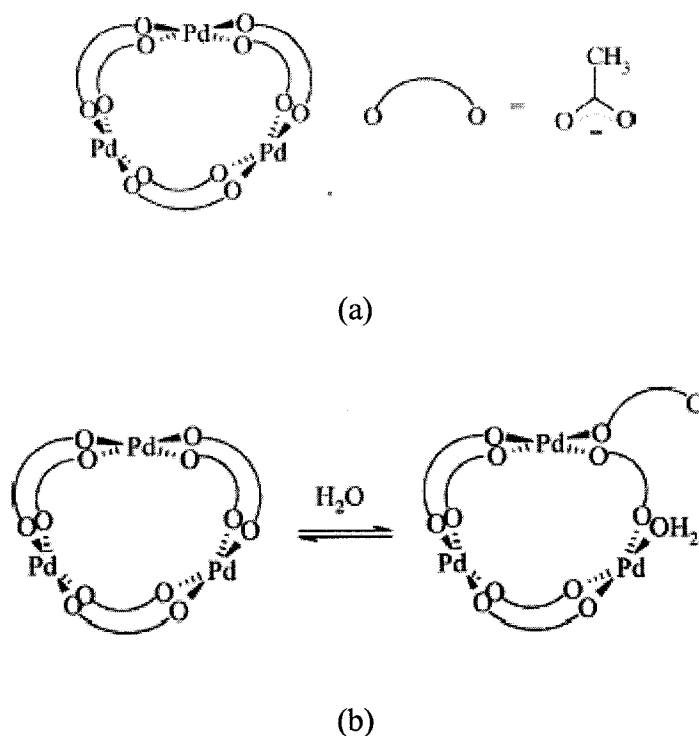


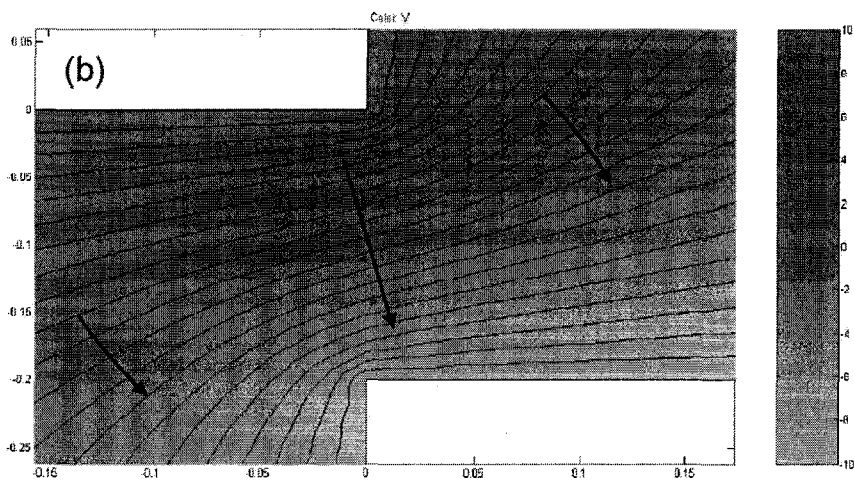
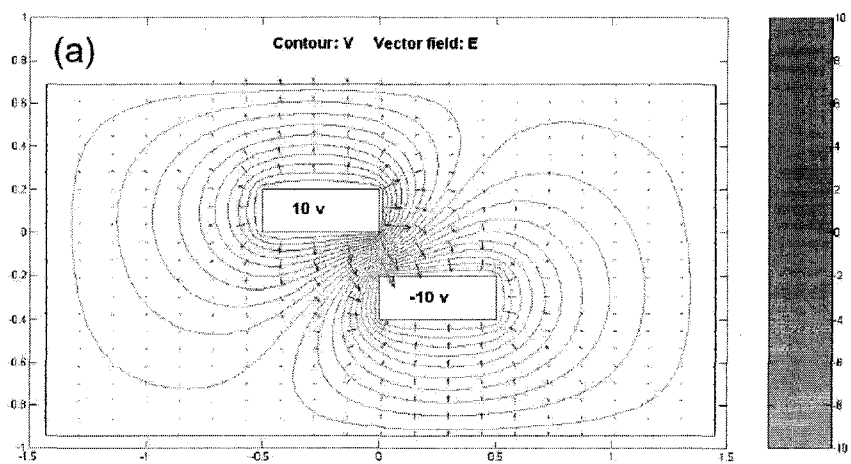
Figure 6-1 Structure of palladium acetate [91].

## 6.2 Electric Field Simulation

Electric field played an important role in growth of nanowires. When the applied voltage was too low, the growth could not be initiated. Moreover, the force of electric field determined the direction of nanowires.

Figure 6-2 shows the calculated electrical properties of electrode structure calculated by finite element methods by Matlab. Figure 6-2a describes scalar and vector fields. Arrows indicate field magnitude and direction. Figure 6-2b shows equipotential surfaces between electrodes. The direction of the electric field is everywhere perpendicular to an equipotential surface. The magnitude of the field at any point is given by the gradient of the potential. Arrows indicate field magnitude and direction. Figure 6-2c indicates density of field lines. It is evident from a comparison with all other electrode

structures studied in this work, that nanowires grew at or very close to where the field strength between electrodes was maximal, and along the direction of electric field force.



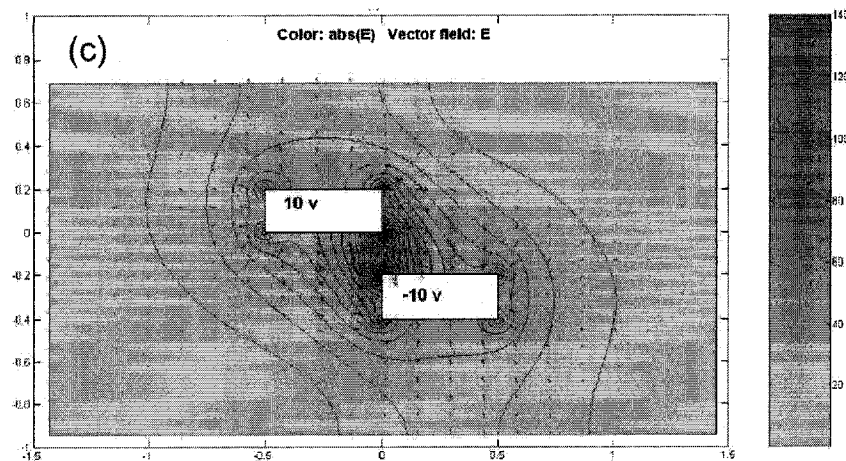


Figure 6-2 Simulation of equal potential lines and electric field around the specific electrode structure.

We also simulated the change of electric field during the growth of a single nanowire with 200 nm diameter. Figure 6-3 shows the electric field before nanowire growth. The highest electric field, around  $1.1 \times 10^6$  V/m, at the tips of electrodes. Figure 6-4 shows the electric field change during growth. With electric field getting higher and higher, we can presume nanowires grow at an accelerating speed.

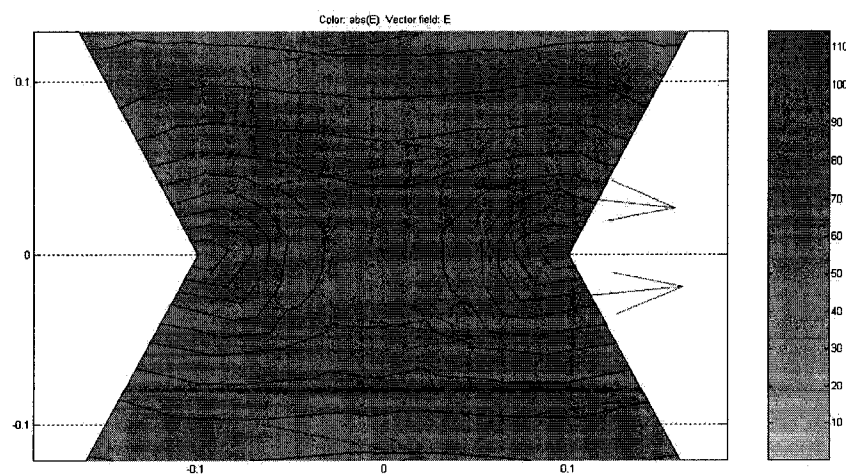
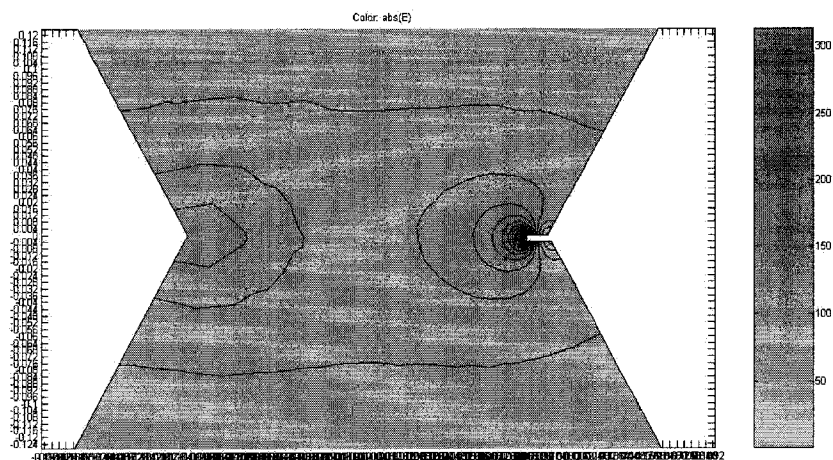
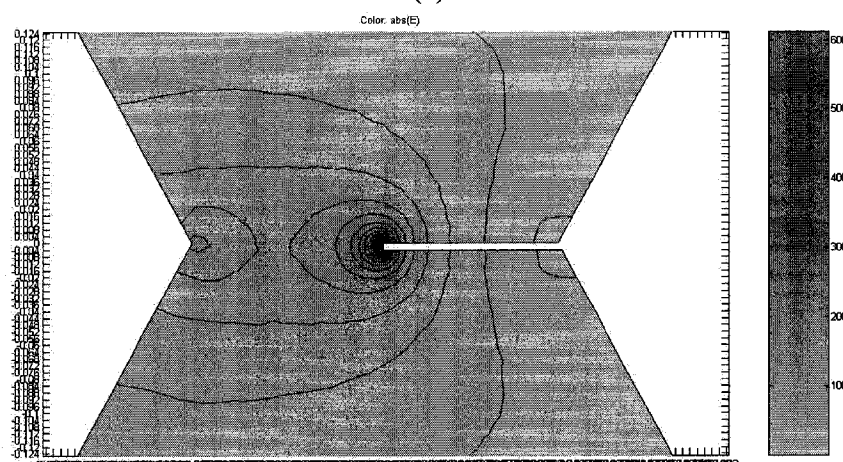


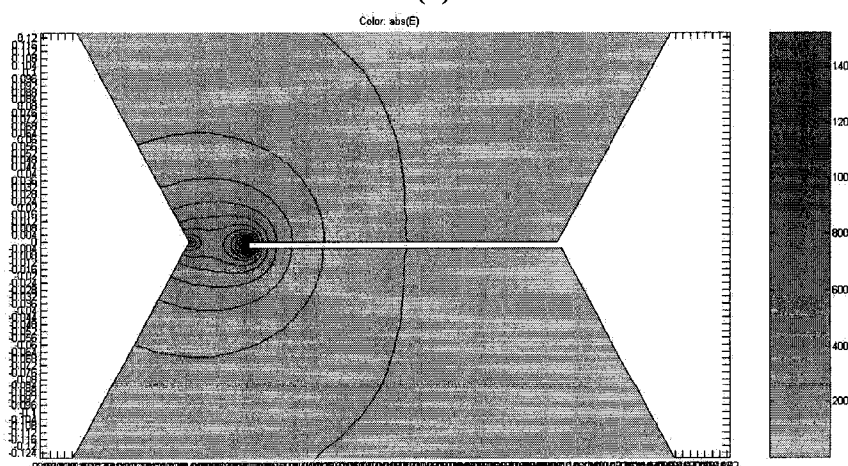
Figure 6-3 Electric field before nanowire growth.



(a)



(b)



(c)

Figure 6-4 Electric field during nanowire growth.

### 6.3 Discussion

The samples of palladium acetate for TEM were prepared by dropping 10  $\mu$ l solution onto carbon substrate followed by completely drying.

From Figure 6-5 we can see small particles are around 3 nm and big ones are tens nm. When water evaporates, palladium acetate complex carried on a crystallization process. After crystallization several nm to tens nm particles were formed and left on the substrate surface. The real size of the palladium acetate complex could be determined from this TEM figure. When the liquid media contain a small amount of water one or more hydrolysis process occurs. It is likely that the trinuclear core is retained. The occurrence of hydrolysis is also consistent with the known reactivity of palladium acetate complex toward ligands such as amines, phosphates, and arsines.

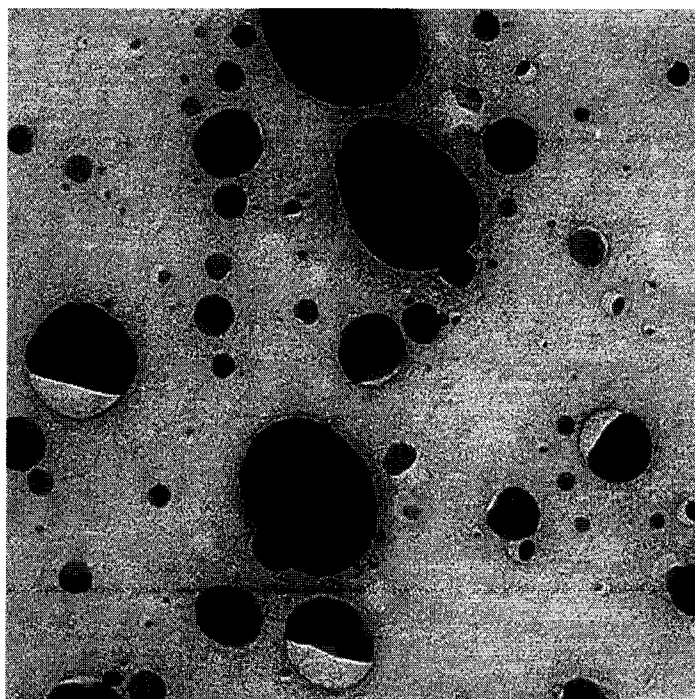


Figure 6-5 Palladium acetate particles.

The dielectrophoresis force that is acting on a polarizable particle, which is placed inside a divergent electric field, can be quantified according to the following equation [92]:

$$\langle F_{DEP} \rangle = 2\pi r^3 \varepsilon_r \varepsilon_0 \text{Re}[K_e] \nabla E_{rms}^2 \quad (6.1)$$

where  $\langle F_{DEP} \rangle$  is the time-averaged vector of the force,  $r$  is the radius of the polarizable particle,  $\varepsilon_r$  is the relative dielectric permittivity of liquid media,  $E_{rms}$  is the electric field intensity, and  $\text{Re}[K_e]$  is the real part of the effective polarizability which is also known as Clausius-Mossotti factor. From the simulation of electric field, we could estimate the gradient to be of order  $\nabla E_{rms}^2 = 10^{17} \text{ V}^2/\text{m}^3$  and  $\text{Re}[K_e]$  is around 1, so calculated  $\langle F_{DEP} \rangle$  is in the order of  $10^{-18} \text{ N}$ . At the same time, if we suppose one electronic charge exists on one palladium complex the coulomb force could be estimated to be around  $10^{-13} \text{ N}$  by  $F = qE$ . We can see when complex brings charge on it, the coulomb force is the dominant force.

Any charged particle in electric field has a force induced by electric field on it. If the particle brings one electron charge, the force will be  $F = qE$ . At the same time, when this particle move in the water, a frictional force by water is working on it in the reverse direction, which is defined by using Stokes' law,  $F_f = 6\pi\eta aV$ , where  $\eta$  is the viscosity of water ( $0.001 \text{ Ns/m}^2$  at room temperature),  $a$  is the effective radius considering water molecules or called Stokes radius, and  $V$  is drift speed of the particle. When the two forces are equal, the particle reaches its end speed, or drift speed. The equation is given as  $V = qE/(6\pi\eta a)$  and  $\mu = q/(6\pi\eta a)$  where  $\mu$  is the ion mobility in water (Table 6-1).

Table 6-1 Ionic mobilities in water at 298 K.  $\mu/(10^{-8} \text{ m}^2\text{s}^{-1}\text{V}^{-1})$ 

Cations		Anions	
Ag <sup>+</sup>	6.42	Cl <sup>-</sup>	7.91
Ca <sup>2+</sup>	6.17	CO <sub>3</sub> <sup>2-</sup>	7.46
Cu <sup>2+</sup>	5.56	NO <sub>3</sub> <sup>-</sup>	7.40
NH <sub>4</sub> <sup>+</sup>	7.63	OH <sup>-</sup>	20.64
Zn <sup>2+</sup>	5.47	SO <sub>4</sub> <sup>2-</sup>	8.29

If Pd<sup>2+</sup> exists in water, we suppose its mobility is around  $6.0 \times 10^{-8} \text{ m}^2\text{s}^{-1}\text{V}^{-1}$ . Its drift speed under an electric field of  $10^6 \text{ V/m}$  is  $6.0 \times 10^4 \mu\text{m/s}$ . For convenient calculation, we use electrode gap distance  $10 \mu\text{m}$ . So the time that a Pd<sup>2+</sup> need to drift from on electrode to the other is  $t = 170 \mu\text{s}$ . As in our experiments, nanowire growth is strictly frequency-dependent, we can calculate the period time that the electric field changes its direction (Table 6-2).

Table 6-2 Period time at different frequency

Frequency (Hz)	Period time ( $\mu\text{s}$ )
300k	1.6
30k	16
3k	160
300	1600

We can easily see at the high frequency the ions only move back and forth near their original places, while at the low frequency ions have enough time to drift and strike onto electrodes before electric field changes its direction. The data match the experiment results that nanowires can grow only at high frequency, and irregular deposition happened at low frequency. In other words, nanowires only grow between electrodes when most of ions stay in the status of back and forth movement. This is interesting as if our calculation is right, only very few ions near electrode or growing nanowire (we name active area, around 100 nm thick at 300 kHz) are involved into growth.

We can easily understand that why most electrochemists use DC or low frequency AC. This is because under DC and low frequency ions in solution can drift in one direction and deposit onto substrate to get thin film structures, or nanowires based on templates (Figure 6-6). Under the high frequency, only ions in the active area (the place very near electrodes) drift onto electrodes, and if there is some defect at the edge of electrode, the electric field near the defect will be nonuniform, electric field force applied on the ions will move them onto the specific defect and aggregate there to initialize nanowire growth.

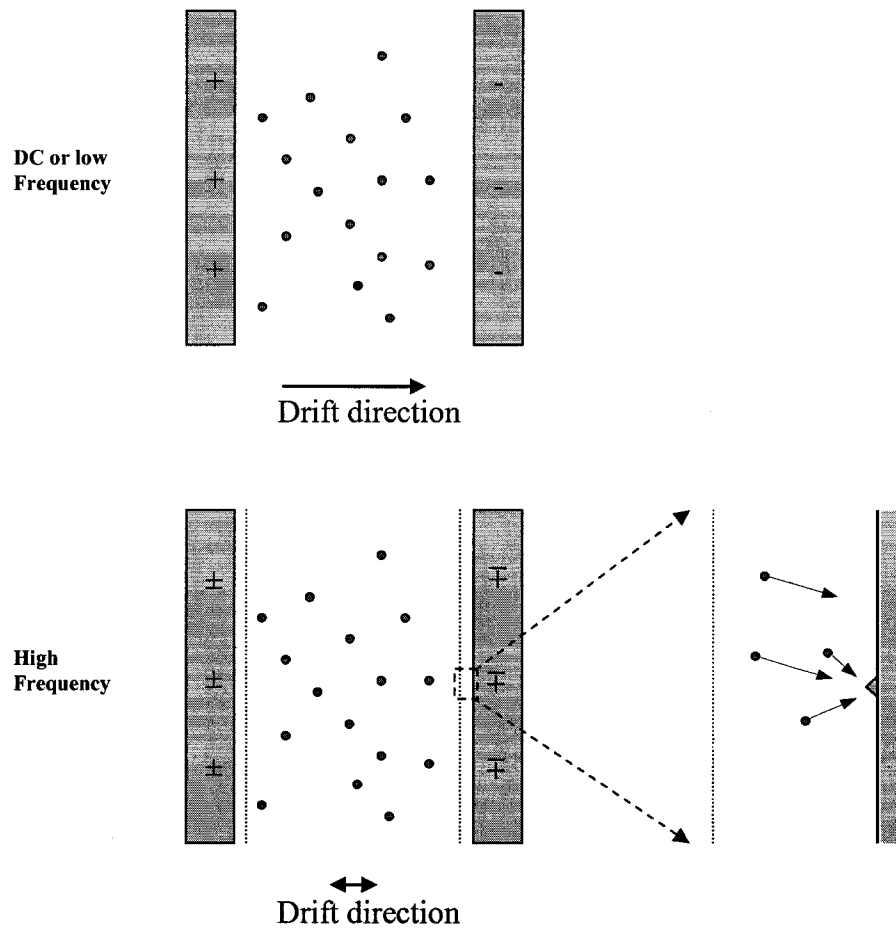


Figure 6-6 Ions drift at different frequencies.

## CHAPTER 7

### CONCLUSION AND FUTURE WORK

#### 7.1 Conclusion

To summarize, our approach of direct assembly of metallic nanowires between electrodes from aqueous solution has a number of features which make it potentially better-suited to practical application than similar methods reported recently. Dielectrophoretic assembly of microwires from gold nanoparticles in solution [19] is characterized by high resistivity and poor mechanical stability, and field emission-induced growth of nanowires from organometallic compound gas [20] involves critical environmental conditions and complicated process control. By contrast, the simplicity of the fabrication process described here and the favorable electrical properties of the resulting nanowires suggest a promising future for wide practical applications.

Single palladium nanowires were also successfully synthesized in our experiments. Nanowire formation decreases the energy of the electric field by reducing the electric field strength in the region surrounding the wires, inhibiting the growth of nanowires nearby. We studied and simulation of current-limiting circuits which was used to control the growth of nanowires. The mechanism of growing of nanowires was discussed, and further details of the mechanism of assembly are still under investigation. The present work has elucidated a simple means of precise positioning of nanowires

between electrical devices. Self-assembly of single Pd nanowires at defined locations between electrodes is not merely possible but in fact achievable and reproducible. In principle, vertical structures could be realized by a similar approach. We have provided a novel means of achieving nanoscale interconnections, potentially useful for futuristic device development, integration, and packaging.

## 7.2 Future Work

Figure 7-1 shows the presumed mechanism of nanowire growth.

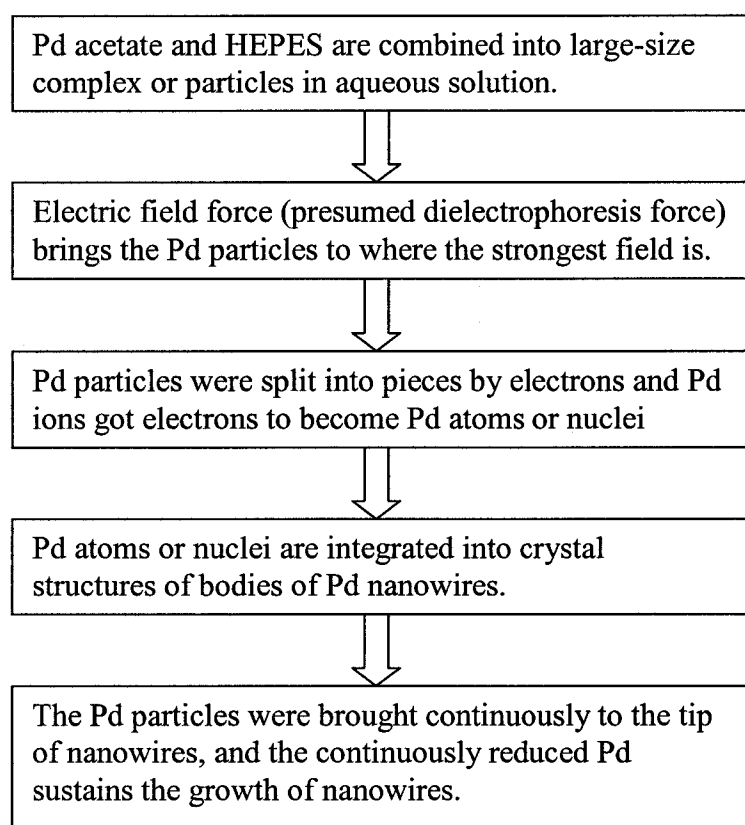


Figure 7-1 Presumed mechanism of nanowire growth.

The synthesized single nanowires and nanowire arrays are potential for device integration, bio or chemical sensor, etc. Some research work could be done in Pd alloys and metal sheath structures based on the Pd nanowire templates. Pd is a precious metal,

one of the platinum group metals, has been widely used in industries of autocatalysts, electronics, fuel cells, hydrogen purification, and petroleum refining etc. Following the previous work, Pd nanowires assembled at predefined location between electrodes, we expect the studies of Pd alloys and metal sheath structures based on the Pd nanowire templates could pave the way to application of interconnects, hydrogen storage, and chemical or biological sensors.

Pd/Cu is one investigated goal because Cu and low-k dielectric materials are widely used interconnection technology. We expect the Pd/Cu structures could largely improve the conductivity over single Pd nanowire and could be compatible with current CMOS, interconnections, and packaging technology.

Pd/Ag alloy is the most used materials for hydrogen extraction in industry, and many Pd alloys have been demonstrated to have more solubility and permeability of hydrogen than pure Pd. Besides, nanoscale structures can provide more surface area and grain boundaries which largely enhance hydrogen adsorption-absorption. We will also investigate on the 3D (vertical structures on large surface area) Pd nanowire arrays instead of two dimensional and one dimensional structures we got before.

Based on the Pd nanowire template, Au nanowires between electrodes could provide an applicable platform for chemical and biological sensors. Many kinds of bonds such as thiol bond and biotin-streptavidin bond can efficiently connect chemical or biological objects with gold. Supposed principle of sensors is that the securing of the chemical or biological objects onto the nanowire results in the current change going through it.

The fabrication of metal sheath structures could be carried by catalyzed deposition of metal ions onto Pd nanowire template in an appropriate reducing bath. We have recently reported the selective deposition of Co onto Pd-covered DNA by a similar method. Pd alloy could be made by annealing the preformed metal sheath structures. Deposition of Cu, Ag, and Au onto Pd nanowires needs to be investigated in the next experiments.

## REFERENCES

1. X. Duan, Y. Huang, Y. Cui, J. Wang, and C. M. Lieber, "Indium phosphide nanowires as building blocks for nanoscale electronic and optoelectronic devices," *Nature* 2001, **409**, 66.
2. T. Rueckes, K. Kim, E. Joselevich, G. Y. Tseng, C. Cheung, and C. M. Lieber, "Carbon nanotube-Based nonvolatile random access memory for molecular computing," *Science* 2000, **289**, 94.
3. A. M. Morales, and C. M. Lieber, "A laser ablation method for the synthesis of crystalline semiconductor nanowires," *Science* 1998, **279**, 208.
4. Y. Wu, and P. Yang, "Direct observation of vapor-liquid-solid nanowire growth," *Journal American Chemical Society* 2001, **123**, 3165.
5. Z. W. Pan, Z. R. Dai, and Z. L. Wang, "Nanobelts of semiconducting oxides," *Science* 2001, **291**, 1947.
6. J. Yin, J. Li, W. Jian, A. J. Bennett, and J. M. Xu, "Fabrication of highly ordered metallic nanowire arrays by electrodeposition," *Applied Physics Letter* 2001, **79**, 1039.
7. M. P. Zach, K. H. Ng, R. M. Penner, "Molybdenum nanowires by electrodeposition," *Science* 2000, **290**, 2120.
8. E. Braun, Y. Eichen, U. Sivan, and G. Ben-Yoseph, "DNA-templated assembly and electrode attachment of a conducting silver wire," *Nature* 1998, **391**, 775.
9. J. Richter, M. Mertig, W. Pompe, I. Monch, and H. K. Schackert, "Construction of highly conductive nanowires on a DNA template," *Applied Physics Letter* 2001, **78**, 536.
10. R. Djalali, Y. Chen, and H. Matsui, "Au nanowire fabrication from sequenced histidine-rich peptide," *Journal American Chemical Society* 2002, **124**, 13660.
11. C. Mao, D. J. Solis, B. D. Reiss, S. T. Kottmann, R. Y. Sweeney, A. Hayhurst, G. Georgiou, B. Iverson, and A. M. Belcher, "Virus-based toolkit for the directed synthesis of magnetic and semiconducting nanowires," *Science* 2004, **303**, 213.

12. W. Han, S. Fan, Q. Li, and Y. Hu, "Synthesis of gallium nitride nanorods through a carbon nanotube-confined reaction," *Science* 1997, **277**, 1287.
13. B. Mayers, X. Jiang, D. Sunderland, B. Cattle, and Y. Xia, "Hollow nanostructures of platinum with controllable dimensions can be synthesized by templating against selenium nanowires and colloids," *Journal American Chemical Society* 2003, **125**, 13364.
14. B. Gates, Y. Yin, and Y. Xia, "A solution-phase approach to the synthesis of uniform nanowires of crystalline selenium with lateral dimensions in the range of 10-30 nm," *Journal American Chemical Society* 2000, **122**, 12582.
15. C. Qian, F. Kim, L. Ma, F. Tsui, P. Yang, and J. Liu, "Solution-phase synthesis of single-crystalline iron phosphide nanorods/nanowires," *Journal American Chemical Society* 2004, **126**, 1195.
16. Y. Huang, X. Duan, Q. Wei, and C. M. Lieber, "Directed assembly of one-dimensional nanostructures into functional networks," *Science* 2001, **291**, 630.
17. B. Messer, J. H. Song, and P. Yang, "Microchannel networks for nanowire patterning," *Journal American Chemical Society* 2000, **122**, 10232.
18. H. He, and N. J. Tao, "Electrochemical fabrication of metal nanowires," *Encyclopedia of Nanoscience and Nanotechnology*, Volume X, 1-18.
19. K. D. Hermanson, S. O. Lumsdon, J. P. Williams, E. W. Kaler, and O. D. Velev, "Dielectrophoretic assembly of electrically functional microwires from nanoparticle suspensions," *Science* 2001, **294**, 1082.
20. J. T. L. Thong, C. H. Oon, M. Yeadon, and W. D. Zhang, "Field-emission induced growth of nanowires," *Applied Physics Letter* 2002, **81**, 4823.
21. J. Bradley, H. Chen, J. Crawford, J. Eckert, K. Ernazarova, T. Kurzeja, M. Lin, M. McGee, W. Nadler, and S. G. Stephens, "Creating electrical contacts between metal particles using directed electrochemical growth," *Nature* 1997, **389**, 268.
22. P. A. Smith, C. D. Nordquist, T. N. Jackson, T. S. Mayer, B. R. Martin, J. Mbindyo, and T. E. Mallouk, "Electric-field assisted assembly and alignment of metallic nanowires," *Applied Physics Letter* 2000, **77**, 1399.
23. C. Cheng, R. K. Gonela, Q. Gu, and D. T. Haynie, "Self-assembly of metallic nanowires from aqueous solution," *Nano Letter* 2005, **5**, 175.
24. Y. Cui, Q. Wei, H. Park, C.M. Lieber, "Nanowire nanosensors for highly sensitive and selective detection of biological and chemical species," *Science* 2001, **293**, 1289.

25. A. Maiti, J.A. Rodriguez, M. Law, P. Kung, J.R. McKinney, P. Yang, "SnO<sub>2</sub> nanoribbons as NO<sub>2</sub> sensors: insights from first-principles calculations," *Nano. Letter* 2003, **3**, 1025.
26. J. Hahn and C.M. Lieber, "Direct ultrasensitive electrical detection of DNA and DNA sequence variations using nanowire nanosensors," *Nano Letter* 2004, **4**, 51.
27. L. Piraux, J. George, J. Despres, C. Leroy, E. Ferain, R. Legres, K. Ounadjela, A. Fert, "Giant magnetoresistance in magnetic multilayered nanowires," *Applied Physics Letter* 1994, **65**, 2484.
28. T. Thurn-Albrecht, J. Schotter, C.A. Kastle, N. Emley, T. Shibauchi, L. Krusin-Elbaum, K. Guarini, C.T. Black, M.T. Tuominen, T.P. Russell, "Ultrahigh density nanowire arrays grown in self-assembled diblock copolymer templates," *Science* 2000, **290**, 2126.
29. K. Nielsch, R.B. Wehrspohn, J. Barthel, J. Kirschner, U. Gosele, "Hexagonally ordered 100 nm period nickel nanowire arrays," *Applied Physics Letter* 2001, **79**, 1360.
30. J. Richter, R. Seidel, R. Kirsch, M. Mertig, W. Pompe, J. Plaschke, H.K. Schackert, "Nanoscale palladium metallization of DNA," *Advanced Materials* 2000, **12**, 507.
31. J. Richter, M. Mertig, W. Pompe, H. Vinzelberg, "Low-temperature resistance of DNA-templated nanowires," *Applied Physics A* 2002, **74**, 725.
32. W.E. Ford, O. Harnack, A. Yasuda, J.M. Wessels, "Platinated DNA as precursors to templated chains of metal nanoparticles," *Advanced Materials* 2001, **13**, 1793.
33. R. Seidel, M. Mertig, W. Pompe, "Scanning force microscopy of DNA metallization," *Surface Interface Analysis* 2002, **33**, 151.
34. M. Mertig, L.C. Ciacchi, R. Seidel, W. Pompe, "DNA as a selective metallization template," *Nano Letter* 2002, **2**, 841.
35. R. Seidel, L.C. Ciacchi, M. Weigel, W. Pompe, M. Mertig, "Synthesis of platinum cluster chains on DNA templates: conditions for template-controlled cluster growth," *Journal of Physical Chemistry B* 2004, **108**, 10801.
36. K. Keren, M. Krueger, R. Gilad, G. Ben-Yoseph, U. Sivan, E. Braun, "Sequence-specific molecular lithography on single DNA molecules," *Science* 2002, **297**, 72.
37. K. Keren, R.S. Berman, E. Braun, "Patterned DNA metallization by sequence-specific localization of a reducing agent," *Nano Letter* 2004, **4**, 323.

38. A. Kumar, M. Pattarkine, M. Bhadbhade, A.B. Mandale, K.N. Ganesh, S.S. Datar, C.V. Dharmadhikari, M. Sastry, "Linear superclusters of colloidal gold particles by electrostatic assembly on DNA templates," *Advanced Materials* 2001, **13**, 341.
39. M. Sastry, A. Kumar, S. Datar, C.V. Dharmadhikari, K.N. Ganesh, "DNA-mediated electrostatic assembly of gold nanoparticles into linear arrays by a simple drop-coating procedure," *Applied Physics Letter* 2001, **78**, 2943.
40. F. Patolsky, Y. Weizmann, O. Lioubashevski, I. Willner, "Au-particle nanowires based on DNA and polylysine templates," *Angewandte Chemie International Edition* 2002, **41**, 2323.
41. O. Harnack, W.E. Ford, A. Yasuda, J.M. Wessels, "Tris(hydroxymethyl) phosphine-capped gold particles templated by DNA as nanowire precursors," *Nano Letter* 2002, **2**, 919.
42. C.F. Monson and A.T. Woolley, "DNA-templated construction of copper nanowires," *Nano Letter* 2003, **3**, 359.
43. H.A. Becerril, R.M. Stoltenberg, C.F. Monson, A.T. Woolley, "Ionic surface masking for low background in single- and double-stranded DNA-templated silver and copper nanorods," *Journal of Material Chemistry* 2004, **14**, 611.
44. Q. Gu, C. Cheng, D.T. Haynie, "Cobalt metallization of DNA: toward magnetic nanowires," *Nanotechnology* 2005, **16**, 1358.
45. J.L. Coffey, S.R. Bigham, X. Li, R.F. Pinizzotto, Y.G. Rho, R.M. Pirtle, I. L. Pirtle, "Dictation of the shape of mesoscale semiconductor nanoparticle assemblies by plasmid DNA," *Applied Physics Letter* 1996, **69**, 3851.
46. T. Torimoto, M. Yamashita, S. Kuwabata, T. Sakata, H. Mori, H. Yoneyama, "Fabrication of CdS Nanoparticle Chains along DNA double strands," *Journal of Physical Chemistry B* 1999, **103**, 8799.
47. W. U. Dittmer and F. C. Simmel, "Chains of semiconductor nanoparticles templated on DNA," *Applied Physics Letter* 2004, **85**, 633.
48. Y. Eichen, E. Braun, U. Sivan, G. Ben-Yoseph, "Self-assembly of nanoelectronic components and circuits using biological templates," *Acta Polymerica* 1998, **49**, 663.
49. Y. F. Ma, J. M. Zhang, G. J. Zhang, H. X. He, "Polyaniline nanowires on Si surfaces fabricated with DNA templates," *Journal American Chemical Society* 2004, **126**, 7097.
50. P. Nickels, W. U. Dittmer, S. Beyer, J. Kotthaus and F. C. Simmel, "Polyaniline nanowire synthesis templated by DNA," *Nanotechnology* 2004, **15**, 1524.

51. P.H. Raven, R.F. Evert, S.E. Eichhorn, *Biology of Plants* (5th ed.), Worth Publishers Inc., New York, 1992, p. 138.
52. P. M. Takahara, A. C. Rosenzweig, S. J. Lippard, "Crystal structure of a double-stranded DNA containing the major adduct of the anticancer drug cisplatin," *Nature* 1995, **377**, 649.
53. H. Huang, L. Zhu, P. B. Hopkins, "Solution structure of a cisplatin-induced DNA interstrand cross-link," *Science* 1995, **270**, 1842.
54. G.B. Onoa, G. Cervantes, V. Moreno, M.J. Prieto, "Study of the interaction of DNA with cisplatin and other Pd(II) and Pt(II) complexes by atomic force microscopy," *Nucleic Acid Research* 1998, **26**, 1473.
55. J. Duguid, V.A. Bloomfield, J. Benevides, G.J. Thomas, "Raman spectroscopy of DNA-metal complexes. I. Interactions and conformational effects of the divalent cations: Mg, Ca, Sr, Ba, Mn, Co, Ni, Cu, Pd, and Cd," *Biophysical Journal* 1993, **65**, 1916.
56. C.J. Loweth, W.B. Caldwell, X. Peng, A.P. Alisatos, P.G. Schultz, "DNA-based assembly of gold nanocrystals," *Angewandte Chemie International Edition* 1999, **38**, 1808.
57. A. Bensimon, A. Simon, A. Chiffaudel, V. Croquette, F. Heslot, D. Bensimon, "Alignment and sensitive detection of DNA by a moving interface," *Science* 1994, **265**, 2096.
58. D. Bensimon, A.J. Simon, V. Croquette, A. Bensimon, "Stretching DNA with a receding meniscus: experiments and models," *Physical Review Letter* 1995, **74**, 4754.
59. J.-F. Allemand, D. Bensimon, L. Jullien, A. Bensimon, V. Croquette, "pH-dependent specific binding and combing of DNA," *Biophysical Journal* 1997, **73**, 2064.
60. H. Yokota, F. Johnson, H. Lu, R.M. Robinson, A.M. Belu, M.D. Garrison, B.D. Ratner, B.J. Trask, D.L. Miller, "A new method for straightening DNA molecules for optical restriction mapping," *Nucleic Acids Research* 1997, **25**, 1064.
61. K. Otobe and T. Ohtani, "Behavior of DNA fibers stretched by precise meniscus motion control," *Nucleic Acids Research* 2001, **29**, e109.
62. X. Michalet, R. Ekong, F. Fougereuse, S. Rousseaux, C. Schurra, N. Hornigold, M. Slegtenhorst, J. Wolfe, S. Povey, J.S. Beckmann, A. Bensimon, "Dynamic molecular combing: stretching the whole human genome for high-resolution studies," *Science* 1997, **277**, 1518.

63. Z. Gueroui, C. Place, E. Freyssingeas, B. Berge, "Observation by fluorescence microscopy of transcription on single combed DNA," *Proceeding of National Academic Science USA* 2002, **99**, 6005.
64. J.M. Schurr and S.B. Smith, "Theory for the extension of a linear polyelectrolyte attached at one end in an electric field," *Biopolymers* 1999, **29**, 1161.
65. S.B. Smith and A.J. Bendich, "Electrophoretic charge density and persistence length of DNA as measured by fluorescence microscopy," *Biopolymers* 1999, **29**, 1167.
66. R.M. Zimmermann and E.C. Cox, "DNA stretching on functionalized gold surfaces," *Nucleic Acid Research* 1994, **22**, 492.
67. M. Washizu and O. Kurosawa, "Electrostatic manipulation of DNA in microfabricated structures," *IEEE Industry Application* 1990, **26**, 1165.
68. M. Washizu, O. Kurosawa, I. Arai, S. Suzuki, N. Shimamoto, "Applications of electrostatic stretch and positioning of DNA," *IEEE Industry Application* 1995, **31**, 447.
69. T. Yamamoto, O. Kurosawa, H. Kabata, N. Shimamoto, M. Washizu, "Molecular surgery of DNA based on electrostatic micromanipulation," *IEEE Industry Application* 2000, **36**, 1010.
70. V. Namasivayam, R.G. Larson, D.T. Burke, M.A. Burns, "Electrostretching DNA molecules using polymer-enhanced media within microfabricated devices," *Analytical Chemistry* 2002, **74**, 3378.
71. W A. Germishuizen, C. Wälti, R. Wirtz, M. B Johnston, M. Pepper, A G. Davies, A. P J Middelberg, "Selective dielectrophoretic manipulation of surface-immobilized DNA molecules," *Nanotechnology* 2003, **14**, 896.
72. N. Kaji, M. Ueda, Y. Baba, "Molecular stretching of long DNA in agarose gel using alternating current electric fields," *Biophysical Journal* 2002, **82**, 335.
73. T.T. Perkins, S.R. Quake, D.E. Smith, S. Chu, "Relaxation of a single DNA molecule observed by optical microscopy," *Science* 1994, **264**, 822.
74. T.T. Perkins, D.E. Smith, R.G. Larson, S. Chu, "Stretching of a single tethered polymer in a uniform flow," *Science* 1995, **268**, 83.
75. S. B. Smith, Y. Cui, C. Bustamante, "Overstretching B-DNA: the elastic response of individual double-stranded and single-stranded DNA molecules," *Science* 1996, **271**, 795.

76. H. Yokota, J. Sunwoo, M. Sarikaya, G. van den Engh, R. Aebersold, "Spin-stretching of DNA and protein molecules for detection by fluorescence and atomic force microscopy," *Analytical Chemistry* 1999, **71**, 4418.
77. J.Y. Ye, K. Umemura, M. Ishikawa, R. Kuroda, "Atomic force microscopy of DNA molecules stretched by spin-coating technique," *Analytical Biochemistry* 2000, **281**, 21.
78. A. Bezryadin, A. Bollinger, D. Hopkins; M. Murphey, M. Remeika, A. Rogachev, "Superconducting nanowires templated by single molecules," *Dekker Encyclopedia of Nanoscience and Nanotechnology*, J.A. Schwarz, C.I. Contescu, and K. Putyera (Eds.), ISBN 0-8247-5055-1, Marcel Dekker, Inc., New York, 2004; pp 3761-3773.
79. J. K. N. Mbindyo, B.R. Reiss, B.R. Martin, C.D. Keating, M.J. Natan, T.E. Mallouk, "DNA-directed assembly of gold nanowires on complementary surfaces," *Advanced Materials* 2001, **13**, 249.
80. D.D Eley, R.B. Leslie, "Conduction in nucleic acid components," *Nature* 1963, **197**, 898.
81. M. Bockrath, N. Markovic, A. Shepard, M. Tinkham, L. Gurevich, L.P. Kouwenhoven, M.W. Wu, L.L. Sohn, "Scanned conductance microscopy of carbon nanotubes and  $\lambda$ -DNA," *Nano Letter* 2002, **2**, 187.
82. E. Abrahams, P.W. Anderson, D.C. Licciardello, T.V. Ramakrishnan, "Scaling theory of localization: absence of quantum diffusion in two dimensions," *Physical Review Letter* 1979, **42**, 673.
83. N.F. Mott, M. Kaveh, "Metal-insulator transitions in non-crystalline Systems," *Advanced Physics* 1985, **34**, 329.
84. P.W. Anderson, "Absence of diffusion in certain random lattices," *Physical Review* 1958, **109**, 1492.
85. S.R. Quake and A. Scherer, "From micro to nano fabrication with soft materials," *Science* 2000, **290**, 1536.
86. D.S. Hopkins, D. Pekker, P.M. Goldbart, A. Bezryadin, "Quantum interference device made by DNA templating of superconducting nanowires," *Science* 2005, **308**, 1762.
87. *International Technology Roadmap for Semiconductors* 2003 edn (<http://public.itrs.net/Files/2003ITRS/Interconnect2003.pdf>).
88. F. Okuyama, "Cr needle crystals with fcc structure plasma grown from  $\text{Cr}(\text{CO})_6$ ," *Journal of Applied Physics* **53**, 6226 (1982).

89. F. Okuyama, Y. Fujimoto, "Fcc needle crystals of molybdenum grown from  $\text{Mo}(\text{CO})_6$ ," *Journal of Applied Physics* **56**, 566 (1984).
90. E. A. Cotton, G. Wilkinson, and P. L. Gaus, *Basic Inorganic Chemistry*, third Edition, 1995.
91. V. I. Bakhmutov, J. F. Berry, F. A. Cotton, S. Ibragimov and C. A. Murillo, "Non-trivial behavior of palladium acetate," *Dalton Transactions* 2005, 1989.
92. A. Docoslis, and P. Alexandridis, "One-, two-, and three-dimensional organization of colloidal particles using nonuniform alternating current electric fields," *Electrophoresis* 2002, **23**, 2174.